

Eclipsing Binaries as Benchmarks for Trigonometric Parallaxes in the *Gaia* Era

Keivan G. Stassun^{1,2} and Guillermo Torres³

ABSTRACT

We present fits to the broadband photometric spectral energy distributions (SEDs) of 158 eclipsing binaries (EBs) in the *Tycho-2* catalog. These EBs were selected because they have highly precise stellar radii, effective temperatures, and in many cases metallicities previously determined in the literature, and thus have bolometric luminosities that are typically good to $\lesssim 10\%$. In most cases the available broadband photometry spans a wavelength range 0.4–10 μm , and in many cases spans 0.15–22 μm . The resulting SED fits, which have only extinction as a free parameter, provide a virtually model-independent measure of the bolometric flux at Earth. The SED fits are satisfactory for 156 of the EBs, for which we achieve typical precisions in the bolometric flux of $\approx 3\%$. Combined with the accurately known bolometric luminosity, the result for each EB is a predicted parallax that is typically precise to $\lesssim 5\%$. These predicted parallaxes—with typical uncertainties of 200 μas —are 4–5 times more precise than those determined by *Hipparcos* for 99 of the EBs in our sample, with which we find excellent agreement. There is no evidence among this sample for significant systematics in the *Hipparcos* parallaxes of the sort that notoriously afflicted the Pleiades measurement. The EBs are distributed over the entire sky, span more than 10 mag in brightness, reach distances of more than 5 kpc, and in many cases our predicted parallaxes should also be more precise than those expected from the *Gaia* first data release. The EBs studied here can thus serve as empirical, independent benchmarks for these upcoming fundamental parallax measurements.

1. Introduction

There is arguably no astronomical measurement more fundamental than distance from trigonometric parallax. Such parallax measurements are foundational to the cosmic distance scale generally and to stellar astrophysics specifically, including our basic understanding of stellar evolution, stellar populations, and Galactic structure. Thus, the parallaxes provided by the *Hipparcos* mission (Perryman et al. 1997; van Leeuwen 2007) have had important, unrivaled impact across many areas of study for the past 20 years.

Yet the *Hipparcos* parallaxes were not without problems, perhaps the most significant of which was the aberrant distance to the Pleiades which the *Hipparcos* parallax placed at 120.2 ± 1.9 pc (van Leeuwen 2009) as compared to the broadly accepted distance of ≈ 135 pc from a variety of methods (e.g., Munari et al. 2004; Zwahlen et al. 2004; Soderblom et al. 2005; Groenewegen et al. 2007; Melis et al. 2014; Madler et al. 2016, and others cited therein). Several of these recent determinations are formally highly precise ($\sigma = 1.2$ – 1.7 pc). The discrepancy in the *Hipparcos* distance for the Pleiades was identified almost immediately (e.g., Pinsonneault et al. 1998; Soderblom et al. 1998), thanks to the unusual combination of proximity and cluster richness

¹Vanderbilt University, Department of Physics & Astronomy, 6301 Stevenson Center Ln., Nashville, TN 37235, USA; keivan.stassun@vanderbilt.edu

²Fisk University, Department of Physics, 1000 17th Ave. N., Nashville, TN 37208, USA

³Harvard-Smithsonian Center for Astrophysics, 60 Garden St., Cambridge, MA 02138, USA

afforded by the Pleiades. In general, however, heretofore there have been very few *fundamental* benchmarks against which to test the *Hipparcos* parallaxes across the sky, across various stellar environments, and across stellar parameter space. One notable example is the use of spatially resolved double-lined spectroscopic binaries, which can yield highly accurate and precise orbital parallaxes (see, e.g., Tomkin 2005).

Eclipsing binary (EB) stars have long served as fundamental benchmarks for stellar astrophysics. Through analysis of the light curve and radial velocities, EBs yield direct measurement of the component stellar masses and radii, and temperatures, with accuracies of $\sim 1\%$ for the best cases. As a result, the bolometric luminosity (L_{bol}) of an EB can be determined to very high precision and—importantly—without need of a distance measurement because it depends only on the measured radii and effective temperatures.

EBs with such accurately determined L_{bol} can therefore serve as empirical, independent benchmarks for stellar distances obtained by other methods such as trigonometric parallax, if the bolometric flux at Earth (F_{bol}) can also be measured empirically and with sufficient precision. For example, in the recent analysis of newly discovered Pleiades EBs in the *K2* (successor to *Kepler*) mission data, David et al. (2016) used the available broadband photometry from *GALEX* ultraviolet bands through *WISE* mid-infrared bands to determine an empirical distance of 132 ± 5 pc to the Pleiades EB HCG 76, consistent with the consensus distance and again showing the *Hipparcos* distance to be biased. Impressively, this new empirical EB-based distance has a precision of better than 4%, significantly more precise than the 12% discrepancy in the *Hipparcos* distance, making it useful as a meaningful benchmark.

Variants of this idea have been used to determine distances to EBs in the near field (relying on bolometric corrections) and even in external galaxies such as M31, the LMC or the SMC (e.g., Ribas et al. 2005; Pietrzyński et al. 2009; Graczyk et al. 2014), sometimes based on application of surface brightness relations. These latter EB studies and others like them have been extremely important in establishing the lower rungs of the cosmological distance ladder, serving as calibrators for other methods reaching larger distances.

The upcoming *Gaia* mission holds great promise for many areas of stellar and Galactic astrophysics through the provision of fundamental trigonometric parallax measurements for $\sim 10^9$ stars. At the same time, there now exists a large sample of benchmark-grade EBs with accurate radii and temperatures, and in many cases metallicities, which provide accurate and distance-independent L_{bol} . In addition, there now exist all-sky, broadband photometric measurements for stars spanning a very broad range of wavelengths, from the *GALEX* far-UV at $\sim 0.1 \mu\text{m}$ to the *WISE* mid-IR at $\sim 22 \mu\text{m}$. These measurements permit construction of spectral energy distributions (SEDs) that effectively sample the majority of the flux for all but the hottest stars. Consequently the bolometric fluxes, and in turn the distances to the EBs, can in principle be determined in a largely empirical manner that preserves the accuracy of the fundamental EB parameters.

In this paper, we use available broadband photometry to construct empirical SEDs and to calculate F_{bol} for 158 EBs in the *Tycho-2* catalog whose fundamental physical properties have previously been established with accuracies of better than 3% (e.g., Torres et al. 2010). The wavelength coverage of the SEDs for most of the EBs in our sample is sufficiently large that the resulting F_{bol} are typically precise to 3%, leading to predicted parallaxes that are in most cases precise to better than 5%. For 99 of the EBs in our study sample, previous *Hipparcos* parallaxes are available for direct comparison to the parallaxes predicted from the EBs.

In Section 2, we present our study sample, the data that we use from the literature, and our SED fitting procedures. The main results of the work, including empirical F_{bol} and predicted parallaxes for the full sample, and a comparison to *Hipparcos* parallaxes where available, are presented in Section 3. In Section 4 we briefly discuss the upcoming applicability of this work to *Gaia*, which is expected to include all of these EBs as early as its first public data release. We summarize our conclusions in Section 5.

2. Data and Methods

2.1. Benchmark EB study sample

For this work we have focused on detached EBs with well determined radii and effective temperatures, to allow the derivation of bolometric luminosities of the highest precision. We set a threshold of 3% for the uncertainties in the absolute radii, although a handful of our objects were allowed to exceed this limit slightly, as described below. More than half of the sample was drawn directly from the compilation by Torres et al. (2010), featuring binaries that have been carefully vetted with special attention paid to the number and quality of the observations, the consistency of the light curve and radial-velocity curve solutions and other details of the analysis, external checks, and efforts to assess and control systematic errors. Additional systems were gathered from the more recent (or sometimes earlier) literature including Stassun et al. (2014) and the DEBCAT list¹ maintained by Southworth (2015), though some have not necessarily received the same level of vetting beyond the requirement of 3% or better formal uncertainties in the radii. While we have attempted to capture the most relevant systems for our study, our search was not intended to be exhaustive so we make no claims of completeness. All EBs were required to have entries in the *Tycho-2* catalog (Høg et al. 2000), and many are contained also in the *Hipparcos* catalog.

Spectral types in our sample span a very wide range from late O to mid M. Most are main-sequence stars, but a few are giants. The challenges involved in analyzing the spectroscopic and photometric observations of these binaries vary greatly depending on the nature of the system, and in some cases unrecognized systematic errors or other problems may not be fully reflected in the formal errors we have adopted. It is also important to note that the temperature estimates are much less fundamental in nature than the radius estimates. This is largely because temperatures often rely on external calibrations, and have been derived in many different ways by different authors. While a light curve typically contains very precise information about the ratio between the primary and secondary temperatures, the value for the primary that sets the absolute scale for the system must generally be determined independently. This is sometimes done from an analysis of disentangled spectra, from color indices, or even simply from its spectral classification. The radii, on the other hand, are always based purely on geometry and dynamics. It is not surprising, therefore, that the temperature uncertainties in our sample can be as large as 10% in some cases.

Small departures from spherical star shapes for most of the binaries in our sample, or even moderate departures for the closest ones, along with associated limb-darkening, reflection, tidal/rotational, and other effects, are assumed to have been adequately accounted for in the light-curve modeling, as suggested by the typically good agreement these systems show when compared against stellar evolution models in the original publications. In particular, the stellar sizes we have adopted are the volumetric radii, as published.

The complete list of 158 EBs for this study is given in Table 1, sorted by *Tycho* number. We have made an effort to collect available estimates of the interstellar reddening for these systems, as well as spectroscopic or photometric measures of the metallicity, both of which can serve to constrain the SED fits described later. A number of the binary components have been found to be metallic-line A or F stars and are so noted in the table, with estimates of the iron abundances given when available. Four of our EBs belong to open clusters for which the *Hipparcos* Mission has provided highly precise average parallaxes based on individual measurements for half a dozen or more members (van Leeuwen 2009). They are V906 Sco (in NGC 6475), GV Car (NGC 3532), V392 Car (NGC 2516), and TX Cnc (Praesepe). The first also has an individual

¹<http://www.astro.keele.ac.uk/jkt/debcats/>

Hipparcos parallax. GV Car and TX Cnc have somewhat poorer radius and/or temperature determinations than the rest (and are only preliminary in the first case), but they were included to enable a check on the *Hipparcos* cluster distances. TX Cnc is an over-contact (W UMa) system rather than a detached one, though this should not affect its usefulness for distance determinations (see, e.g., Wilson et al. 2010).

2.2. Broadband photometric data from the literature

The 158 EBs that comprise our study sample are, by virtue of having previously determined EB solutions and being in the *Tycho-2* catalog, relatively bright and well studied. Therefore, in most cases the EBs appear in many published photometric catalogs. In order to systematize and simplify our procedures, we opted to assemble for each EB the available broadband photometry from only the following large, all-sky catalogs (listed here in approximate order by wavelength coverage) via the *VizieR*² query service:

- *GALEX* All-sky Imaging Survey (AIS): FUV and NUV at $\approx 0.15 \mu\text{m}$ and $\approx 0.22 \mu\text{m}$, respectively.
- Catalog of Homogeneous Means in the *UBV* System for bright stars from Mermilliod (2006): Johnson *UBV* bands ($\approx 0.35\text{--}0.55 \mu\text{m}$).
- *Tycho-2*: Tycho *B* (B_T) and Tycho *V* (V_T) bands ($\approx 0.42 \mu\text{m}$ and $\approx 0.54 \mu\text{m}$, respectively).
- Strömngren Photometric Catalog by Paunzen (2015): Strömngren *uvby* bands ($\approx 0.34\text{--}0.55 \mu\text{m}$).
- AAVSO Photometric All-Sky Survey (APASS) DR6 (obtained from the UCAC-4 catalog): Johnson *BV* and SDSS *gri* bands ($\approx 0.45\text{--}0.75 \mu\text{m}$).
- Two-Micron All-Sky Survey (2MASS): *JHK_S* bands ($\approx 1.2\text{--}2.2 \mu\text{m}$).
- All-WISE: *WISE1-4* bands ($\approx 3.5\text{--}22 \mu\text{m}$).

We found B_TV_T , *JHK_S*, and *WISE1-3* photometry—spanning a wavelength range $\approx 0.4\text{--}10 \mu\text{m}$ —for nearly all of the EBs in our study sample. Most of the EBs also have *WISE4* photometry, and many of the EBs also have Strömngren and/or *GALEX* photometry, thus extending the wavelength coverage to $\approx 0.15\text{--}22 \mu\text{m}$. We adopted the reported measurement uncertainties unless they were less than 0.01 mag, in which case we assumed an uncertainty of 0.01 mag. In addition, to account for an artifact in the Kurucz atmospheres at $10 \mu\text{m}$, we artificially inflated the *WISE3* uncertainty to 0.1 mag unless the reported uncertainty was already larger than 0.1 mag.

Although the likelihood is small, it is always possible that some of these brightness measurements were obtained during an eclipse, in which case they would underestimate the total flux of the system. However, most of the catalogs listed above report averages of multi-epoch observations, from as many as 100 or more individual measurements taken over three years in the case of *Tycho-2*, so they are less likely to be affected. Single-epoch measurements such as those in the 2MASS catalog, on the other hand, are more susceptible to this problem. We found eleven systems in which the 2MASS measurements were clearly obtained in eclipse, and in those cases we applied adjustments by referring back to the original optical light curves at the exact phase of the observation, with small corrections from the optical to the near-infrared for binaries with unequal component temperatures, or corrections for third light if significant. The adjustments in *JHK_S* range from about 0.25 mag to 0.68 mag. The assembled SEDs are presented in Appendix A.

²<http://vizier.u-strasbg.fr/>

2.3. Spectral energy distribution fitting

The observed SEDs were fitted with standard stellar atmosphere models. For the EBs in our sample with $T_{\text{eff}} > 4000$ K (all but two EBs), we adopted the atmospheres of Kurucz (2013), whereas for the two EBs with $T_{\text{eff}} < 4000$ K (CU Cnc and YY Gem) we adopted the NextGen atmospheres of Hauschildt et al. (1999). The model atmosphere grids are parametrized by T_{eff} , $\log g$, and $[\text{Fe}/\text{H}]$, in steps of approximately 100 K, 0.5 dex, and 0.1 dex, respectively.

As summarized in Table 1, for each star in each EB we have T_{eff} and radius (with the masses listed in the original publications, the radius also gives $\log g$), and in many cases $[\text{Fe}/\text{H}]$ as well (we assume $[\text{Fe}/\text{H}] = +0.2$ for the Am-type stars, solar metallicity otherwise). We interpolated in the model grid to obtain the appropriate model atmosphere for each star in units of emergent flux, and then summed the two model atmospheres scaled by the stars’ surface areas to produce the total SED model for the EB. To redden the SED model, we adopted the interstellar extinction law of Cardelli et al. (1989). We then fitted the summed atmosphere model to the flux measurements to minimize χ^2 by varying just two fit parameters: extinction (A_V) and overall normalization. (The adopted stellar radii and T_{eff} also have associated uncertainties, of course; these are handled in a later step via the propagation of errors through L_{bol} ; see Section 3.2.) Where an A_V estimate was available from the literature, we adopted it as an initial guess but allowed the fit to vary A_V by as much as 3σ or 20%, whichever was larger. Where no prior A_V estimate was available, the A_V fit was unconstrained except that we limited the maximum value to that from the Schlegel et al. (1998) dust maps for the given line of sight.

The best-fit model SED with extinction is shown for each EB in Appendix A, and the reduced χ^2 values (χ^2_ν) are given in Table 2. The fits were satisfactory in 156 cases, leaving 2 EBs with very large χ^2_ν flagged in Table 2. We were not able to discern the cause of the very poor fits in these 2 cases—we rechecked that the stellar radii and T_{eff} from the original publications appear reliable and that the photometric measurements are not flagged as bad. Thus we simply discarded these 2 cases for the remainder of our analyses.

The primary quantity of interest for each EB is F_{bol} , which we obtained via direct summation of the fitted SED, *without* extinction, over all wavelengths. The formal uncertainty in F_{bol} was determined according to the standard criterion of $\Delta\chi^2 = 2.30$ for the case of two fitted parameters (e.g., Press et al. 1992), where we first renormalized the χ^2 of the fits such that $\chi^2_\nu = 1$ for the best fit model. Because χ^2_ν is in almost all cases greater than 1 (see Table 2), this χ^2 renormalization is equivalent to inflating the photometric measurement errors by a constant factor and results in a more conservative final uncertainty in F_{bol} according to the $\Delta\chi^2$ criterion. While not strictly equivalent to 1σ errors, we consider these uncertainties to be representative of our true errors, and evidence presented in Section 3.4 supports this.

Finally, because the model atmosphere grids do not extend to wavelengths shorter than $0.1 \mu\text{m}$, we found it necessary to augment the model atmospheres at the blue end for hot stars with $T_{\text{eff}} > 15,000$ K, for which the emergent flux at $\lambda < 0.1 \mu\text{m}$ becomes comparable to the typical uncertainty in F_{bol} of 3%. Therefore, for these hot stars we appended to the model SED a simple blackbody representing the sum of two blackbodies corresponding to the two stars’ temperatures scaled by their surface areas. To account for the non-blackbody nature of the SED at $\lambda > 0.1 \mu\text{m}$, we adjusted the blackbody portion at $\lambda < 0.1 \mu\text{m}$ by the flux difference of the actual SED relative to a blackbody at $\lambda > 0.1 \mu\text{m}$.

2.4. How model-dependent are the bolometric fluxes?

For the purposes of the present work, the ultimate aim of the SED fitting is to obtain a measure of F_{bol} for each EB that is as model-independent as possible. It could be argued that the procedure is dependent on the model atmospheres used, which of course it is to some extent. This model dependence is mitigated, however, by the very large wavelength range covered by the actual flux measurements, which for most of the EBs includes a very large fraction of the emergent stellar flux.

To quantify this, we have calculated the fraction of each EB’s F_{bol} that is from beyond the span of the flux measurements, which for hot stars is most important at the blue end. For 50% of the EBs this flux fraction is less than 4%, and for only 25% of the EBs is it greater than 25%; for 5% of the EBs, representing the very hottest stars, it is greater than 90%. Given the large span of the flux measurements, in principle one could perform a simple linear interpolation between the measurements and, say, a simple polynomial extrapolation at the ends. The atmosphere model essentially serves as a more intelligent, more physically motivated way of performing the interpolation (and extrapolation, where needed), grounded in basic stellar astrophysics. Hot EBs, for which the extension of the SED model to the blue represents a relatively large contribution of the total F_{bol} , could be of concern. However, as we show in Sec. 3, the efficacy of the procedure appears to be independent of T_{eff} .

Other concerns may be that we have had to assume solar metallicity for some of the EBs. We therefore performed a check by varying the adopted $[\text{Fe}/\text{H}]$ from -0.5 to $+0.3$ —representing the range of metallicity for the vast majority of Milky Way stars—for several EBs in our sample over the full range of T_{eff} . We find that the effect on the resulting F_{bol} is negligible for the hot stars and as much as $\sim 0.5\%$ for the cool stars, in all cases much smaller than the typical F_{bol} uncertainty of 3% (Table 2).

Arguably the most important purpose of the fitting procedure is to determine A_V , for determining what F_{bol} would be in the absence of extinction, thus permitting the distance to be calculated simply via

$$d = (L_{\text{bol}}/4\pi F_{\text{bol}})^{1/2} \quad (1)$$

For 67 of the 156 EBs with good SED fits, A_V estimates can be derived from published reddening values previously reported in the literature via $A_V = 3.1 E(B - V)$. The comparison between our fitted A_V and the literature values is shown in Fig. 1, where the agreement is very good. Indeed, we expect that the A_V values newly determined here should represent an improvement over the original values in many cases. We have adopted a single ratio of total-to-selective extinction, $R_V = 3.1$ in our fits. R_V values in the literature span the range ≈ 2.5 –4 for most Galactic sight lines, and thus in principle fitting for R_V could further improve the SED fits. However, we have opted for simplicity not to introduce a third free parameter to the SED fitting procedure. In any event, if any of the SED fits are poorer due to our choice of R_V , the resulting increased χ^2_ν will in turn result in more conservative uncertainties on F_{bol} .

3. Results

The results of the SED fitting procedure described in Section 2.3 are summarized in Table 2, and the full set of 158 SED fits provided in Figure Set 11 in Appendix A. In this section we discuss several representative SED fits that demonstrate the range of cases, and then present the resulting F_{bol} for our sample of EBs. Next, we present the predicted parallaxes that result from combining F_{bol} together with the L_{bol} values from the literature. Finally, we compare our predicted parallaxes with the subset measured by *Hipparcos*, and we assess the reliability of the uncertainties in our predicted parallaxes.

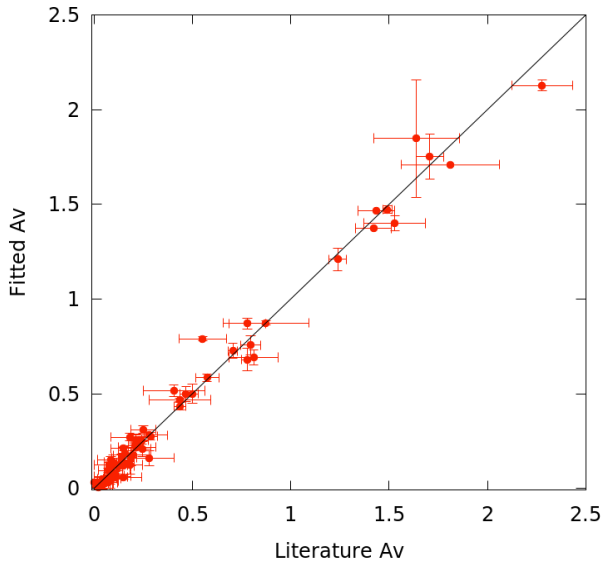


Fig. 1.— Comparison of fitted A_V versus literature A_V for the EBs possessing such literature measurements.

3.1. SED Fits and Bolometric Fluxes

Satisfactory SED fits were achieved for 156 of the 158 EBs in our study sample. For context, these 156 EBs are represented in the T_{eff} -radius plane in Figure 2, color coded according to the χ^2_ν of the SED fit.

Six representative SED fits, covering a range of T_{eff} , radius, and χ^2_ν from Fig. 2, are presented in Fig. 3: YY Gem, BD +36:3317, CW Cep, V380 Cyg, WX Cep, and HD 187669. V380 Cyg, with $\chi^2_\nu = 0.90$, is a good example of the best fits achieved by our procedures. WX Cep, with $\chi^2_\nu = 12.5$, is an example of one of the worst fits that we nonetheless deem acceptable. In this case, the quality of the fit has been affected by the 2MASS data, which appear systematically offset upward relative to the rest of the fit. BD +36:3317 is an example of a case in which the original 2MASS measurements have been corrected for having been observed during eclipse (see Sec. 2), with a very good resulting $\chi^2_\nu = 1.96$.

For comparison, the 2 cases of truly unacceptable SED fits with $\chi^2_\nu > 20$ are shown in Figure 4. Both of these are cases for which we adjusted the 2MASS measurements for having been observed in eclipse, but this did not improve the fits sufficiently. It is possible that alternative photometric measurements from among the many catalogs in which these EBs appear could salvage these cases. However, for the sake of consistency in methodology and in the data sources used, we have opted in this work to simply discard these 2 cases.

Eight of the EBs with otherwise satisfactory SED fits were flagged by *Hipparcos* as possessing sub-arcsecond companions. Such close companions could be contributing flux to the catalog photometric measurements, which typically have spatial resolutions on the order of 1 arcsec. This additional flux in the data would lead to an incorrectly high F_{bol} and thus an erroneously short inferred distance (i.e., erroneously large predicted parallax). In fact, the quality of the SED fits in these cases is in general quite good. For example, CW Cep in Figure 3 is one such EB; its $\chi^2_\nu = 1.22$ gives no indication of problems. Nonetheless, to be conservative we have opted in the analysis that follows to disregard these eight cases.

A key empirical product of this work is the F_{bol} for each EB that results from direct summation of the SED. These F_{bol} values are tabulated in Table 2, and the distribution of their uncertainties presented

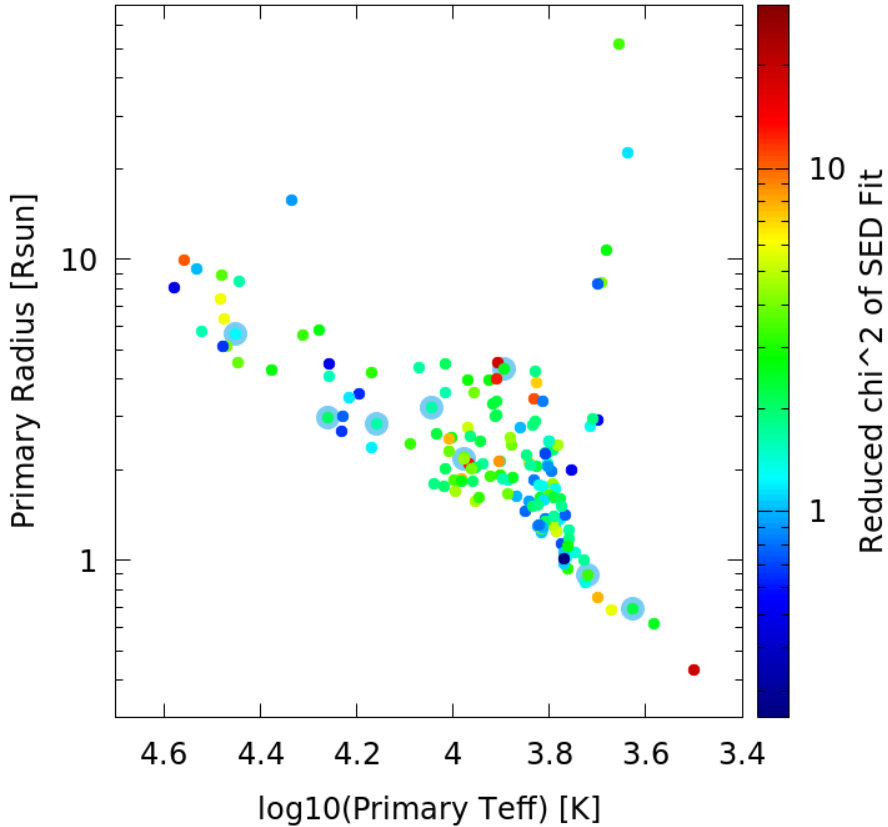


Fig. 2.— T_{eff} -radius diagram of the primary stars in the 156 EBs with satisfactory SED fits, color coded by the χ^2_{ν} of the fit. Points highlighted with blue halos represent EBs with otherwise satisfactory SED fits that are flagged by *Hipparcos* as having sub-arcsecond companions that could compromise the F_{bol} .

in Figure 5. The best cases have uncertainties of $\lesssim 1.5\%$. The median uncertainty for the full EB sample is 3.0%, and is better than 5% for 90% of the sample. This means that the uncertainty in the predicted parallaxes for the EBs will in almost all cases be dominated by the uncertainty in the EB L_{bol} , which is typically $\lesssim 10\%$.

3.2. Predicted Parallaxes

With F_{bol} and L_{bol} and in hand for each EB, we can calculate the predicted distance to each EB according to Equation 1. The uncertainty in F_{bol} comes directly from our SED fitting procedure (Section 2.3). The uncertainty in L_{bol} is less straightforward, as it requires propagation of uncertainties in the stellar radii and T_{eff} , which themselves require a proper handling of correlated uncertainties in the measured quantities from the original EB analyses. Our procedure for determining the uncertainties in L_{bol} is explained in Appendix B.

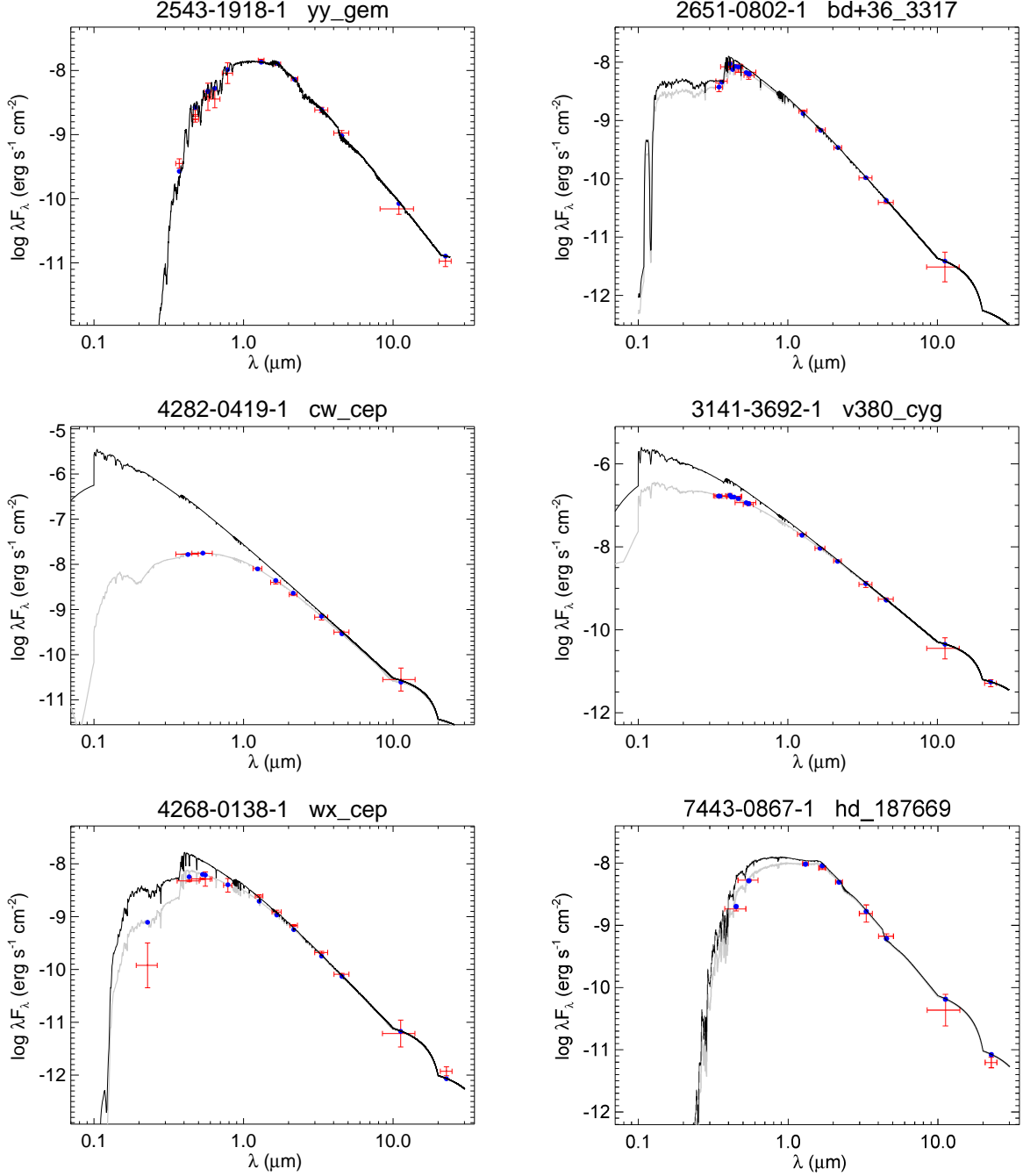


Fig. 3.— Representative SED fits for six EBs spanning a range of primary T_{eff} , primary radius, and χ^2_{ν} from Figure 2: YY Gem ($T_{\text{eff}} = 3820$ K, $R = 0.62 R_{\odot}$, $\chi^2_{\nu} = 2.49$), BD +36:3317 ($T_{\text{eff}} = 10450$ K, $R = 1.76 R_{\odot}$, $\chi^2_{\nu} = 1.96$), CW Cep ($T_{\text{eff}} = 28300$ K, $R = 5.64 R_{\odot}$, $\chi^2_{\nu} = 1.22$), V380 Cyg ($T_{\text{eff}} = 21700$ K, $R = 15.71 R_{\odot}$, $\chi^2_{\nu} = 0.90$), WX Cep ($T_{\text{eff}} = 8150$ K, $R = 4.00 R_{\odot}$, $\chi^2_{\nu} = 12.47$), and HD 187669 ($T_{\text{eff}} = 4330$ K, $R = 22.62 R_{\odot}$, $\chi^2_{\nu} = 1.13$). Note that CW Cep is flagged by *Hipparcos* as possessing a sub-arcsecond companion and thus is excluded from our analyses (see the text). The discontinuity in the model SED at $0.1 \mu\text{m}$ among the hot stars is due to the blackbody addition to the model for $\lambda < 0.1 \mu\text{m}$ for stars with $T_{\text{eff}} > 15,000$ K (see Section 2.3). All labels, symbols, lines, and colors are as in Figure Set 11 in Appendix A.

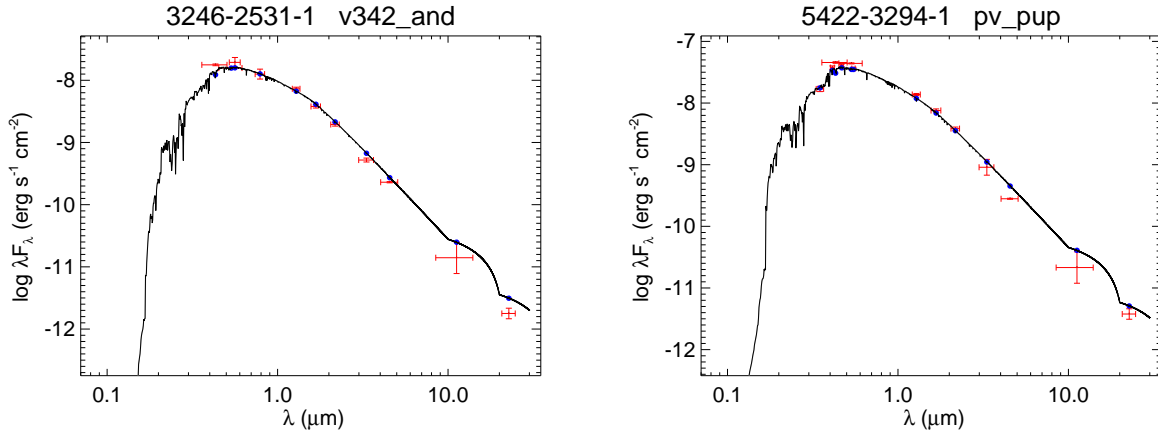


Fig. 4.— As in Figure 3, but for the 2 EBs whose SED fits have unacceptably large χ^2 : V342 And ($T_{\text{eff}} = 6200$ K, $R = 1.25 R_{\odot}$, $\chi_{\nu}^2 = 24.2$) and PV Pup ($T_{\text{eff}} = 6920$ K, $R = 1.54 R_{\odot}$, $\chi_{\nu}^2 = 85.1$). We do not consider these EBs in the rest of our analyses.

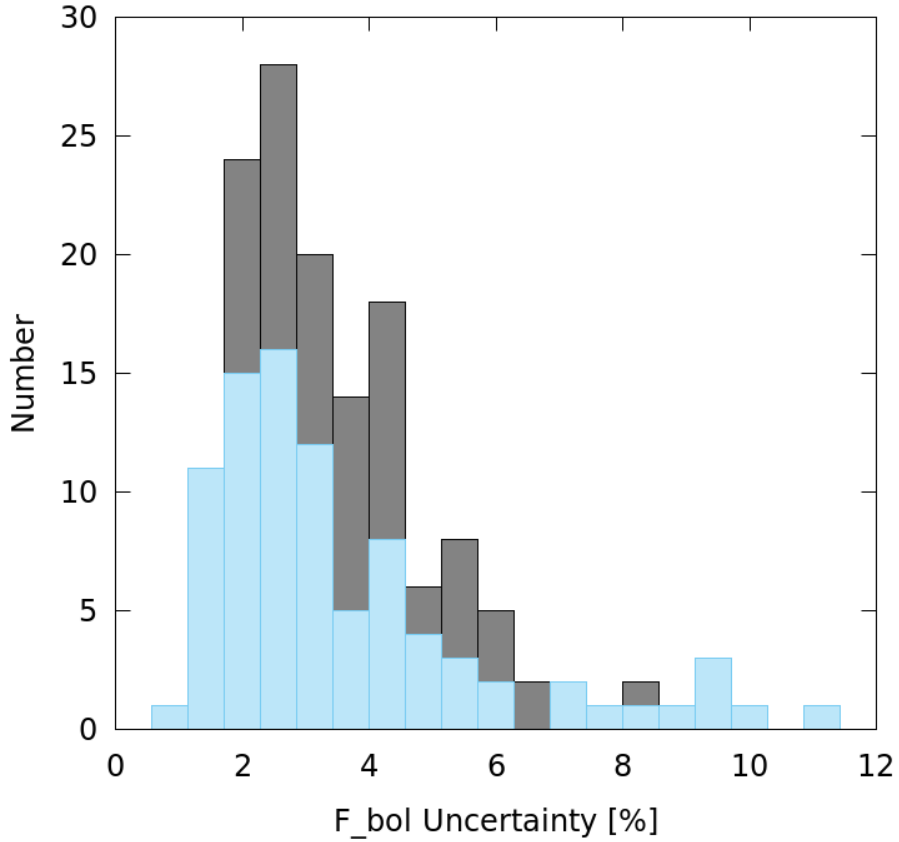


Fig. 5.— Distribution of F_{bol} uncertainties for the full EB sample (grey) and for the subset with *Hipparcos* parallaxes (blue). The typical uncertainty is 3%.

The predicted distances so computed, and the parallaxes derived from them, are tabulated in Table 2. The distribution of their uncertainties is presented in Figure 6. We note that, as explained by Bailer-Jones (2015) and others, estimating a distance from a parallax, or in our case a parallax from a distance, is not trivial when the relative errors are larger than about 20%, and becomes sensitive to prior assumptions. The EBs in our sample all have relative errors well below 20%, so a straightforward conversion to parallaxes is sufficient for our purposes.

The implied precision of the predicted EB parallaxes is remarkably good: The uncertainty is $\sim 30 \mu\text{as}$ in the best cases, and the median for the entire sample is $190 \mu\text{as}$. The precision is better than $\sim 500 \mu\text{as}$ for 90% of the sample.

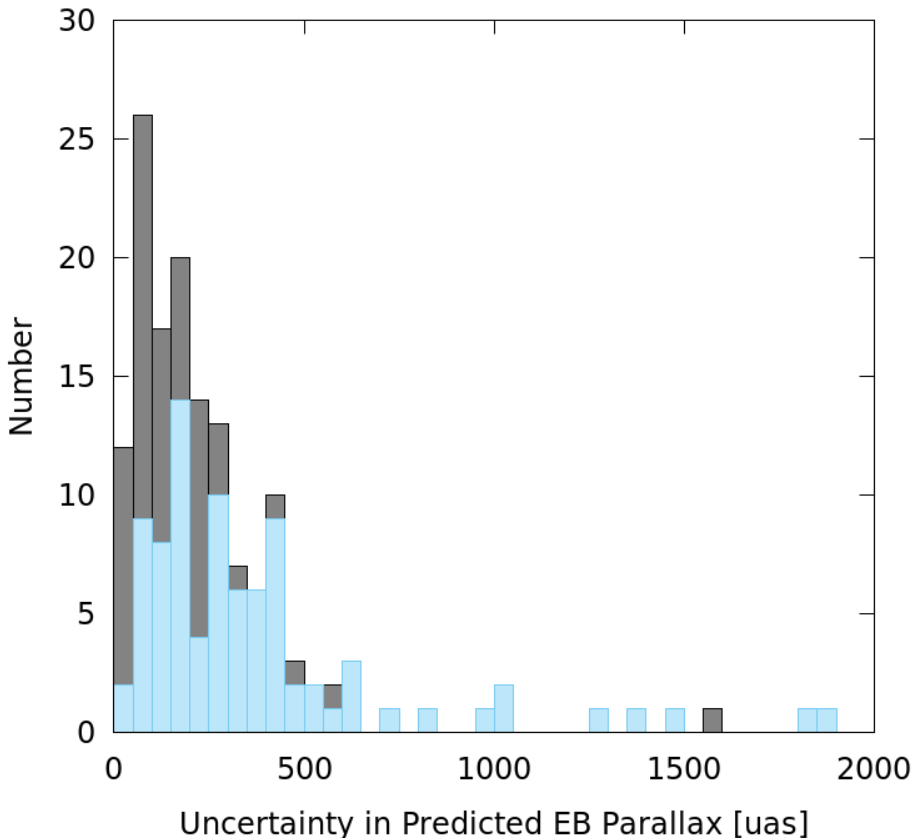


Fig. 6.— Distribution of uncertainties in the predicted parallaxes (in units of micro-arcseconds) for the full EB sample (grey) and for the subset with *Hipparcos* parallaxes (blue). Two EBs with parallax uncertainties larger than $2000 \mu\text{as}$ are off the plot. The typical uncertainty is $200 \mu\text{as}$.

3.3. Comparison to *Hipparcos*

As just mentioned the precision of the predicted EB parallaxes is typically 4 to 5 times better than the formal uncertainties in the *Hipparcos* trigonometric parallaxes (van Leeuwen 2007). Although the latter are therefore poorer than the EB parallaxes on an individual basis, collectively they do allow for a check on the

accuracy of our results, by comparing values for the 86 EBs that were observed by the satellite and that have acceptable SED fits.

Figure 7 presents the direct comparison of our predicted EB parallaxes against the trigonometric parallaxes reported by Perryman et al. (1997) in the original reduction (hereafter referred to as “old Hipparcos”) and as reported in the “new Hipparcos” reduction of van Leeuwen (2007). In both cases the overall agreement is excellent. The EB parallaxes appear to slightly better follow the new *Hipparcos* parallaxes for the most distant EBs (i.e., the smallest parallaxes) for which the old *Hipparcos* parallaxes appear systematically smaller than the EB parallaxes. However, this small trend is well within the errors. Indeed, the old *Hipparcos* parallaxes on the whole exhibit fewer large residuals relative to the EB parallaxes, and much of this difference occurs among the smallest parallaxes for which the new *Hipparcos* reported uncertainties are much smaller than in the old *Hipparcos* reduction.

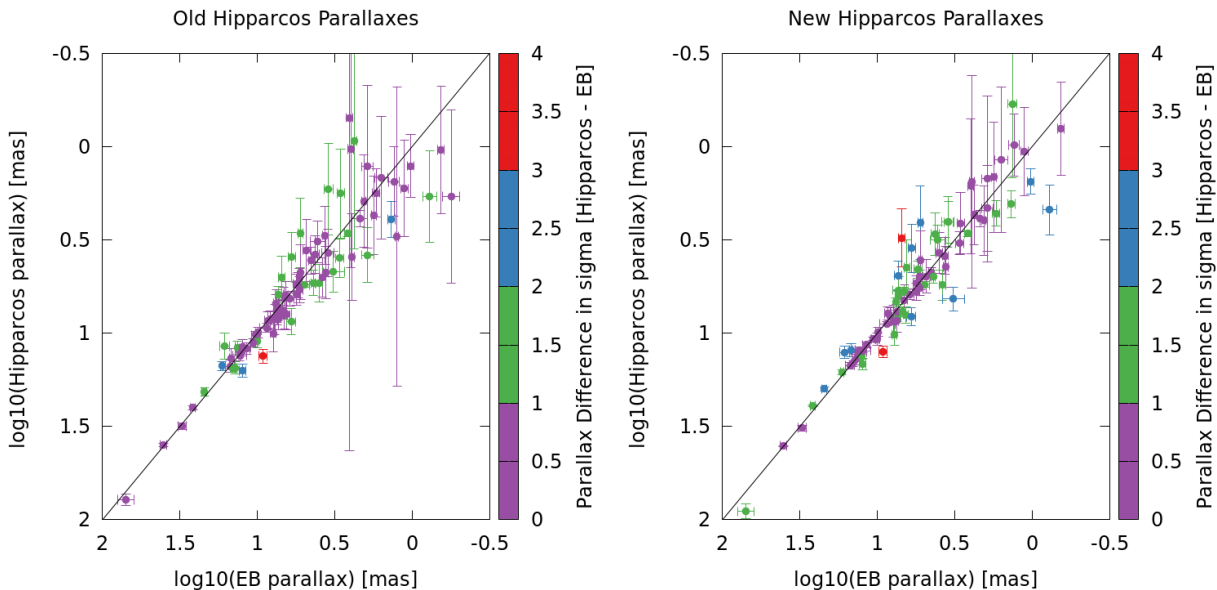


Fig. 7.— Comparison of predicted EB parallaxes versus their trigonometric parallaxes measured by *Hipparcos* according to the old (left) and new (right) *Hipparcos* reductions. The color bar represents the difference of the *Hipparcos* parallax relative to our predicted EB parallax in units of the parallax uncertainties, σ_π .

We show this directly in Figure 8, where we observe that while the overall distribution of parallax residuals is similar for both the old and new *Hipparcos* parallaxes, there are more outliers larger than 2σ with the new *Hipparcos* parallaxes (12 in the new, 4 in the old). In addition, for the nearest EB in our sample (CU Cnc), the old *Hipparcos* parallax agrees with the EB parallax within 1σ , whereas the difference is nearly 2σ for the new *Hipparcos* parallax. These outliers are identified by name in Figure 8 so that the SED fits may be readily compared (Fig. 11).

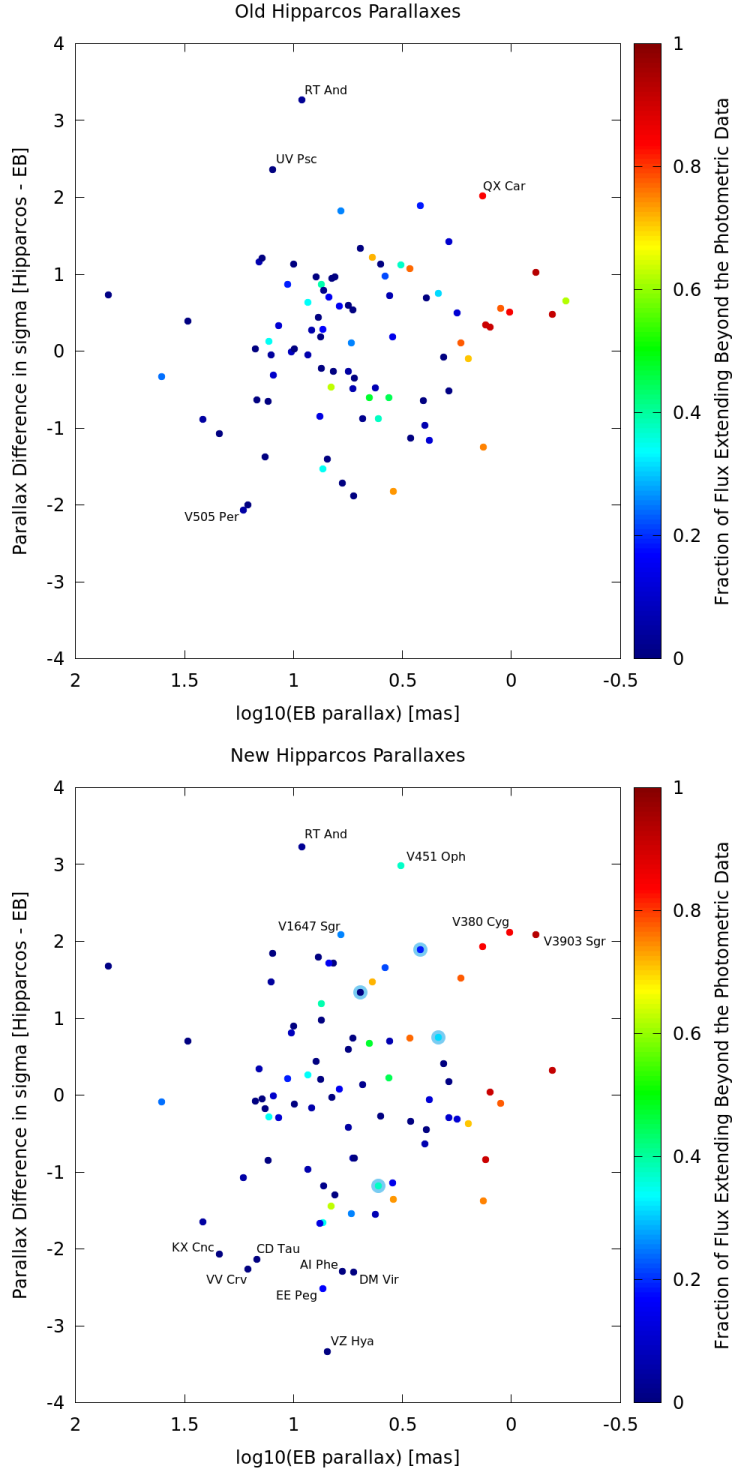


Fig. 8.— Differences between predicted EB parallaxes and their trigonometric parallaxes measured by *Hipparcos*, in units of the parallax uncertainties, according the old (top) and new (bottom) *Hipparcos* reductions. The color bar represents the fraction of each EB’s F_{bol} that is from the portion of the SED fit beyond the span of the photometric measurements (see Section 2.4). Points highlighted with blue halos in the bottom panel are EBs that are members of clusters with average parallaxes reported in the new *Hipparcos* reduction (see Section 2). Specific EBs that disagree by more than 2σ are identified; their SED fits may be inspected in Figure 11.

We have checked for any indications of potential problems that might be common to the outliers. We checked the EBs that were reported in the original EB publications to possess tertiary companions (although any “third light” in these cases should already be accounted for in the EB solutions from which the radii and T_{eff} were derived); we checked the EBs containing metallic A (Am) stars whose metallicities are less well determined and/or anomalous (although metallicity in general has a negligible effect on the derived F_{bol} , see Section 2.4); we checked the EBs flagged by *Hipparcos* as “Variability-Induced Movers” (although this should have been accounted for in the *Hipparcos* reduction); we checked the EBs with the largest A_V values (although our SED-derived A_V values agree very well with the published values, see Fig. 1); finally, we checked the EBs with large amounts of flux in the SED fits that are beyond the span of the photometric measurements (this is represented in Fig. 8). The outliers have none of these factors in common.

It is notable that the predicted EB parallaxes compare so favorably even when the F_{bol} determination involves a large contribution from beyond the span of the photometric measurements, considering that this contribution to F_{bol} is as large as $\sim 90\%$ in the most extreme cases. Though this may seem surprising, it is simply a consequence of the fact that the SED fit is very stringently constrained by the stellar properties—which are in turn very accurately determined from the published EB solutions—and of the fact that the available photometry spans a sufficiently large range of wavelengths to stringently constrain A_V , the only remaining free parameter. It is an extrapolation only in the sense that the model extends beyond the data, not in the sense that there is no knowledge of the nature of the SED beyond the data.

It is also notable that the predicted EB parallaxes retain their high precision regardless of distance. This is a consequence of the fact that the accuracy of the stellar properties arising from the EB solutions does not depend on the EB distance, as long as the light curves and radial velocities used in the EB analysis are of sufficient quality. Indeed, even the EB-based distance to the Large Magellanic Cloud at ~ 50 kpc has a demonstrated precision of $\sim 2\%$ (Pietrzyński et al. 2013).

3.4. Reliability of the EB Parallax Uncertainties

The comparison of the predicted EB parallaxes to the available *Hipparcos* parallaxes suggests that our estimated EB parallax precisions are reliable. With only a few exceptions, the residuals relative to the *Hipparcos* parallaxes are distributed as expected, especially when compared to the old *Hipparcos* parallaxes. The two large outliers seen in Figure 8 (top) may represent nothing more than the few $> 2\sigma$ deviations expected from a normal sample of ~ 100 .

The larger number of $> 2\sigma$ outliers relative to the new *Hipparcos* parallaxes (Figure 8, bottom), however, suggests that our EB parallax uncertainties may be underestimated in some cases. Another way of checking our EB parallaxes and uncertainties is to use the distances to those EBs in our sample that reside in star clusters for which accurate distances have been determined. There are four such EBs in our sample, from the new *Hipparcos* parallaxes (we exclude the Pleiades for reasons discussed in Section 1), and these are highlighted in Figure 8 (bottom). In all four cases, the agreement between our predicted EB parallax and the *Hipparcos* cluster parallax is within 2σ . At the same time, the distribution of the four residuals is strictly speaking slightly broader than for a normal distribution: Two of the four EBs agree to within 1σ , whereas a normal distribution would expect three of the four to agree with 1σ .

It is difficult to say more than this on the basis of only four measurements. Certainly, there is not compelling evidence that the uncertainties in our predicted EB parallaxes are not reliable. However, more conservatively, these four measurements could also be interpreted as suggesting that our EB parallax uncer-

tainties are underestimated by $\sim 50\%$. This is depicted in Figure 9, where now the four EBs with cluster parallaxes are more normally distributed, although the large number of systems that deviate by more than 2σ remains large, suggesting that perhaps it is some of the new *Hipparcos* parallax uncertainties that are underestimated. In any event, these comparisons allow us to conclude that the EB parallaxes are very precise, with typical errors in the range of 200–300 μas .

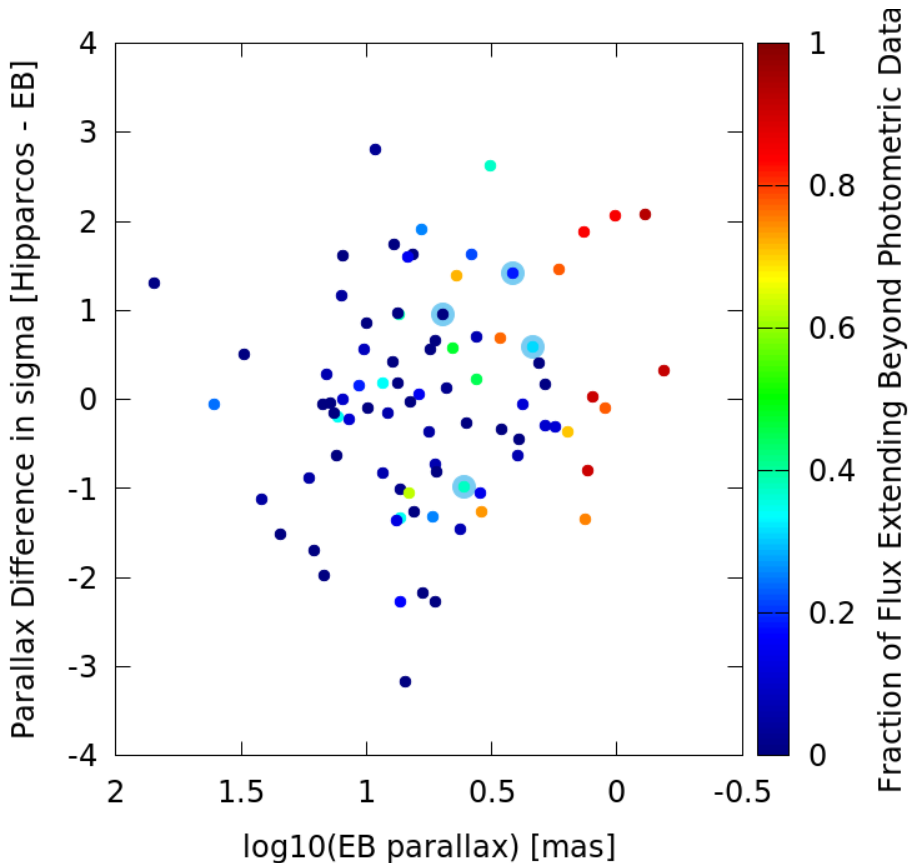


Fig. 9.— Same as Figure 8 (bottom), except with the EB parallax uncertainties increased by 50%.

We can also assess the *accuracy* of the EB parallaxes. We have measured this by computing the mean and median parallax difference compared to *Hipparcos*. For the old *Hipparcos* reduction, we obtain mean and median differences of $-60 \mu\text{as}$ and $+60 \mu\text{as}$ (in the sense of *Hipparcos*–EB), respectively. For the new *Hipparcos* reduction, we obtain mean and median differences of $-40 \mu\text{as}$ and $-55 \mu\text{as}$, respectively. For both the old and new *Hipparcos* reductions, these differences are $\lesssim 1/3$ of our typical random errors. This is important, as it not only confirms that our EB parallaxes are highly accurate as well as very precise, but also that our estimated uncertainties are realistic and reflect any systematics inherent to the method.

4. Discussion: Applicability to *Gaia*

The *Gaia* Mission is poised to revolutionize many areas of astrophysics by mapping the entire sky and delivering high-precision astrometry, photometry, and spectroscopy for up to a billion stars. Most notably,

it will provide trigonometric parallaxes that in some cases will be as precise as a few μas , yielding useful distances to individual objects halfway across the Galaxy. While the final results from the nominal 5-year mission are not expected until after 2020, interim data releases will already provide extremely valuable information beginning with the first (DR1) slated for late 2016.

In addition to accurate positions and mean magnitudes for stars over at least 90% of the sky, and additional information for sources at the ecliptic poles, DR1 will contain parallaxes for up to 2.5 million stars based on the Tycho-Gaia Astrometric Solution (TGAS; Michalik et al. 2015). This full-sky solution takes advantage of the *Tycho-2* astrometry (Høg et al. 2000) gathered 20 years ago during the *Hipparcos* Mission, and combines it with the first six months of *Gaia* data to solve for the positions, proper motions, and parallaxes of the majority of the *Tycho-2* stars. The precision expected for these parallaxes is comparable to or better than that of *Hipparcos* for most stars, with typical nominal errors below a milli-arc second, and somewhat poorer precision up to about 3 mas along the ecliptic. The data set should be almost complete down to $V \approx 11.5$, or about 3 to 4 magnitudes deeper than *Hipparcos*.

Even if it is preliminary, this large collection of parallaxes featuring 20 times more stars than *Hipparcos* will have numerous scientific applications. In particular, it will significantly improve the stellar characterization of targets of exoplanet searches, including transit surveys, many of which observe relatively bright stars that are contained in the *Tycho-2* catalog. This, in turn, should have an immediate impact on the precision and accuracy of the derived planetary properties. NASA’s Transiting Exoplanet Survey Satellite Mission (TESS; Ricker et al. 2015) will benefit enormously as well, as *Gaia* DR1 will supply parallaxes for a large fraction of the bright nearby stars being considered for observation, enabling a better selection of the optimal targets in preparation for launch at the end of 2017.

While the external *accuracy* of the *Gaia* DR1 parallaxes is expected to be very good, and perhaps similar to that of *Hipparcos* according to simulations by (Michalik et al. 2015), independent checks are highly desirable as a means to validate the new astrometric results. The set of predicted EB parallaxes derived in this work, obtained in a completely different way, offers an excellent opportunity for this test given that our typical 200 μas precision is at least as good as, and often better than, that expected of *Gaia* DR1. We note also that our parallax errors do not tend to increase as stars get fainter or more distant. Our faintest system, CoRoT 102918586 ($V = 12.4$), has a predicted parallax with an uncertainty of 30 μas ; our most distant system, V467 Vel, is more than 5 kpc away and has a correspondingly well-determined parallax under 0.2 mas also with an uncertainty of only 20–30 μas . Furthermore, as shown in Figure 10, our stars are distributed over the entire sky, and span more than a 10 magnitude range in brightness ($V = 1.9\text{--}12.4$) potentially allowing the discovery of magnitude-dependent parallax discrepancies, should they be present.

5. Summary and Conclusions

Eclipsing binaries with well-measured physical properties allow the determination of distances that are essentially model-independent, and can be both highly accurate and highly precise. They are therefore ideal as benchmarks for validating other methods of establishing distances, and can often be used out to many kiloparsecs without loss of precision. They have been employed to great advantage even in external galaxies such as the LMC, the SMC, and others.

In this paper we have assembled an all-sky list of 158 EBs contained in the *Tycho-2* catalog with high-quality determinations of the component radii and effective temperatures from the literature, and combined this information with constrained SED fits using existing photometric measurements over a wide range of

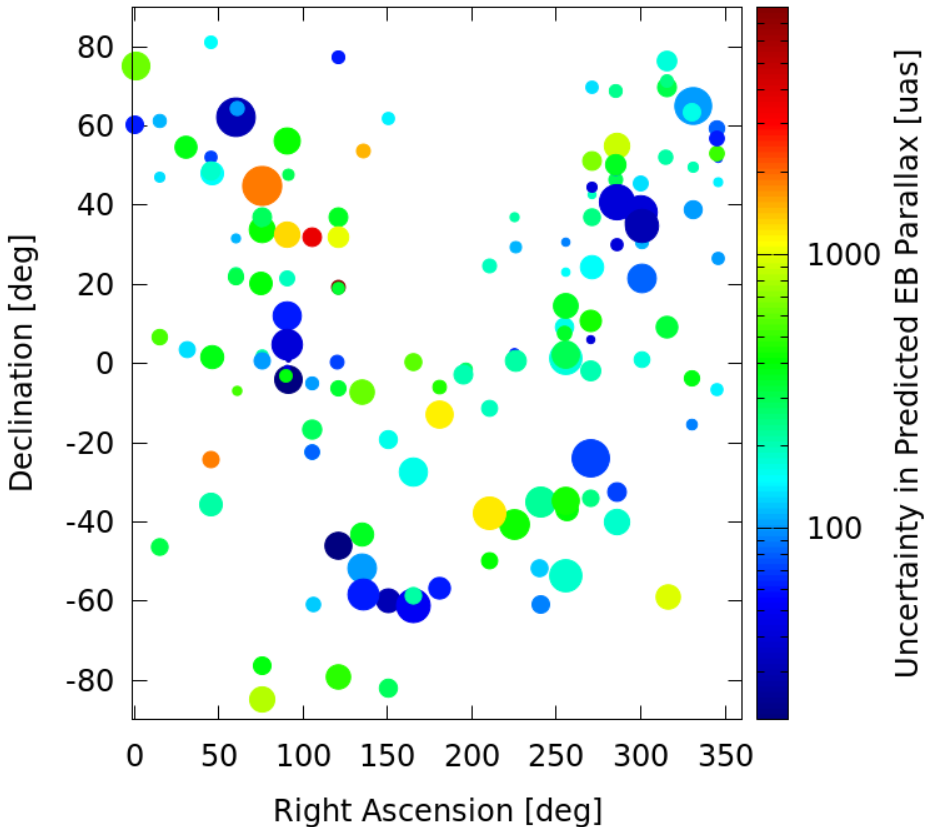


Fig. 10.— Map in equatorial coordinates of the EBs in our sample. Color represents the uncertainty in our predicted parallaxes. Symbol size is proportional to EB brightness, with the largest symbols corresponding to $V \approx 2$ and the smallest corresponding to $V \approx 12$.

wavelengths. The distances calculated from the accurate absolute stellar luminosities and bolometric fluxes lead to predicted parallaxes having typical precisions of $200 \mu\text{as}$ (5% relative errors), which are 4–5 times better than the trigonometric parallaxes from *Hipparcos*. We find excellent overall agreement between our results and those from *Hipparcos*. To the extent that our EB parallaxes represent a test of the *Hipparcos* parallaxes, we find no obvious systematic deviations of the sort that appear to have affected the Pleiades, at least for this particular sample. In any case, the good agreement between our EB parallaxes and the *Hipparcos* parallaxes supports the accuracy of our measurements, and other tests suggest that our precision estimates are also realistic.

The quality of our predicted parallaxes also compares very favorably with that expected for the *Gaia* parallaxes from the Tycho-Gaia Astrometric Solution (Michalik et al. 2015), soon to be delivered as part of the mission’s first Data Release. Our results will therefore serve as an important external check on the spacecraft’s astrometric performance early on in the mission. While subsequent *Gaia* releases will feature steadily increasing parallax precision for larger numbers of stars as the time base lengthens, we anticipate that predicted parallaxes from EBs will continue to provide a valuable reference that is completely independent of astrometry and whose precision does not degrade with increasing distance or diminishing brightness.

K.G.S. acknowledges partial support from NSF PAARE grant AST-1358862. G.T. acknowledges partial support from NSF grant AST-1509375. This work made extensive use of the Filtergraph data visualization system (Burger et al. 2013) at filtergraph.vanderbilt.edu.

REFERENCES

- Albrecht, S., Setiawan, J., Torres, G., Fabrycky, D. C., & Winn, J. N. 2013, *ApJ*, 767, 32
- Bailer-Jones, C. A. L. 2015, *PASP*, 127, 994
- Bakış, V., Bakış, H., Demircan, O., & Eker, Z. 2008, *MNRAS*, 384, 1657
- Bruntt, H., Southworth, J., Torres, G., et al. 2006, *A&A*, 456, 651
- Burger, D., Stassun, K. G., Pepper, J., et al. 2013, *Astronomy and Computing*, 2, 40
- Çakırlı, Ö., Ibanoglu, C., Southworth, J., Frasca, A., & Hernandez, J. 2008, *MNRAS*, 389, 205
- Çakırlı, Ö., Dervişoğlu, A., Sipahi, E., Ibanoglu, C. 2012, *New A*, 17, 215
- Cardelli, J. A., Clayton, G. C., & Mathis, J. S. 1989, *ApJ*, 345, 245
- Clausen, J. V., Olsen, E. H., Helt, B. E., & Claret, A. 2010a, *A&A*, 510, A91
- Clausen, J. V., Frandsen, S., Bruntt, H., et al. 2010b, *A&A*, 516, A42
- da Silva, R., Maceroni, C., Gandolfi, D., Lehmann, H., & Hatzes, A. P. 2014, *A&A*, 565, A55
- David, T. J., Conroy, K. E., Hillenbrand, L. A., et al. 2016, *AJ*, 151, 112
- Debosscher, J., Aerts, C., Tkachenko, A., et al. 2013, *A&A*, 556, A56
- Dimitrov, W., Kamiński, K., Lehmann, H., et al. 2015, *A&A*, 575, A101
- Erdem, A., Sürgit, D., Engelbrecht, C. A., & Van Heerden, H. P. 2015, *PASA*, 32, e028
- Fekel, F. C., Henry, G. W., & Sowell, J. R. 2013, *AJ*, 146, 146
- Frandsen, S., Lehmann, H., Hekker, S., et al. 2013, *A&A*, 556, A138
- Graczyk, D., Pietrzyński, G., Thompson, I. B., et al. 2014, *ApJ*, 780, 59
- Graczyk, D., Maxted, P. F. L., Pietrzyński, G., et al. 2015, *A&A*, 581, A106
- Graczyk, D., Smolec, R., Pavlovski, K., et al. 2016, *A&A*, in press (arXiv:1608.01000)
- Groenewegen, M. A. T., Decin, L., Salaris, M., & De Cat, P. 2007, *A&A*, 463, 579
- Harmanec, P., Božić, H., Mayer, P., et al. 2011, *A&A*, 531, A49
- Harmanec, P., Holmgren, D. E., Wolf, M., et al. 2014, *A&A*, 563, A120
- Hauschildt, P. H., Allard, F., & Baron, E. 1999, *ApJ*, 512, 377
- Hełminiak, K. G., Ukita, N., Kambe, E., & Konacki, M. 2015a, *ApJ*, 813, L25

- Helminiak, K. G., & Konacki, M. 2011, *A&A*, 526, A29
- Helminiak, K. G., Brahm, R., Ratajczak, M., et al. 2014, *A&A*, 567, A64
- Helminiak, K. G., Graczyk, D., Konacki, M., et al. 2015b, *MNRAS*, 448, 1945
- Høg, E., Fabricius, C., Makarov, V. V., et al. 2000, *A&A*, 355, L27
- Hubrig, S., González, J. F., Ilyin, I., et al. 2012, *A&A*, 547, A90
- Ibanoğlu, C., Evren, S., Taş, G., et al. 2008, *MNRAS*, 384, 331
- Kıran, E., Harmanec, P., Değirmenci, Ö. L., et al. 2016, *A&A*, 587, A127
- Koo, J.-R., Lee, J. W., Lee, B.-C., et al. 2014, *AJ*, 147, 104
- Kurucz, R. L. 2013, *Astrophysics Source Code Library*, ascl:1303.024
- Lacy, C. H. S., Torres, G., Wolf, M., & Burks, C. L. 2014a, *AJ*, 147, 1
- Lacy, C. H. S., Torres, G., Fekel, F. C., Muterspaugh, M. W., & Southworth, J. 2015, *AJ*, 149, 34
- Lacy, C. H. S., Torres, G., Fekel, F. C., & Muterspaugh, M. W. 2014b, *AJ*, 147, 148
- Lacy, C. H. S., Torres, G., Fekel, F. C., Sabby, J. A., & Claret, A. 2012, *AJ*, 143, 129
- Lacy, C. H., Gulmen, O., Gudur, N., & Sezer, C. 1989, *AJ*, 97, 822
- Lehmann, H., Borkovits, T., Rappaport, S. A., et al. 2016, *ApJ*, 819, 33
- Maceroni, C., Lehmann, H., da Silva, R., et al. 2014, *A&A*, 563, A59
- Maceroni, C., Montalbán, J., Gandolfi, D., Pavlovski, K., & Rainer, M. 2013, *A&A*, 552, A60
- Mädler, T., Jofré, P., Gilmore, G., et al. 2016, *arXiv:1606.03015*
- Mantegazza, L., Rainer, M., & Antonello, E. 2010, *A&A*, 512, A42
- Matson, R. A., Gies, D. R., Guo, Z., & Orosz, J. A. 2016, *AJ*, 151, 139
- Maxted, P. F. L., Hutcheon, R. J., Torres, G., et al. 2015, *A&A*, 578, A25
- Melis, C., Reid, M. J., Mioduszewski, A. J., Stauffer, J. R., & Bower, G. C. 2014, *Science*, 345, 1029
- Mermilliod, J. C. 2006, *VizieR Online Data Catalog*, 2168,
- Michalik, D., Lindegren, L., & Hobbs, D. 2015, *A&A*, 574, A115
- Michalska, G., Niemczura, E., Pigulski, A., Steślicki, M., & Williams, A. 2013, *MNRAS*, 429, 1354
- Milone, E. F., Kurpińska-Winiarska, M., & Oblak, E. 2010, *AJ*, 140, 129
- Morales, J. C., Torres, G., Marschall, L. A., & Brehm, W. 2009, *ApJ*, 707, 671
- Munari, U., Dallaporta, S., Siviero, A., et al. 2004, *A&A*, 418, L31
- Nordstrom, B., & Johansen, K. T. 1994, *A&A*, 282, 787

- North, P., Studer, M., & Kunzli, M. 1997, *A&A*, 324, 137
- Paunzen, E. 2015, *A&A*, 580, A23
- Perryman, M. A. C., Lindegren, L., Kovalevsky, J., et al. 1997, *A&A*, 323,
- Pietrzyński, G., Graczyk, D., Gieren, W., et al. 2013, *Nature*, 495, 76
- Pietrzyński, G., Thompson, I. B., Graczyk, D., et al. 2009, *ApJ*, 697, 862
- Pinsonneault, M. H., Stauffer, J., Soderblom, D. R., King, J. R., & Hanson, R. B. 1998, *ApJ*, 504, 170
- Press, W. H., Teukolsky, S. A., Vetterling, W. T., & Flannery, B. P. 1992, Cambridge: University Press, —c1992, 2nd ed.,
- Ratajczak, M., Kwiatkowski, T., Schwarzenberg-Czerny, A., et al. 2010, *MNRAS*, 402, 2424
- Rawls, M. L., Gaulme, P., McKeever, J., et al. 2016, *ApJ*, 818, 108
- Ribas, I., Jordi, C., Vilardell, F., et al. 2005, *ApJ*, 635, L37
- Ricker, G. R., Winn, J. N., Vanderspek, R., et al. 2015, *Journal of Astronomical Telescopes, Instruments, and Systems*, 1, 014003
- Rozyczka, M., Kaluzny, J., Pych, W., et al. 2011, *MNRAS*, 414, 2479
- Sabby, J. A., Sandberg Lacy, C. H., Ibanoglu, C., & Claret, A. 2011, *AJ*, 141, 195
- Sabby, J. A., & Lacy, C. H. S. 2003, *AJ*, 125, 1448
- Sandberg Lacy, C. H., Fekel, F. C., & Claret, A. 2012a, *AJ*, 144, 63
- Sandberg Lacy, C. H., Torres, G., & Claret, A. 2012b, *AJ*, 144, 167
- Sandberg Lacy, C. H., Fekel, F. C., Pavlovski, K., Torres, G., & Muterspaugh, M. W. 2016, *AJ*, 152, 2
- Sandberg Lacy, C. H., & Fekel, F. C. 2014, *AJ*, 148, 71
- Sandberg Lacy, C. H., & Fekel, F. C. 2011, *AJ*, 142, 185
- Sandberg Lacy, C. H., Torres, G., Claret, A., et al. 2010, *AJ*, 139, 2347
- Schlegel, D. J., Finkbeiner, D. P., & Davis, M. 1998, *ApJ*, 500, 525
- Soderblom, D. R., Nelan, E., Benedict, G. F., et al. 2005, *AJ*, 129, 1616
- Soderblom, D. R., King, J. R., Hanson, R. B., et al. 1998, *ApJ*, 504, 192
- Southworth, J., Pavlovski, K., Tamajo, E., et al. 2011, *MNRAS*, 414, 3740
- Southworth, J. 2013, *A&A*, 557, A119
- Southworth, J., & Clausen, J. V. 2006, *Ap&SS*, 304, 199
- Southworth, J. 2015, *Living Together: Planets, Host Stars and Binaries*, 496, 164
- Sowell, J. R., Henry, G. W., & Fekel, F. C. 2012, *AJ*, 143, 5

- Stassun, K. G., Feiden, G. A., & Torres, G. 2014, *New A Rev.*, 60, 1
- Suchomska, K., Graczyk, D., Smolec, R., et al. 2015, *MNRAS*, 451, 651
- Tamajo, E., Munari, U., Siviero, A., Tomasella, L., & Dallaporta, S. 2012, *A&A*, 539, A139
- Tkachenko, A., Degroote, P., Aerts, C., et al. 2014, *MNRAS*, 438, 3093
- Tomkin, J. 2005, *The Observatory*, 125, 232
- Tomkin, J., & Fekel, F. C. 2006, *AJ*, 131, 2652
- Torres, G., Andersen, J., & Giménez, A. 2010, *A&A Rev.*, 18, 67
- Torres, G., Vaz, L. P. R., Sandberg Lacy, C. H., & Claret, A. 2014a, *AJ*, 147, 36
- Torres, G., Sandberg Lacy, C. H., & Claret, A. 2009a, *AJ*, 138, 1622
- Torres, G., & Lacy, C. H. S. 2009b, *AJ*, 137, 507
- Torres, G., Sandberg Lacy, C. H., Pavlovski, K., et al. 2014b, *ApJ*, 797, 31
- Torres, G., Sandberg Lacy, C. H., Pavlovski, K., Fekel, F. C., & Muterspaugh, M. W. 2015, *AJ*, 150, 154
- Torres, G., Clausen, J. V., Bruntt, H., et al. 2012, *A&A*, 537, A117
- Torres, G., Lacy, C. H. S., Claret, A., & Sabby, J. A. 2000, *AJ*, 120, 3226
- Trudel, J.-L., Fernie, J. D., & Mochnecki, S. 1993, *AJ*, 105, 2291
- van Leeuwen, F. 2009, *A&A*, 497, 209
- van Leeuwen, F. 2007, *A&A*, 474, 653
- Veramendi, M. E., & González, J. F. 2015, *New A*, 34, 266
- Vos, J., Clausen, J. V., Jørgensen, U. G., et al. 2012, *A&A*, 540, A64
- Williams, S. J., Gies, D. R., Helsel, J. W., Matson, R. A., & Caballero-Nieves, S. 2011, *AJ*, 142, 5
- Wilson, R. E., Van Hammme, W., & Terrell, D. 2010, *ApJ*, 723, 1469
- Zhang, X. B., Deng, L., & Lu, P. 2009, *AJ*, 138, 680
- Zwahlen, N., North, P., Debernardi, Y., et al. 2004, *A&A*, 425, L45

Table 1. Stellar properties of our sample of EBs

System	<i>Tycho</i> ID	<i>Hipparcos</i> ID	R_1 (R_\odot)	R_2 (R_\odot)	Primary T_{eff} (K)	Secondary T_{eff} (K)	$E(B - V)$ (mag)	[Fe/H]	Source
UV Psc	0026-0577-1	5980	1.110 ± 0.023	0.835 ± 0.018	5780 ± 100	4750 ± 80	1
XY Cet	0051-0832-1	13937	1.873 ± 0.035	1.773 ± 0.029	7870 ± 115	7620 ± 125	0.04 ± 0.02	Am / Am	2
V1130 Tau	0066-1108-1	17988	1.782 ± 0.011	1.489 ± 0.010	6625 ± 70	6650 ± 70	0.000 ± 0.011	-0.25 ± 0.10	3
EW Ori	0104-1206-1	...	1.133 ± 0.011	1.083 ± 0.011	5970 ± 100	5780 ± 100	0.014 ± 0.012	...	1
V578 Mon	0154-2528-1	...	5.149 ± 0.091	4.21 ± 0.10	30000 ± 740	26400 ± 600	0.455 ± 0.029	-0.30 ± 0.13	1
AI Hya	0196-0626-1	...	3.916 ± 0.031	2.767 ± 0.019	6700 ± 60	7100 ± 65	0	Am / -	1
FM Leo	0263-0727-1	54766	1.648 ± 0.043	1.511 ± 0.049	6316 ± 240	6190 ± 211	0.043	...	4
AQ Ser	0340-0588-1	...	2.281 ± 0.014	2.451 ± 0.027	6430 ± 100	6340 ± 100	0.029 ± 0.010	-0.19 ± 0.15	5
V335 Ser	0353-0301-1	...	2.03 ± 0.03	1.73 ± 0.04	9020 ± 150	8510 ± 150	0.068 ± 0.007	...	6
U Oph	0400-1862-1	84500	3.484 ± 0.021	3.110 ± 0.034	16440 ± 250	15590 ± 250	0.226 ± 0.007	...	1
V2368 Oph	0404-2156-1	84479	3.99 ± 0.03	3.87 ± 0.02	9300 ± 200	9500 ± 200	0.20	...	7
V413 Ser	0446-0091-1	91113	3.21 ± 0.05	2.93 ± 0.05	11100 ± 300	10350 ± 280	0.79	...	8
CoRoT 105906206	0459-0892-1	...	4.24 ± 0.02	1.34 ± 0.01	6750 ± 150	6152 ± 162	...	0.0 ± 0.1	9
IO Aqr	0511-0960-1	102041	2.493 ± 0.017	2.191 ± 0.015	6336 ± 125	6475 ± 138	0.027 ± 0.020	...	10
V1388 Ori	0738-0244-1	29321	5.60 ± 0.08	3.76 ± 0.06	20500 ± 500	18500 ± 500	0.15 ± 0.01	...	1
WZ Oph	0977-0216-1	83719	1.402 ± 0.012	1.419 ± 0.012	6165 ± 100	6115 ± 100	0.045 ± 0.016	-0.27 ± 0.07	1
V2365 Oph	0977-0547-1	83891	2.190 ± 0.009	0.934 ± 0.001	9500 ± 200	6400 ± 210	0.25 ± 0.01	...	11
V624 Her	1005-2131-1	86809	3.031 ± 0.051	2.210 ± 0.034	8150 ± 150	7950 ± 150	0.05 ± 0.01	Am / Am	1
V451 Oph	1027-1355-1	90599	2.642 ± 0.031	2.029 ± 0.028	10800 ± 800	9800 ± 500	0.158	...	1
EE Peg	1120-0161-1	106981	2.090 ± 0.025	1.312 ± 0.013	8700 ± 200	6450 ± 300	0	Am / -	1
CF Tau	1262-0050-1	...	2.797 ± 0.011	2.048 ± 0.016	5200 ± 150	6000 ± 150	0.28 ± 0.07	...	12
V1094 Tau	1263-0642-1	...	1.4109 ± 0.0058	1.1063 ± 0.0066	5850 ± 100	5700 ± 100	0.026 ± 0.009	-0.09 ± 0.11	13
CD Tau	1291-0292-1	24663	1.798 ± 0.015	1.584 ± 0.018	6200 ± 50	6200 ± 50	0	+0.08 ± 0.15	1
FT Ori	1326-0910-1	...	1.860 ± 0.013	1.616 ± 0.013	9600 ± 400	8600 ± 300	0.09 ± 0.04	...	14
CU Cnc	1387-0884-1	41824	0.4323 ± 0.0055	0.3916 ± 0.0094	3160 ± 150	3125 ± 150	0	...	1
TX Cnc ^a	1395-0907-1	...	1.27 ± 0.04	0.89 ± 0.03	6537 ± 200	6250 ± 200	15
HD 194495	1644-1635-1	100719	5.82 ± 0.03	3.14 ± 0.08	19000 ± 550	17800 ± 600	0.08 ± 0.02	...	16
BP Vul	1644-2113-1	100745	1.852 ± 0.014	1.489 ± 0.013	7715 ± 150	6810 ± 150	0.030 ± 0.014	Am / Am	1
AD Boo	2015-0216-1	...	1.613 ± 0.014	1.2165 ± 0.0097	6575 ± 120	6145 ± 120	0.027 ± 0.021	+0.10 ± 0.15	1
RT CrB	2039-1337-1	76551	2.946 ± 0.051	2.615 ± 0.044	5134 ± 100	5781 ± 100	0.011 ± 0.001	...	17
LV Her	2076-1042-1	...	1.358 ± 0.012	1.313 ± 0.011	6060 ± 150	6030 ± 150	0.03 ± 0.03	+0.08 ± 0.21	18
DI Her	2109-0775-1	92708	2.681 ± 0.046	2.478 ± 0.046	17000 ± 800	15100 ± 700	0.18	...	1
BK Peg	2254-2563-1	...	1.988 ± 0.008	1.474 ± 0.017	6265 ± 85	6320 ± 90	0.059 ± 0.020	-0.12 ± 0.07	19
AG Per	2362-0115-1	19201	2.995 ± 0.071	2.605 ± 0.070	18200 ± 800	17400 ± 800	0.19	...	1
NP Per	2371-0390-1	...	1.372 ± 0.013	1.229 ± 0.013	6420 ± 90	4540 ± 160	0.26 ± 0.04	+0.02 ± 0.08	20

Table 1—Continued

System	<i>Tycho</i> ID	<i>Hipparcos</i> ID	R_1 (R_\odot)	R_2 (R_\odot)	Primary T_{eff} (K)	Secondary T_{eff} (K)	$E(B - V)$ (mag)	[Fe/H]	Source
AR Aur	2398-1311-1	24740	1.799 ± 0.013	1.834 ± 0.019	10950 ± 300	10350 ± 300	0	...	21,22
HP Aur	2401-1263-1	...	1.0278 ± 0.0042	0.7758 ± 0.0034	5810 ± 120	5160 ± 120	0.048 ± 0.020	...	23
V432 Aur	2416-0768-1	26434	2.429 ± 0.023	1.2239 ± 0.0072	6080 ± 85	6685 ± 85	0	-0.60 ± 0.05	1
WW Aur	2426-0345-1	31173	1.929 ± 0.011	1.838 ± 0.011	7960 ± 420	7670 ± 410	...	Am / Am	1
GX Gem	2444-0267-1	32427	2.326 ± 0.012	2.236 ± 0.012	6195 ± 100	6165 ± 100	0.092 ± 0.011	...	1
KX Cnc	2484-0592-1	42753	1.064 ± 0.002	1.049 ± 0.002	5900 ± 100	5843 ± 100	...	+0.07 ± 0.10	24
HD 71636	2489-1972-1	41691	1.571 ± 0.026	1.363 ± 0.026	6950 ± 140	6440 ± 140	0.02	...	1
YY Gem	2543-1918-1	...	0.6194 ± 0.0057	0.6194 ± 0.0057	3820 ± 100	3820 ± 100	0	...	1
CV Boo	2570-0843-1	...	1.263 ± 0.023	1.174 ± 0.023	5760 ± 150	5670 ± 150	0	...	1
V501 Her	2606-1905-1	...	2.0016 ± 0.0031	1.5112 ± 0.0027	5683 ± 100	5720 ± 100	0.048 ± 0.018	...	25
BD+36 3317	2651-0802-1	...	1.76 ± 0.01	1.46 ± 0.01	10450 ± 420	7623 ± 328	0.06 ± 0.01	...	26
V885 Cyg	2655-1877-1	...	3.387 ± 0.026	2.346 ± 0.017	8150 ± 150	8375 ± 150	0.079 ± 0.014	Am / Am	1
MY Cyg	2680-1529-1	100258	2.242 ± 0.050	2.178 ± 0.050	7050 ± 200	7000 ± 200	0.048 ± 0.03	Am / Am	1
V453 Cyg	2683-3326-1	...	8.445 ± 0.068	5.420 ± 0.068	27800 ± 400	26200 ± 500	0.46 ± 0.03	-0.25 ± 0.05	1
V442 Cyg	2685-1903-1	...	2.073 ± 0.034	1.663 ± 0.033	6900 ± 100	6800 ± 100	0.085	...	1
CG Cyg	2696-2945-1	103505	0.893 ± 0.012	0.838 ± 0.011	5260 ± 180	4720 ± 60	0.11	...	1
Y Cyg	2696-3486-1	102999	5.785 ± 0.091	5.816 ± 0.063	33200 ± 600	33521 ± 600	27
β Aur	2924-2742-1	28360	2.765 ± 0.018	2.571 ± 0.018	9350 ± 200	9200 ± 200	0	Am / Am	1
KIC 7177553	3127-0167-1	...	10.74 ± 0.11	0.941 ± 0.005	5800 ± 130	5740 ± 140	...	-0.05 ± 0.09	28
KIC 8410637	3130-2385-1	...	3.45 ± 0.01	1.571 ± 0.031	4800 ± 80	6490 ± 160	0.14 ± 0.05	+0.08 ± 0.13	29
KIC 3858884	3135-0651-1	96299	1.85 ± 0.02	3.05 ± 0.01	6800 ± 70	6606 ± 70	30
KIC 5738698	3141-1400-1	...	1.85 ± 0.02	1.71 ± 0.02	6792 ± 50	6740 ± 52	...	-0.4 ± 0.1	31
V380 Cyg	3141-3692-1	97634	15.71 ± 0.13	3.819 ± 0.048	21700 ± 400	22700 ± 1200	...	+0.03 ± 0.10	32
V478 Cyg	3151-2222-1	100227	7.426 ± 0.072	7.426 ± 0.072	30479 ± 1000	30549 ± 1000	0.85	...	1
V364 Lac	3215-0971-1	112928	3.309 ± 0.021	2.986 ± 0.020	8250 ± 150	8500 ± 150	0.068 ± 0.010	Am / Am	1
V342 And	3246-2531-1	817	1.25 ± 0.01	1.21 ± 0.01	6200 ± 100	6395 ± 100	...	-0.10 ± 0.12	33
CO And	3268-0398-1	...	1.727 ± 0.021	1.694 ± 0.017	6140 ± 130	6170 ± 130	0.09 ± 0.03	+0.01 ± 0.15	34
V570 Per	3314-1225-1	14673	1.521 ± 0.034	1.386 ± 0.019	6842 ± 50	6562 ± 50	0.023 ± 0.007	+0.02 ± 0.03	1
IM Per	3323-1123-1	...	2.409 ± 0.018	2.366 ± 0.017	7580 ± 150	7570 ± 160	0.49 ± 0.05	...	35
IQ Per	3331-1175-1	18662	2.445 ± 0.024	1.499 ± 0.016	12300 ± 230	7700 ± 140	0.14 ± 0.01	...	1
HS Aur	3394-0326-1	32900	1.004 ± 0.024	0.874 ± 0.024	5350 ± 75	5200 ± 75	0.015 ± 0.010	...	1
FL Lyr	3542-1492-1	94335	1.283 ± 0.028	0.962 ± 0.028	6150 ± 100	5300 ± 100	0.007 ± 0.005	...	1
KIC 11285625	3549-2141-1	...	2.123 ± 0.010	1.472 ± 0.014	6960 ± 100	7195 ± 200	...	-0.58 ± 0.15	36
V2080 Cyg	3551-1744-1	95611	1.596 ± 0.008	1.599 ± 0.008	6000 ± 75	5987 ± 75	...	-0.46	11
HP Dra	3552-0394-1	92835	1.371 ± 0.012	1.052 ± 0.010	6000 ± 150	5895 ± 150	0.025	...	37

Table 1—Continued

System	<i>Tycho</i> ID	<i>Hipparcos</i> ID	R_1 (R_\odot)	R_2 (R_\odot)	Primary T_{eff} (K)	Secondary T_{eff} (K)	$E(B - V)$ (mag)	[Fe/H]	Source
KIC 9246715	3559-0102-1	...	8.37 ± 0.05	8.30 ± 0.04	4930 ± 190	4930 ± 190	...	-0.15 ± 0.08	38,39
V1061 Cyg	3600-0472-1	104263	1.616 ± 0.017	0.967 ± 0.011	6180 ± 100	5300 ± 150	0	...	1
RW Lac	3629-0740-1	...	1.1864 ± 0.0038	0.9638 ± 0.0040	5760 ± 100	5560 ± 150	0.068 ± 0.012	...	1
AP And	3639-0915-1	...	1.2335 ± 0.0062	1.1954 ± 0.0053	6565 ± 150	6495 ± 150	0.058 ± 0.030	...	40
IT Cas	3650-0959-1	...	1.594 ± 0.018	1.562 ± 0.018	6470 ± 100	6470 ± 100	0.062 ± 0.031	...	1
V505 Per	3690-0536-1	10961	1.287 ± 0.024	1.266 ± 0.024	6510 ± 50	6460 ± 50	0.005	-0.12 ± 0.03	1
RR Lyn	3772-2770-1	30651	2.57 ± 0.02	1.59 ± 0.03	7600 ± 100	7000 ± 100	...	Am / -	41
ISWASP J093010.78+533859.5	3807-0759-1	...	0.757 ± 0.008	0.743 ± 0.010	5000 ± 200	4240 ± 200	0.01	...	42
V1143 Cyg	3938-1983-1	96620	1.347 ± 0.023	1.324 ± 0.023	6450 ± 100	6400 ± 100	0	...	1
RT And	3998-2167-1	114484	1.256 ± 0.015	0.906 ± 0.011	6100 ± 150	4880 ± 100	0	...	1
V396 Cas	4006-1219-1	...	2.592 ± 0.014	1.779 ± 0.010	9225 ± 150	8550 ± 120	0.160 ± 0.010	...	1
PV Cas	4010-1411-1	...	2.301 ± 0.020	2.257 ± 0.019	10200 ± 250	10190 ± 250	0.217	...	1
MU Cas	4014-1119-1	1263	4.195 ± 0.058	3.670 ± 0.057	14750 ± 800	15100 ± 800	0.478 ± 0.007	...	1
V459 Cas	4030-1001-1	...	2.014 ± 0.020	1.970 ± 0.020	9140 ± 300	9100 ± 300	0.255 ± 0.016	Am / Am	1
SZ Cam	4068-1651-1	19270	8.91 ± 0.05	6.70 ± 0.12	30320 ± 150	28015 ± 130	0.73 ± 0.05	...	143
WW Cam	4073-1191-1	...	1.912 ± 0.016	1.808 ± 0.016	8350 ± 135	8240 ± 135	0.397 ± 0.014	Am / Am	241
ZZ UMa	4144-0400-1	51411	1.513 ± 0.019	1.1562 ± 0.0096	5960 ± 70	5270 ± 90	0.008 ± 0.004	...	1
WX Cep	4268-0138-1	111166	3.996 ± 0.030	2.712 ± 0.023	8150 ± 250	8900 ± 250	1
AH Cep	4273-0857-1	112562	6.346 ± 0.071	5.836 ± 0.085	29900 ± 1000	28600 ± 1000	0.58 ± 0.08	...	1
CW Cep	4282-0419-1	113907	5.64 ± 0.12	5.14 ± 0.12	28300 ± 1000	27700 ± 1000	0.69	...	1
YZ Cas	4307-2167-1	3572	2.539 ± 0.026	1.350 ± 0.014	10200 ± 300	7200 ± 300	0.07	Am / -	1
BF Dra	4435-1750-1	92489	2.086 ± 0.012	1.922 ± 0.012	6360 ± 150	6400 ± 150	0.026 ± 0.014	-0.03 ± 0.15	44
UZ Dra	4444-1595-1	...	1.31 ± 0.01	1.15 ± 0.02	6200 ± 100	6000 ± 100	45
EK Cep	4466-2120-1	107083	1.5800 ± 0.0065	1.3153 ± 0.0057	9000 ± 200	5700 ± 200	0.01	+0.07 ± 0.05	1
VZ Cep	4470-1334-1	...	1.534 ± 0.012	1.042 ± 0.039	6670 ± 160	5720 ± 120	...	+0.06 ± 0.09	46
EY Cep	4521-0349-1	...	1.463 ± 0.011	1.470 ± 0.011	7090 ± 150	6970 ± 150	0.049 ± 0.012	...	1
AY Cam	4540-1742-1	...	2.772 ± 0.020	2.026 ± 0.017	7250 ± 100	7395 ± 100	0.06	...	1
EI Cep	4599-0082-1	106024	2.897 ± 0.048	2.330 ± 0.044	6750 ± 100	6950 ± 100	0	- / Am	1
ASAS J045304-0700.4	4749-0560-1	...	0.848 ± 0.005	0.833 ± 0.005	5324 ± 200	5105 ± 200	0.13	...	47
GG Ori	4767-0857-1	...	1.854 ± 0.025	1.831 ± 0.025	9950 ± 200	9950 ± 200	0.547 ± 0.022	...	1
V530 Ori	4786-0571-1	...	0.980 ± 0.013	0.5873 ± 0.0067	5890 ± 100	3880 ± 120	0.045 ± 0.020	-0.12 ± 0.08	48
V501 Mon	4799-1943-1	...	1.888 ± 0.029	1.592 ± 0.028	7510 ± 100	7000 ± 90	0.177 ± 0.039	Am / -	49
CoRoT 102918586	4800-1540-1	...	1.64 ± 0.01	1.48 ± 0.01	7400 ± 90	7144 ± 110	...	0.00 ± 0.10	50
HI Mon	4809-0245-1	...	5.13 ± 0.11	4.99 ± 0.07	29500 ± 600	28400 ± 400	0.34	...	51
FS Mon	4825-2374-1	...	2.052 ± 0.012	1.6293 ± 0.0098	6715 ± 100	6550 ± 100	0.023 ± 0.008	...	1

Table 1—Continued

System	<i>Tycho</i> ID	<i>Hipparcos</i> ID	R_1 (R_\odot)	R_2 (R_\odot)	Primary T_{eff} (K)	Secondary T_{eff} (K)	$E(B - V)$ (mag)	[Fe/H]	Source
VZ Hya	4874-0811-1	41834	1.3141 ± 0.0053	1.1129 ± 0.0072	6645 ± 150	6290 ± 150	0.027 ± 0.027	-0.20 ± 0.12	1
KW Hya	4891-1371-1	45184	2.126 ± 0.016	1.480 ± 0.013	8000 ± 200	6900 ± 200	0	Am / -	1
IM Vir	4955-0912-1	...	1.061 ± 0.016	0.681 ± 0.013	5570 ± 100	4250 ± 130	52
HY Vir	4960-0976-1	64120	2.806 ± 0.008	1.519 ± 0.008	6850 ± 125	6550 ± 120	0.026 ± 0.011	Am / -	53
BH Vir	4968-0569-1	68258	1.247 ± 0.024	1.135 ± 0.023	6100 ± 100	5500 ± 200	0.036	...	1
EG Ser	5099-0149-1	...	1.69 ± 0.01	1.55 ± 0.01	9900 ± 200	9100 ± 200	0.142	...	54
LL Aqr	5236-0883-1	111454	1.321 ± 0.006	1.002 ± 0.005	6080 ± 45	5703 ± 50	0.018 ± 0.014	+0.02 ± 0.06	55,72
EF Aqr	5248-1030-1	...	1.338 ± 0.012	0.956 ± 0.012	6150 ± 65	5185 ± 110	0.023 ± 0.015	0.00 ± 0.10	56
V1031 Ori	5351-0761-1	27341	4.323 ± 0.034	2.978 ± 0.064	7850 ± 500	8400 ± 500	0.034	...	1
PV Pup	5422-3294-1	37842	1.543 ± 0.016	1.499 ± 0.016	6920 ± 300	6930 ± 300	0	...	1
VV Crv	5534-1488-1	61910	3.375 ± 0.010	1.650 ± 0.008	6500 ± 200	6638 ± 200	57
DM Vir	5558-1683-1	69029	1.764 ± 0.017	1.764 ± 0.017	6500 ± 100	6500 ± 300	0.023	...	1
GZ CMa	5965-0860-1	35187	2.494 ± 0.031	2.132 ± 0.037	8800 ± 350	8500 ± 350	0.07 ± 0.03	Am / -	1
SW CMa	5976-0630-1	34431	3.014 ± 0.020	2.495 ± 0.042	8200 ± 150	8100 ± 150	0.031 ± 0.014	Am / Am	58
HW CMa	5976-1266-1	...	1.662 ± 0.021	1.643 ± 0.018	7700 ± 150	7560 ± 150	58
ASAS J082552-1622.8	5998-1918-1	41322	0.694 ± 0.008	0.699 ± 0.013	4230 ± 200	4080 ± 200	47
VV Pys	6010-5044-1	41475	2.168 ± 0.020	2.168 ± 0.020	9500 ± 200	9500 ± 200	0.022	...	1
HS Hya	6069-1131-1	50966	1.2753 ± 0.0073	1.2169 ± 0.0073	6500 ± 50	6400 ± 50	0	...	1
BW Aqr	6378-0804-1	110514	2.062 ± 0.044	1.786 ± 0.043	6350 ± 100	6450 ± 100	0.04	-0.07 ± 0.11	1
AK For	6446-0342-1	16247	0.687 ± 0.020	0.609 ± 0.016	4690 ± 100	4390 ± 150	0	-0.2 ± 0.1	59
χ^2 Hya	6644-1330-1	54255	4.390 ± 0.039	2.159 ± 0.030	11750 ± 190	11100 ± 230	0.016	...	1
ASAS J180057-2333.8	6842-1399-1	...	52.12 ± 1.38	67.63 ± 1.40	4535 ± 80	4211 ± 80	0.525 ± .07	-0.20 ± 0.1	60
V3903 Sgr	6843-0543-1	88943	8.088 ± 0.086	6.125 ± 0.060	38000 ± 1900	34100 ± 1700	0.44	...	1
TZ For	7026-0633-1	15092	8.32 ± 0.12	3.965 ± 0.088	5000 ± 100	6350 ± 100	0.034	+0.10 ± 0.15	1
V760 Sco	7352-1162-1	80405	3.015 ± 0.066	2.641 ± 0.066	16900 ± 500	16300 ± 500	0.33	...	1
V906 Sco	7386-0562-1	87616	4.521 ± 0.035	3.515 ± 0.039	10400 ± 500	10700 ± 500	0.078 ± 0.010	+0.14 ± 0.06	1
V1647 Sgr	7390-1395-1	88069	1.832 ± 0.018	1.667 ± 0.017	9600 ± 300	9100 ± 300	0.04	...	1
V4403 Sgr	7415-4484-1	91718	2.50 ± 0.03	1.74 ± 0.02	6316 ± 151	6517 ± 150	61
HD 187669	7443-0867-1	...	22.62 ± 0.50	11.33 ± 0.28	4330 ± 70	4650 ± 80	0.13 ± 0.05	-0.25 ± 0.10	62
PT Vel	7690-2859-1	45079	2.094 ± 0.020	1.559 ± 0.020	9250 ± 150	7650 ± 200	0.005	...	63
ψ Cen	7805-2696-1	70090	3.621 ± 0.007	1.804 ± 0.004	10400 ± 500	8800 ± 300	64,65
GG Lup	7826-3079-1	74950	2.380 ± 0.025	1.726 ± 0.019	14750 ± 450	11000 ± 600	0.027	...	1
V4089 Sgr	7936-2270-1	96234	3.959 ± 0.013	1.605 ± 0.016	8433 ± 97	7361 ± 105	66
AI Phe	8032-0625-1	5438	2.932 ± 0.048	1.818 ± 0.024	5010 ± 120	6310 ± 150	...	-0.14 ± 0.10	1
V467 Vel	8151-1072-1	...	9.99 ± 0.09	3.49 ± 0.03	36200 ± 2500	25260 ± 2500	67

Table 1—Continued

System	<i>Tycho</i> ID	<i>Hipparcos</i> ID	R_1 (R_\odot)	R_2 (R_\odot)	Primary T_{eff} (K)	Secondary T_{eff} (K)	$E(B - V)$ (mag)	[Fe/H]	Source
CV Vel	8177-1750-1	44245	4.089 ± 0.036	3.950 ± 0.036	18100 ± 500	17900 ± 500	0.035	-0.14 ± 0.15	1
V636 Cen	8285-0847-1	69781	1.0186 ± 0.0043	0.8300 ± 0.0043	5900 ± 85	5000 ± 100	0.007 ± 0.011	-0.20 ± 0.08	1
TV Nor	8322-0334-1	...	1.839 ± 0.012	1.550 ± 0.014	9120 ± 150	7800 ± 110	0.184 ± 0.019	...	68
ζ Phe	8476-1302-1	5348	2.852 ± 0.015	1.854 ± 0.011	14400 ± 800	12000 ± 600	0	...	1
QX Car	8610-2639-1	48589	4.291 ± 0.091	4.053 ± 0.091	23800 ± 500	22600 ± 500	0.049	...	1
G V Car	8627-1797-1	...	2.57 ± 0.05	1.43 ± 0.06	10100 ± 300	7750 ± 350	69
EP Cru	8654-0806-1	...	3.590 ± 0.035	3.495 ± 0.034	15700 ± 500	15400 ± 500	0.118	...	70
SZ Cen	8676-2330-1	67556	4.556 ± 0.032	3.626 ± 0.026	8100 ± 300	8380 ± 300	0.065	...	1
V539 Ara	8742-3096-1	87314	4.516 ± 0.084	3.428 ± 0.083	18100 ± 500	17100 ± 500	0.071	...	1
BG Ind	8820-0477-1	108478	2.290 ± 0.017	1.680 ± 0.038	6350 ± 200	6650 ± 100	...	-0.2 ± 0.1	71
V392 Car	8911-3412-1	...	1.624 ± 0.022	1.600 ± 0.022	8850 ± 200	8630 ± 200	0.101	...	1
DW Car	8957-1314-1	...	4.561 ± 0.050	4.299 ± 0.058	27900 ± 1000	26500 ± 1000	0.25 ± 0.03	...	1
EM Car	8959-0569-1	...	9.35 ± 0.17	8.35 ± 0.16	34000 ± 2000	34000 ± 2000	0.60	...	1
V349 Ara	9038-0641-1	...	3.60 ± 0.07	4.15 ± 0.07	9074 ± 200	8180 ± 202	61
UX Men	9378-0190-1	25760	1.348 ± 0.013	1.275 ± 0.013	6200 ± 100	6150 ± 100	0.027 ± 0.027	+0.04 ± 0.10	1
RS Cha	9403-1987-1	42794	2.138 ± 0.055	2.339 ± 0.055	7640 ± 180	7240 ± 170	0	+0.17 ± 0.01	1,73
RZ Cha	9422-0104-1	52381	2.256 ± 0.016	2.256 ± 0.016	6450 ± 150	6450 ± 150	0.004	...	1
TZ Men	9496-0590-1	25776	2.017 ± 0.020	1.433 ± 0.014	10400 ± 500	7200 ± 300	0	...	1

^aOver-contact system (W UMa).

Note. — Sources: (1) Torres et al. (2010); (2) Southworth et al. (2011); (3) Clausen et al. (2010a); (4) Ratajczak et al. (2010); (5) Torres et al. (2014a); (6) Sandberg Lacy et al. (2012a); (7) Harmanec et al. (2011); (8) Çakırhı et al. (2008); (9) da Silva et al. (2014); (10) Graczyk et al. (2015); (11) İbanoglu et al. (2008); (12) Sandberg Lacy et al. (2012b); (13) Maxted et al. (2015); (14) Sabby et al. (2011); (15) Zhang et al. (2009); (16) Çakırhı et al. (2012); (17) Sabby & Lacy (2003); (18) Torres et al. (2009a); (19) Clausen et al. (2010b); (20) Sandberg Lacy et al. (2016); (21) Hubrig et al. (2012); (22) Nördstrom & Johansen (1994); (23) Lacy et al. (2014a); (24) Sowell et al. (2012); (25) Sandberg Lacy & Fekel (2014); (26) Kiran et al. (2016); (27) Harmanec et al. (2014); (28) Lehmann et al. (2016); (29) Frandsen et al. (2013); (30) Maceroni et al. (2014); (31) Matson et al. (2016); (32) Tkachenko et al. (2014); (33) Dimitrov et al. (2015); (34) Sandberg Lacy et al. (2010); (35) Lacy et al. (2015); (36) Debosscher et al. (2013); (37) Millone et al. (2010); (38) Rawls et al. (2016); (39) Helminiak et al. (2015a); (40) Lacy et al. (2014b); (41) Tomkin & Fekel (2006); (42) Koo et al. (2014); (43) Tamajo et al. (2012); (44) Lacy et al. (2012); (45) Lacy et al. (1989); (46) Torres & Lacy (2009b); (47) Helminiak & Konacki (2011); (48) Torres et al. (2014b); (49) Torres et al. (2015); (50) Maceroni et al. (2013); (51) Williams et al. (2011); (52) Morales et al. (2009); (53) Sandberg Lacy & Fekel (2011); (54) Trudel et al. (1993); (55) Southworth (2013); (56) Vos et al. (2012); (57) Fekel et al. (2013); (58) Torres et al. (2012); (59) Helminiak et al. (2014); (60) Suchomska et al. (2015); (61) Erden et al. (2015); (62) Helminiak et al. (2015b); (63) Bakış et al. (2008); (64) Mantegazza et al. (2010); (65) Bruntt et al. (2006); (66) Veramendi & González (2015); (67) Michalska et al. (2013); (68) North et al. (1997); (69) Southworth & Clausen (2006); (70) Albrecht et al. (2013); (71) Rozyczka et al. (2011); (72) Graczyk et al. (2016); (73) Stassun et al. (2014).

The notation “Am / Am” indicates both components are metallic-line stars; “Am / -” means only the primary is known to have that anomaly. Am systems having components with individually measured [Fe/H]: YZ Cas ($+0.54 \pm 0.11$, Am) + ($+0.01 \pm 0.11$, normal), V501 Mon ($+0.33 \pm 0.08$, Am) + ($+0.01 \pm 0.06$, normal), SW CMa ($+0.49 \pm 0.15$, Am) + ($+0.61 \pm 0.15$, Am), HW CMa ($+0.28 \pm 0.10$, Am) + ($+0.33 \pm 0.10$, Am).

All uncertainties correspond to 1σ errors.

Table 2. Results

System	<i>Tycho</i> ID	<i>V</i> (mag)	χ^2_ν	F_{bol} ($\text{erg s}^{-1} \text{cm}^{-2}$)	A_V (mag)	Distance (pc)	Parallax (mas)
UV Psc	0026-0577-1	9.01	2.72	$7.748\text{e-}09 \pm (3.4\text{e-}10/3.2\text{e-}10)$	$0.01 \pm (0.00/0.01)$	$80.2 \pm (3.6/3.5)$	$12.47 \pm (0.57/0.53)$
XY Cet	0051-0832-1	8.75	1.60	$9.072\text{e-}09 \pm (3.9\text{e-}10/3.2\text{e-}10)$	$0.11 \pm (0.07/0.05)$	$276.5 \pm (10.2/10.7)$	$3.62 \pm (0.14/0.13)$
V1130 Tau	0066-1108-1	6.66	1.34	$6.202\text{e-}08 \pm (1.4\text{e-}09/1.7\text{e-}09)$	$0.03 \pm (0.00/0.02)$	$69.7 \pm (1.9/1.7)$	$14.35 \pm (0.36/0.37)$
EW Ori	0104-1206-1	9.78	0.71	$2.945\text{e-}09 \pm (6.3\text{e-}11/6.1\text{e-}11)$	$0.02 \pm (0.02/0.00)$	$169.6 \pm (6.3/6.1)$	$5.90 \pm (0.22/0.21)$
V578 Mon	0154-2528-1	8.55	0.65 *	$4.922\text{e-}07 \pm (1.3\text{e-}08/1.1\text{e-}08)$	$1.37 \pm (0.02/0.02)$	$1327.2 \pm (71.9/70.9)$	$0.75 \pm (0.04/0.04)$
AI Hya	0196-0626-1	9.35	7.02	$4.826\text{e-}09 \pm (3.1\text{e-}10/2.9\text{e-}10)$	$0.21 \pm (0.03/0.00)$	$548.4 \pm (20.5/19.6)$	$1.82 \pm (0.07/0.07)$
FM Leo	0263-0727-1	8.45	3.49	$1.175\text{e-}08 \pm (5.3\text{e-}10/5.0\text{e-}10)$	$0.11 \pm (0.02/0.00)$	$137.2 \pm (11.7/11.1)$	$7.29 \pm (0.64/0.57)$
AQ Ser	0340-0588-1	10.65	1.89	$1.576\text{e-}09 \pm (3.6\text{e-}11/3.2\text{e-}11)$	$0.12 \pm (0.00/0.01)$	$583.2 \pm (20.0/20.0)$	$1.71 \pm (0.06/0.06)$
V335 Ser	0353-0301-1	7.49	1.99	$3.495\text{e-}08 \pm (7.5\text{e-}10/1.2\text{e-}09)$	$0.23 \pm (0.00/0.03)$	$188.2 \pm (7.9/6.8)$	$5.31 \pm (0.20/0.21)$
U Oph	0400-1862-1	5.90	1.15 *	$7.968\text{e-}07 \pm (1.4\text{e-}08/3.1\text{e-}08)$	$0.73 \pm (0.00/0.04)$	$229.7 \pm (9.1/6.9)$	$4.35 \pm (0.14/0.17)$
V2368 Oph	0404-2156-1	6.18	2.84	$2.056\text{e-}07 \pm (1.5\text{e-}08/1.3\text{e-}08)$	$0.76 \pm (0.07/0.06)$	$183.8 \pm (10.4/10.1)$	$5.44 \pm (0.32/0.29)$
V413 Ser	0446-0091-1	7.99	1.64	$2.097\text{e-}07 \pm (1.2\text{e-}08/1.1\text{e-}08)$	$2.29 \pm (0.06/0.06)$	$187.2 \pm (12.0/11.4)$	$5.34 \pm (0.35/0.32)$
CoRoT 105906206	0459-0892-1	12.21	1.80	$1.016\text{e-}09 \pm (4.1\text{e-}11/3.5\text{e-}11)$	$0.64 \pm (0.19/0.04)$	$1063.5 \pm (51.5/52.0)$	$0.94 \pm (0.05/0.04)$
IO Aqr	0511-0960-1	8.86	0.87	$8.378\text{e-}09 \pm (2.9\text{e-}10/2.6\text{e-}10)$	$0.09 \pm (0.04/0.04)$	$252.0 \pm (11.1/11.0)$	$3.97 \pm (0.18/0.17)$
V1388 Ori	0738-0244-1	7.50	3.28 *	$2.598\text{e-}07 \pm (7.8\text{e-}09/1.1\text{e-}08)$	$0.50 \pm (0.00/0.04)$	$893.4 \pm (51.3/45.0)$	$1.12 \pm (0.06/0.06)$
V2365 Oph	0977-0547-1	8.86	1.68	$7.243\text{e-}09 \pm (3.2\text{e-}10/3.3\text{e-}10)$	$0.16 \pm (0.03/0.05)$	$150.0 \pm (6.2/5.9)$	$6.67 \pm (0.27/0.27)$
WZ Oph	0977-0216-1	9.12	3.60	$1.698\text{e-}08 \pm (8.0\text{e-}10/5.7\text{e-}10)$	$0.68 \pm (0.06/0.00)$	$262.3 \pm (11.8/12.8)$	$3.81 \pm (0.19/0.16)$
V624 Her	1005-2131-1	6.20	2.11	$9.992\text{e-}08 \pm (1.9\text{e-}09/4.4\text{e-}09)$	$0.19 \pm (0.00/0.04)$	$131.6 \pm (6.3/4.9)$	$7.60 \pm (0.29/0.35)$
V451 Oph	1027-1355-1	7.91	2.26	$3.962\text{e-}08 \pm (1.1\text{e-}09/8.8\text{e-}10)$	$0.49 \pm (0.02/0.00)$	$311.0 \pm (48.4/44.9)$	$3.22 \pm (0.54/0.43)$
EE Peg	1120-0161-1	6.98	1.72	$4.341\text{e-}08 \pm (1.6\text{e-}09/6.3\text{e-}10)$	$0.01 \pm (0.03/0.00)$	$136.3 \pm (6.2/7.1)$	$7.33 \pm (0.41/0.32)$
CF Tau	1262-0050-1	10.24	1.31	$5.302\text{e-}09 \pm (2.2\text{e-}10/2.3\text{e-}10)$	$0.87 \pm (0.11/0.12)$	$246.2 \pm (15.9/15.0)$	$4.06 \pm (0.26/0.25)$
V1094 Tau	1263-0642-1	8.97	0.74	$7.374\text{e-}09 \pm (2.3\text{e-}10/1.7\text{e-}10)$	$0.06 \pm (0.04/0.00)$	$119.0 \pm (4.3/4.6)$	$8.40 \pm (0.34/0.30)$
CD Tau	1291-0292-1	6.77	4.36	$5.304\text{e-}08 \pm (2.3\text{e-}09/2.1\text{e-}09)$	$0.01 \pm (0.00/0.00)$	$67.9 \pm (1.9/1.8)$	$14.73 \pm (0.41/0.39)$
FT Ori	1326-0910-1	9.29	7.62	$6.776\text{e-}09 \pm (3.4\text{e-}10/3.3\text{e-}10)$	$0.16 \pm (0.04/0.00)$	$431.0 \pm (39.3/36.9)$	$2.32 \pm (0.22/0.19)$
CU Cnc	1387-0884-1	11.81	18.89	$4.775\text{e-}09 \pm (5.4\text{e-}10/4.9\text{e-}10)$	$0.01 \pm (0.00/0.00)$	$14.2 \pm (1.6/1.5)$	$70.58 \pm (8.49/7.38)$
TX Cnc	1395-0907-1	9.97	3.80	$2.939\text{e-}09 \pm (1.2\text{e-}10/1.1\text{e-}10)$	$0.18 \pm (0.00/0.02)$	$201.8 \pm (14.2/13.7)$	$4.95 \pm (0.36/0.33)$
BP Vul	1644-2113-1	9.95	2.61	$2.797\text{e-}07 \pm (8.5\text{e-}09/8.4\text{e-}09)$	$0.31 \pm (0.00/0.02)$	$746.1 \pm (47.0/44.6)$	$1.34 \pm (0.09/0.08)$
HD 194495	1644-1635-1	7.06	1.45 *	$3.023\text{e-}09 \pm (7.7\text{e-}11/5.9\text{e-}11)$	$0.05 \pm (0.07/0.00)$	$401.6 \pm (16.5/16.8)$	$2.49 \pm (0.11/0.10)$
AD Boo	2015-0216-1	9.44	2.31	$5.001\text{e-}09 \pm (1.1\text{e-}10/1.2\text{e-}10)$	$0.15 \pm (0.00/0.02)$	$200.4 \pm (8.1/7.7)$	$4.99 \pm (0.20/0.19)$
RT CrB	2039-1337-1	10.22	1.84	$2.539\text{e-}09 \pm (5.9\text{e-}11/5.7\text{e-}11)$	$0.03 \pm (0.00/0.00)$	$393.9 \pm (17.2/16.9)$	$2.54 \pm (0.11/0.11)$
LV Her	2076-1042-1	10.97	1.17	$1.096\text{e-}09 \pm (3.8\text{e-}11/3.8\text{e-}11)$	$0.06 \pm (0.05/0.05)$	$354.1 \pm (19.5/18.7)$	$2.82 \pm (0.16/0.15)$
DI Her	2109-0775-1	8.47	0.65 *	$6.596\text{e-}08 \pm (1.7\text{e-}09/2.0\text{e-}09)$	$0.49 \pm (0.03/0.03)$	$633.9 \pm (64.8/59.2)$	$1.58 \pm (0.16/0.15)$
BK Peg	2254-2563-1	10.04	0.82	$3.153\text{e-}09 \pm (8.3\text{e-}11/6.7\text{e-}11)$	$0.12 \pm (0.05/0.00)$	$295.5 \pm (8.8/9.2)$	$3.38 \pm (0.11/0.10)$
AG Per	2362-0115-1	6.69	2.02 *	$4.366\text{e-}07 \pm (1.7\text{e-}08/2.0\text{e-}08)$	$0.68 \pm (0.02/0.05)$	$325.6 \pm (32.1/29.1)$	$3.07 \pm (0.30/0.28)$
NP Per	2371-0390-1	11.24	0.79	$1.329\text{e-}09 \pm (3.0\text{e-}11/2.9\text{e-}11)$	$0.69 \pm (0.04/0.00)$	$288.6 \pm (9.3/9.1)$	$3.47 \pm (0.11/0.11)$

Table 2—Continued

System	<i>Tycho</i> ID	<i>V</i> (mag)	χ^2_ν	F_{bol} (erg s ⁻¹ cm ⁻²)	A_V (mag)	Distance (pc)	Parallax (mas)
AR Aur	2398-1311-1	6.14	1.83	1.354e-07 ± (2.0e-09/2.4e-09)	0.04 ± (0.00/0.00)	134.6 ± (8.0/ 7.4)	7.43 ± (0.43/0.41)
HP Aur	2401-1263-1	11.17	1.31	1.179e-09 ± (3.1e-11/3.0e-11)	0.21 ± (0.00/0.01)	199.7 ± (8.9/ 8.7)	5.01 ± (0.23/0.21)
V432 Aur	2416-0768-1	8.05	4.61	1.898e-08 ± (9.1e-10/8.5e-10)	0.07 ± (0.00/0.02)	129.6 ± (4.8/ 4.7)	7.72 ± (0.29/0.28)
WW Aur	2426-0345-1	5.82	3.06	1.184e-07 ± (3.6e-09/3.4e-09)	0.01 ± (0.00/0.00)	80.5 ± (9.1/ 8.5)	12.42 ± (1.46/1.26)
GX Gem	2444-0267-1	11.71	1.88	9.195e-10 ± (2.7e-11/2.9e-11)	0.27 ± (0.02/0.00)	690.0 ± (25.9/ 24.6)	1.45 ± (0.05/0.05)
KX Cnc	2484-0592-1	7.19	1.05	3.692e-08 ± (8.2e-10/7.2e-10)	0.00 ± (0.00/0.00)	45.5 ± (1.7/ 1.6)	21.97 ± (0.83/0.77)
HD 71636	2489-1972-1	7.90	0.92	1.905e-08 ± (5.0e-10/2.4e-10)	0.06 ± (0.02/0.00)	116.4 ± (4.9/ 5.4)	8.59 ± (0.41/0.35)
YY Gem	2543-1918-1	9.83	2.49	1.831e-08 ± (8.0e-10/7.7e-10)	0.01 ± (0.00/0.00)	16.0 ± (0.9/ 0.9)	62.36 ± (3.77/3.50)
CV Boo	2570-0843-1	10.99	1.64	1.344e-09 ± (4.7e-11/4.0e-11)	0.08 ± (0.02/0.00)	261.2 ± (15.0/ 14.9)	3.83 ± (0.23/0.21)
V501 Her	2606-1905-1	11.12	0.50	1.062e-09 ± (2.3e-11/2.2e-11)	0.12 ± (0.03/0.02)	423.9 ± (16.1/ 15.6)	2.36 ± (0.09/0.09)
BD+36 3317	2651-0802-1	8.77	1.96	1.192e-08 ± (4.1e-10/2.2e-10)	0.16 ± (0.04/0.00)	326.6 ± (26.5/ 27.1)	3.06 ± (0.28/0.23)
V885 Cyg	2655-1877-1	9.99	2.27	3.074e-09 ± (1.2e-10/7.1e-11)	0.21 ± (0.04/0.00)	853.4 ± (32.7/ 36.7)	1.17 ± (0.05/0.04)
MY Cyg	2680-1529-1	8.34	1.79	1.223e-08 ± (2.6e-10/2.0e-10)	0.06 ± (0.01/0.00)	236.8 ± (14.6/ 14.4)	4.22 ± (0.27/0.25)
V453 Cyg	2683-3326-1	8.40	1.62 *	5.471e-07 ± (2.3e-08/2.3e-08)	1.47 ± (0.04/0.04)	1724.3 ± (64.5/ 61.8)	0.58 ± (0.02/0.02)
V442 Cyg	2685-1903-1	9.70	1.68	4.006e-09 ± (7.9e-11/5.9e-11)	0.22 ± (0.02/0.00)	335.6 ± (11.0/ 11.4)	2.98 ± (0.10/0.09)
CG Cyg	2696-2945-1	10.16	3.26	3.770e-09 ± (1.4e-10/1.4e-10)	0.34 ± (0.00/0.00)	85.6 ± (6.3/ 6.1)	11.68 ± (0.89/0.80)
Y Cyg	2696-3486-1	7.32	1.58 *	1.009e-06 ± (1.6e-08/2.1e-08)	0.69 ± (0.00/0.01)	1543.5 ± (63.4/ 58.5)	0.65 ± (0.03/0.03)
β Aur	2924-2742-1	1.90	5.15	4.968e-06 ± (8.1e-08/1.2e-07)	0.00 ± (0.01/0.00)	24.8 ± (1.2/ 1.1)	40.37 ± (1.81/1.83)
KIC 7177553	3127-0167-1	11.54	3.04	1.000e-09 ± (2.2e-11/2.1e-11)	0.13 ± (0.00/0.01)	237.8 ± (11.5/ 11.1)	4.21 ± (0.21/0.19)
KIC 8410637	3130-2385-1	11.33	2.63	1.802e-09 ± (8.0e-11/7.2e-11)	0.47 ± (0.07/0.06)	1024.4 ± (41.5/ 41.8)	0.98 ± (0.04/0.04)
KIC 3858884	3135-0651-1	9.28	10.60	5.204e-09 ± (3.1e-10/2.9e-10)	0.23 ± (0.04/0.00)	488.9 ± (17.6/ 17.1)	2.05 ± (0.07/0.07)
KIC 5738698	3141-1400-1	12.13	0.82	5.766e-10 ± (1.6e-11/1.4e-11)	0.42 ± (0.04/0.04)	815.9 ± (17.2/ 17.7)	1.23 ± (0.03/0.03)
V380 Cyg	3141-3692-1	5.68	0.90 *	1.773e-06 ± (7.5e-08/6.0e-08)	0.62 ± (0.04/0.03)	976.0 ± (40.5/ 42.1)	1.02 ± (0.05/0.04)
V478 Cyg	3151-2222-1	8.68	5.82 *	9.677e-07 ± (7.8e-08/7.2e-08)	2.24 ± (0.11/0.09)	1687.6 ± (135.1/ 127.8)	0.59 ± (0.05/0.04)
V364 Lac	3215-0971-1	8.36	2.30	1.572e-08 ± (4.6e-10/5.4e-10)	0.26 ± (0.00/0.03)	422.2 ± (18.0/ 16.4)	2.37 ± (0.10/0.10)
V342 And	3246-2531-1	7.82	24.15 X	2.025e-08 ± (1.9e-09/1.8e-09)	0.00 ± (0.00/0.00)	82.3 ± (4.9/ 4.4)	12.15 ± (0.69/0.69)
CO And	3268-0398-1	10.77	1.34	1.776e-09 ± (5.9e-11/6.1e-11)	0.28 ± (0.04/0.04)	369.2 ± (17.9/ 17.0)	2.71 ± (0.13/0.13)
V570 Per	3314-1225-1	8.09	1.98	1.698e-08 ± (3.4e-10/3.3e-10)	0.10 ± (0.00/0.01)	121.0 ± (2.7/ 2.7)	8.26 ± (0.19/0.18)
IM Per	3323-1123-1	11.28	3.91	3.052e-09 ± (1.8e-10/1.1e-10)	1.40 ± (0.06/0.02)	595.4 ± (26.1/ 29.7)	1.68 ± (0.09/0.07)
IQ Per	3331-1175-1	7.73	3.20	5.551e-08 ± (2.2e-09/2.0e-09)	0.43 ± (0.02/0.00)	274.1 ± (11.7/ 11.7)	3.65 ± (0.16/0.15)
HS Aur	3394-0326-1	10.05	1.71	2.483e-09 ± (7.0e-11/7.6e-11)	0.05 ± (0.00/0.00)	126.8 ± (4.8/ 4.6)	7.89 ± (0.30/0.29)
FL Lyr	3542-1492-1	9.36	1.53	5.012e-09 ± (1.7e-10/1.5e-10)	0.01 ± (0.02/0.00)	133.2 ± (5.5/ 5.5)	7.51 ± (0.33/0.29)
KIC 11285625	3549-2141-1	10.24	7.08	2.608e-09 ± (7.5e-11/1.2e-10)	0.25 ± (0.00/0.05)	425.5 ± (17.0/ 13.5)	2.35 ± (0.08/0.09)
V2080 Cyg	3551-1744-1	7.40	2.15	3.029e-08 ± (6.6e-10/6.4e-10)	0.00 ± (0.00/0.00)	79.2 ± (2.2/ 2.2)	12.63 ± (0.36/0.35)
HP Dra	3552-0394-1	7.93	1.52	1.866e-08 ± (3.0e-10/2.9e-10)	0.07 ± (0.01/0.00)	76.3 ± (4.0/ 3.9)	13.10 ± (0.70/0.66)

Table 2—Continued

System	<i>Tycho</i> ID	<i>V</i> (mag)	χ^2_ν	F_{bol} ($\text{erg s}^{-1} \text{cm}^{-2}$)	A_V (mag)	Distance (pc)	Parallax (mas)
KIC 9246715	3559-0102-1	9.65	3.92	$6.707\text{e-}09 \pm (3.8\text{e-}10/3.7\text{e-}10)$	$0.45 \pm (0.00/0.07)$	$593.9 \pm (51.6/48.2)$	$1.68 \pm (0.15/0.13)$
V1061 Cyg	3600-0472-1	9.21	2.29	$5.600\text{e-}09 \pm (1.8\text{e-}10/1.0\text{e-}10)$	$0.06 \pm (0.02/0.00)$	$153.0 \pm (5.2/5.8)$	$6.54 \pm (0.26/0.21)$
RW Lac	3629-0740-1	10.81	1.83	$1.866\text{e-}09 \pm (6.7\text{e-}11/6.4\text{e-}11)$	$0.23 \pm (0.00/0.00)$	$194.0 \pm (7.8/7.6)$	$5.15 \pm (0.21/0.20)$
AP And	3639-0915-1	11.19	1.02	$1.293\text{e-}09 \pm (3.2\text{e-}11/3.1\text{e-}11)$	$0.27 \pm (0.00/0.02)$	$345.9 \pm (17.1/16.6)$	$2.89 \pm (0.15/0.14)$
IT Cas	3650-0959-1	11.23	1.13	$1.027\text{e-}09 \pm (3.1\text{e-}11/3.0\text{e-}11)$	$0.18 \pm (0.03/0.04)$	$494.8 \pm (18.0/17.5)$	$2.02 \pm (0.47/0.07)$
V505 Per	3690-0536-1	6.88	0.99	$4.765\text{e-}08 \pm (9.8\text{e-}10/8.0\text{e-}10)$	$0.01 \pm (0.01/0.00)$	$59.1 \pm (1.3/1.4)$	$16.93 \pm (0.41/0.37)$
RR Lyn	3772-2770-1	5.54	4.39	$1.470\text{e-}07 \pm (4.0\text{e-}09/3.9\text{e-}09)$	$0.00 \pm (0.00/0.00)$	$74.2 \pm (2.3/2.3)$	$13.47 \pm (0.43/0.41)$
ISWASP J093010.78+533859.5	3807-0759-1	9.84	7.70	$4.928\text{e-}09 \pm (1.8\text{e-}10/2.1\text{e-}10)$	$0.04 \pm (0.00/0.02)$	$56.0 \pm (5.0/4.5)$	$17.85 \pm (1.56/1.46)$
V1143 Cyg	3938-1983-1	5.90	2.02	$1.195\text{e-}07 \pm (2.2\text{e-}09/1.8\text{e-}09)$	$0.01 \pm (0.00/0.00)$	$38.3 \pm (1.3/1.4)$	$26.11 \pm (0.96/0.88)$
RT And	3998-2167-1	9.04	5.42	$6.416\text{e-}09 \pm (3.4\text{e-}10/3.2\text{e-}10)$	$0.00 \pm (0.04/0.00)$	$109.1 \pm (6.2/6.1)$	$9.17 \pm (0.54/0.50)$
V396 Cas	4006-1219-1	9.58	1.82	$6.433\text{e-}09 \pm (2.8\text{e-}10/1.4\text{e-}10)$	$0.50 \pm (0.05/0.00)$	$542.0 \pm (17.9/22.0)$	$1.85 \pm (0.08/0.06)$
PV Cas	4010-1411-1	9.86	3.77	$7.824\text{e-}09 \pm (2.5\text{e-}10/2.3\text{e-}10)$	$0.64 \pm (0.02/0.00)$	$643.0 \pm (34.4/33.6)$	$1.56 \pm (0.09/0.08)$
MU Cas	4014-1119-1	10.80	3.10 *	$1.369\text{e-}08 \pm (3.2\text{e-}10/2.8\text{e-}10)$	$1.47 \pm (0.02/0.00)$	$1796.7 \pm (207.9/194.2)$	$0.56 \pm (0.07/0.06)$
V459 Cas	4030-1001-1	10.36	3.94	$4.043\text{e-}09 \pm (2.1\text{e-}10/1.9\text{e-}10)$	$0.76 \pm (0.05/0.00)$	$625.7 \pm (46.1/44.2)$	$1.60 \pm (0.12/0.11)$
SZ Cam	4068-1651-1	6.93	3.57 *	$4.292\text{e-}06 \pm (1.6\text{e-}07/1.4\text{e-}07)$	$2.13 \pm (0.03/0.00)$	$797.7 \pm (16.8/17.4)$	$1.25 \pm (0.03/0.03)^{\dagger}$
WW Cam	4073-1191-1	10.09	3.26	$5.507\text{e-}09 \pm (3.2\text{e-}10/2.7\text{e-}10)$	$1.21 \pm (0.07/0.01)$	$414.6 \pm (17.5/17.9)$	$2.41 \pm (0.11/0.10)$
ZZ UMa	4144-0400-1	9.83	1.74	$3.136\text{e-}09 \pm (6.7\text{e-}11/5.9\text{e-}11)$	$0.02 \pm (0.02/0.00)$	$189.8 \pm (5.1/5.2)$	$5.27 \pm (0.15/0.14)^{\dagger}$
WX Cep	4268-0138-1	9.00	12.47	$1.358\text{e-}08 \pm (1.2\text{e-}09/1.1\text{e-}09)$	$0.59 \pm (0.00/0.04)$	$497.4 \pm (38.2/36.7)$	$2.01 \pm (0.16/0.14)$
AH Cep	4273-0857-1	6.88	5.84 *	$2.717\text{e-}06 \pm (2.7\text{e-}07/2.4\text{e-}07)$	$1.71 \pm (0.09/0.09)$	$763.6 \pm (65.3/61.5)$	$1.31 \pm (0.11/0.10)$
CW Cep	4282-0419-1	7.64	1.22 *	$2.200\text{e-}06 \pm (1.1\text{e-}07/9.3\text{e-}08)$	$2.21 \pm (0.05/0.05)$	$686.4 \pm (53.5/52.7)$	$1.46 \pm (0.12/0.11)$
YZ Cas	4307-2167-1	5.65	4.63	$2.228\text{e-}07 \pm (1.1\text{e-}08/8.8\text{e-}09)$	$0.22 \pm (0.02/0.00)$	$85.4 \pm (2.8/2.9)$	$11.71 \pm (0.41/0.37)$
BF Dra	4435-1750-1	9.76	1.42	$3.225\text{e-}09 \pm (1.0\text{e-}10/5.5\text{e-}11)$	$0.04 \pm (0.04/0.00)$	$345.0 \pm (16.6/17.8)$	$2.90 \pm (0.16/0.13)$
UZ Dra	4444-1595-1	9.60	4.95	$3.779\text{e-}09 \pm (2.0\text{e-}10/1.9\text{e-}10)$	$0.06 \pm (0.02/0.00)$	$180.0 \pm (7.9/7.6)$	$5.55 \pm (0.24/0.23)$
EK Cep	4466-2120-1	7.89	4.61	$1.978\text{e-}08 \pm (9.4\text{e-}10/8.8\text{e-}10)$	$0.02 \pm (0.02/0.00)$	$162.9 \pm (8.3/8.1)$	$6.14 \pm (0.32/0.30)$
VZ Cep	4470-1334-1	9.72	1.82	$3.358\text{e-}09 \pm (1.4\text{e-}10/1.4\text{e-}10)$	$0.04 \pm (0.04/0.04)$	$223.5 \pm (12.6/12.0)$	$4.47 \pm (0.25/0.24)$
EY Cep	4521-0349-1	9.81	0.77	$3.440\text{e-}09 \pm (7.1\text{e-}11/6.8\text{e-}11)$	$0.13 \pm (0.02/0.00)$	$296.7 \pm (13.5/13.1)$	$3.37 \pm (0.16/0.15)$
AY Cam	4540-1742-1	9.72	0.99	$3.632\text{e-}09 \pm (8.6\text{e-}11/8.3\text{e-}11)$	$0.18 \pm (0.01/0.00)$	$515.6 \pm (16.0/15.8)$	$1.94 \pm (0.06/0.06)$
EI Cep	4599-0082-1	7.61	1.93	$2.457\text{e-}08 \pm (6.7\text{e-}10/5.1\text{e-}10)$	$0.04 \pm (0.02/0.00)$	$187.9 \pm (6.4/6.7)$	$5.32 \pm (0.20/0.17)$
ASAS J045304-0700.4	4749-0560-1	11.13	1.37	$1.420\text{e-}09 \pm (5.0\text{e-}11/4.9\text{e-}11)$	$0.49 \pm (0.00/0.09)$	$145.9 \pm (11.9/11.2)$	$6.85 \pm (0.57/0.52)$
GG Ori	4767-0857-1	10.49	3.43	$9.748\text{e-}09 \pm (5.0\text{e-}10/4.5\text{e-}10)$	$1.75 \pm (0.12/0.00)$	$443.6 \pm (21.6/21.5)$	$2.25 \pm (0.11/0.10)$
V530 Ori	4786-0571-1	9.96	1.09	$3.392\text{e-}09 \pm (1.4\text{e-}10/1.3\text{e-}10)$	$0.14 \pm (0.06/0.06)$	$102.4 \pm (4.2/4.1)$	$9.77 \pm (0.41/0.38)$
V501 Mon	4799-1943-1	12.32	2.48	$6.050\text{e-}10 \pm (1.7\text{e-}11/1.7\text{e-}11)$	$0.79 \pm (0.01/0.00)$	$911.1 \pm (30.2/29.5)$	$1.10 \pm (0.04/0.04)$
CoRoT 102918586	4800-1540-1	12.43	0.99	$4.203\text{e-}10 \pm (1.1\text{e-}11/6.4\text{e-}12)$	$0.42 \pm (0.03/0.00)$	$971.8 \pm (24.7/28.7)$	$1.03 \pm (0.03/0.03)$
HI Mon	4809-0245-1	9.45	4.10 *	$2.129\text{e-}07 \pm (1.3\text{e-}08/1.2\text{e-}08)$	$1.29 \pm (0.10/0.09)$	$2211.5 \pm (117.3/114.7)$	$0.45 \pm (0.02/0.02)$
FS Mon	4825-2374-1	9.68	2.17	$3.801\text{e-}09 \pm (8.7\text{e-}11/8.0\text{e-}11)$	$0.05 \pm (0.01/0.00)$	$319.3 \pm (10.4/10.4)$	$3.13 \pm (0.10/0.10)$

Table 2—Continued

System	<i>Tycho</i> ID	<i>V</i> (mag)	χ^2_ν	F_{bol} ($\text{erg s}^{-1} \text{cm}^{-2}$)	A_V (mag)	Distance (pc)	Parallax (mas)
VZ Hya	4874-0811-1	9.06	0.80	$7.393\text{e-}09 \pm (2.1\text{e-}10/1.8\text{e-}10)$	$0.12 \pm (0.04/0.04)$	$143.8 \pm (6.9/6.9)$	$6.95 \pm (0.35/0.32)$
KW Hya	4891-1371-1	6.12	1.52	$9.334\text{e-}08 \pm (1.3\text{e-}09/1.7\text{e-}09)$	$0.03 \pm (0.00/0.01)$	$85.1 \pm (4.5/4.2)$	$11.75 \pm (0.62/0.60)$
IM Vir	4955-0912-1	9.69	1.39	$4.548\text{e-}09 \pm (1.4\text{e-}10/1.3\text{e-}10)$	$0.00 \pm (0.00/0.00)$	$88.5 \pm (3.7/3.6)$	$11.30 \pm (0.48/0.45)$
HY Vir	4960-0976-1	7.86	1.87	$1.944\text{e-}08 \pm (5.8\text{e-}10/4.1\text{e-}10)$	$0.05 \pm (0.02/0.00)$	$178.9 \pm (6.8/7.2)$	$5.59 \pm (0.23/0.20)$
BH Vir	4968-0569-1	9.68	1.81	$4.007\text{e-}09 \pm (1.7\text{e-}10/1.7\text{e-}10)$	$0.11 \pm (0.02/0.00)$	$154.8 \pm (6.8/6.5)$	$6.46 \pm (0.28/0.27)$
EG Ser	5099-0149-1	8.24	4.57	$2.664\text{e-}08 \pm (9.0\text{e-}10/8.6\text{e-}10)$	$0.52 \pm (0.00/0.02)$	$217.9 \pm (9.8/9.6)$	$4.59 \pm (0.21/0.20)$
LL Aqr	5236-0883-1	9.32	0.90	$7.492\text{e-}09 \pm (2.4\text{e-}10/2.4\text{e-}10)$	$0.43 \pm (0.05/0.05)$	$115.2 \pm (2.6/2.5)$	$8.68 \pm (0.19/0.19)$
EF Aqr	5248-1030-1	10.04	0.67	$2.974\text{e-}09 \pm (6.8\text{e-}11/6.6\text{e-}11)$	$0.03 \pm (0.03/0.00)$	$176.7 \pm (4.5/4.5)$	$5.66 \pm (0.15/0.14)$
V1031 Ori	5351-0761-1	6.06	2.52	$1.065\text{e-}07 \pm (3.1\text{e-}09/2.1\text{e-}09)$	$0.09 \pm (0.02/0.00)$	$176.5 \pm (23.7/22.4)$	$5.66 \pm (0.82/0.67)$
PV Pup	5422-3294-1	6.93	85.13 X	$4.399\text{e-}08 \pm (7.1\text{e-}09/5.9\text{e-}09)$	$0.01 \pm (0.02/0.00)$	$83.5 \pm (10.0/9.2)$	$11.98 \pm (1.49/1.28)$
VV Crv	5534-1488-1	5.84	0.82	$1.955\text{e-}07 \pm (1.6\text{e-}08/1.5\text{e-}08)$	$0.00 \pm (0.00/0.00)$	$61.5 \pm (4.7/4.4)$	$16.27 \pm (1.26/1.15)$
DM Vir	5558-1683-1	8.79	1.25	$8.970\text{e-}09 \pm (2.4\text{e-}10/2.8\text{e-}10)$	$0.10 \pm (0.00/0.04)$	$188.9 \pm (7.0/6.5)$	$5.29 \pm (0.19/0.19)$
GZ CMa	5965-0860-1	7.98	2.25	$2.158\text{e-}08 \pm (1.3\text{e-}09/1.1\text{e-}09)$	$0.22 \pm (0.07/0.06)$	$285.5 \pm (25.1/24.1)$	$3.50 \pm (0.32/0.28)$
HW CMa	5976-1266-1	9.18	2.14	$6.126\text{e-}09 \pm (1.3\text{e-}10/2.4\text{e-}10)$	$0.14 \pm (0.00/0.04)$	$565.0 \pm (25.8/20.9)$	$1.77 \pm (0.07/0.08)$
SW CMa	5976-0630-1	9.16	3.87	$5.511\text{e-}09 \pm (2.2\text{e-}10/2.1\text{e-}10)$	$0.07 \pm (0.02/0.00)$	$311.3 \pm (14.2/13.9)$	$3.21 \pm (0.15/0.14)$
ASAS J082552-1622.8	5998-1918-1	10.29	2.20	$5.398\text{e-}09 \pm (2.6\text{e-}10/2.6\text{e-}10)$	$0.00 \pm (0.00/0.00)$	$39.3 \pm (4.1/3.8)$	$25.43 \pm (2.72/2.41)$
VV Pys	6010-5044-1	6.58	4.36	$7.737\text{e-}08 \pm (2.3\text{e-}09/2.5\text{e-}09)$	$0.08 \pm (0.00/0.02)$	$168.9 \pm (8.0/7.6)$	$5.92 \pm (0.28/0.27)$
HS Hya	6069-1131-1	8.12	1.04	$1.556\text{e-}08 \pm (4.4\text{e-}10/1.9\text{e-}10)$	$0.03 \pm (0.02/0.00)$	$99.9 \pm (1.6/2.2)$	$10.01 \pm (0.23/0.16)$
BW Aqr	6378-0804-1	10.31	0.89	$2.143\text{e-}09 \pm (2.6\text{e-}11/5.1\text{e-}11)$	$0.14 \pm (0.00/0.02)$	$409.0 \pm (16.4/14.2)$	$2.45 \pm (0.09/0.09)$
AK For	6446-0342-1	9.36	5.68	$9.910\text{e-}09 \pm (7.0\text{e-}10/6.9\text{e-}10)$	$0.00 \pm (0.00/0.00)$	$32.6 \pm (2.0/1.9)$	$30.65 \pm (1.88/1.80)$
χ^2 Hya	6644-1330-1	5.71	1.67	$2.559\text{e-}07 \pm (5.3\text{e-}09/6.8\text{e-}09)$	$0.07 \pm (0.00/0.02)$	$222.1 \pm (8.3/7.6)$	$4.50 \pm (0.16/0.16)$
ASAS J180057-2333.8	6842-1399-1	10.34	3.38	$1.630\text{e-}08 \pm (1.1\text{e-}09/1.4\text{e-}09)$	$1.85 \pm (0.00/0.31)$	$2138.6 \pm (137.1/105.6)$	$0.47 \pm (0.02/0.03)$
V3903 Sgr	6843-0543-1	7.31	0.47 *	$3.163\text{e-}06 \pm (6.9\text{e-}08/7.6\text{e-}08)$	$1.57 \pm (0.04/0.06)$	$1305.8 \pm (138.5/128.4)$	$0.77 \pm (0.08/0.07)$
TZ For	7026-0633-1	6.89	0.75	$5.627\text{e-}08 \pm (1.4\text{e-}09/7.1\text{e-}10)$	$0.09 \pm (0.02/0.00)$	$187.8 \pm (7.8/8.5)$	$5.33 \pm (0.25/0.21)$
V760 Sco	7352-1162-1	7.05	0.75 *	$4.288\text{e-}07 \pm (1.4\text{e-}08/1.3\text{e-}08)$	$1.09 \pm (0.03/0.03)$	$288.0 \pm (19.0/18.2)$	$3.47 \pm (0.23/0.22)$
V906 Sco	7386-0562-1	5.96	2.04	$1.917\text{e-}07 \pm (1.8\text{e-}08/1.9\text{e-}08)$	$0.25 \pm (0.02/0.04)$	$245.6 \pm (28.6/25.4)$	$4.07 \pm (0.47/0.43)$
V1647 Sgr	7390-1395-1	6.94	2.60	$5.001\text{e-}08 \pm (1.2\text{e-}09/1.8\text{e-}09)$	$0.15 \pm (0.00/0.03)$	$165.6 \pm (11.6/10.3)$	$6.04 \pm (0.40/0.39)$
V4403 Sgr	7415-4484-1	8.62	1.50	$1.027\text{e-}08 \pm (3.0\text{e-}10/2.7\text{e-}10)$	$0.09 \pm (0.02/0.00)$	$208.0 \pm (10.8/10.5)$	$4.81 \pm (0.26/0.24)$
HD 187669	7443-0867-1	8.88	1.13	$1.867\text{e-}08 \pm (8.2\text{e-}10/8.3\text{e-}10)$	$0.52 \pm (0.04/0.07)$	$608.5 \pm (26.7/25.6)$	$1.64 \pm (0.07/0.07)$
PT Vel	7690-2859-1	7.03	13.27	$6.226\text{e-}08 \pm (4.9\text{e-}09/4.4\text{e-}09)$	$0.02 \pm (0.00/0.00)$	$136.8 \pm (7.0/6.8)$	$7.31 \pm (0.38/0.35)$
ψ Cen	7805-2696-1	4.05	1.59	$8.410\text{e-}07 \pm (1.3\text{e-}08/1.3\text{e-}08)$	$0.00 \pm (0.00/0.00)$	$77.0 \pm (7.7/7.2)$	$12.99 \pm (1.35/1.18)$
GG Lup	7826-3079-1	5.59	1.17	$4.078\text{e-}07 \pm (7.0\text{e-}09/4.1\text{e-}09)$	$0.06 \pm (0.01/0.00)$	$148.4 \pm (9.3/9.3)$	$6.74 \pm (0.45/0.40)$
V4089 Sgr	7936-2270-1	5.91	2.66	$1.177\text{e-}07 \pm (2.6\text{e-}09/2.8\text{e-}09)$	$0.03 \pm (0.00/0.00)$	$145.8 \pm (3.9/3.7)$	$6.86 \pm (0.18/0.18)$
AI Phe	8032-0625-1	8.60	0.52	$1.097\text{e-}08 \pm (1.3\text{e-}10/1.6\text{e-}10)$	$0.05 \pm (0.00/0.01)$	$167.3 \pm (8.8/8.3)$	$5.98 \pm (0.31/0.30)$
V467 Vel	8151-1072-1	10.90	10.29 *	$1.857\text{e-}07 \pm (1.0\text{e-}08/9.3\text{e-}09)$	$2.12 \pm (0.00/0.02)$	$523.2 \pm (769.2/712.1)$	$0.19 \pm (0.03/0.02)$

Table 2—Continued

System	<i>Tycho</i> ID	<i>V</i> (mag)	χ^2_ν	F_{bol} (erg s ⁻¹ cm ⁻²)	A_V (mag)	Distance (pc)	Parallax (mas)
CV Vel	8177-1750-1	6.69	1.51 *	2.868e-07 ± (4.5e-09/6.8e-09)	0.13 ± (0.00/0.02)	584.2 ± (35.5/32.2)	1.71 ± (0.10/0.10)
V636 Cen	8285-0847-1	9.09	0.25	9.410e-09 ± (1.1e-10/7.8e-11)	0.00 ± (0.01/0.00)	71.9 ± (2.1/2.2)	13.91 ± (0.43/0.40)
TV Nor	8322-0334-1	9.06	1.99	1.173e-08 ± (2.5e-10/2.7e-10)	0.58 ± (0.00/0.02)	281.7 ± (10.2/9.8)	3.55 ± (0.13/0.12)
ζ Phe	8476-1302-1	3.97	1.62	1.746e-06 ± (2.1e-08/5.1e-08)	0.02 ± (0.00/0.01)	83.4 ± (10.0/8.8)	12.00 ± (1.42/1.29)
QX Car	8610-2639-1	6.64	2.69 *	5.440e-07 ± (1.1e-08/1.2e-08)	0.16 ± (0.00/0.01)	734.9 ± (35.4/33.8)	1.36 ± (0.07/0.06)
GV Car	8627-1797-1	8.91	2.72	1.052e-08 ± (5.5e-10/2.3e-10)	0.24 ± (0.06/0.00)	456.7 ± (28.3/32.5)	2.19 ± (0.17/0.13)
EP Cru	8654-0806-1	8.69	0.63 *	4.260e-08 ± (1.1e-09/1.1e-09)	0.42 ± (0.02/0.03)	997.3 ± (68.2/65.2)	1.00 ± (0.07/0.06)
SZ Cen	8676-2330-1	8.59	17.76	1.667e-08 ± (1.6e-09/1.4e-09)	0.44 ± (0.00/0.05)	516.4 ± (47.0/44.0)	1.94 ± (0.18/0.16)
V539 Ara	8742-3096-1	5.71	0.48 *	7.887e-07 ± (1.2e-08/2.3e-08)	0.26 ± (0.00/0.03)	341.6 ± (21.8/18.9)	2.93 ± (0.17/0.18)
BG Ind	8820-0477-1	6.14	2.69	9.099e-08 ± (2.2e-09/2.3e-09)	0.00 ± (0.00/0.00)	66.7 ± (4.5/4.3)	14.99 ± (1.03/0.95)
V392 Car	8911-3412-1	9.48	3.16	5.945e-09 ± (1.7e-10/1.6e-10)	0.38 ± (0.00/0.01)	383.8 ± (19.2/18.6)	2.61 ± (0.13/0.12)
DW Car	8957-1314-1	9.85	3.76 *	9.486e-08 ± (5.3e-09/4.7e-09)	0.87 ± (0.00/0.03)	2568.7 ± (204.4/197.4)	0.39 ± (0.03/0.03)
EM Car	8959-0569-1	8.52	0.99 *	1.353e-06 ± (5.1e-08/3.8e-08)	2.03 ± (0.04/0.03)	2114.8 ± (265.1/251.6)	0.47 ± (0.06/0.05)
V349 Ara	9038-0641-1	8.58	3.91	1.376e-08 ± (5.8e-10/6.1e-10)	0.42 ± (0.00/0.04)	587.8 ± (31.5/29.5)	1.70 ± (0.09/0.09)
UX Men	9378-0190-1	8.24	1.15	1.420e-08 ± (5.2e-10/5.5e-10)	0.06 ± (0.04/0.04)	100.9 ± (4.0/3.8)	9.91 ± (0.39/0.38)
RS Cha	9403-1987-1	6.07	2.76	9.210e-08 ± (3.0e-09/2.1e-09)	0.02 ± (0.02/0.00)	97.9 ± (5.1/5.3)	10.22 ± (0.58/0.51)
RZ Cha	9422-0104-1	8.09	0.68	1.597e-08 ± (3.6e-10/4.4e-10)	0.02 ± (0.01/0.02)	178.3 ± (9.2/8.5)	5.61 ± (0.28/0.28)
TZ Men	9496-0590-1	6.18	2.04	1.141e-07 ± (1.1e-08/7.5e-09)	0.00 ± (0.03/0.00)	115.8 ± (12.0/12.2)	8.63 ± (1.01/0.81)

^aSystems flagged with an asterisk have $T_{\text{eff}} > 15,000$ K and a large fraction of their flux extrapolated from a blackbody distribution on the blue side. Those marked with an “X” are considered to have poor SED fits.

A. Spectral Energy Distribution Measurements and Fits for EB Study Sample

In Figure Set 11 we present the observed and fitted spectral energy distributions of the 158 EBs in our study sample (Table 1).

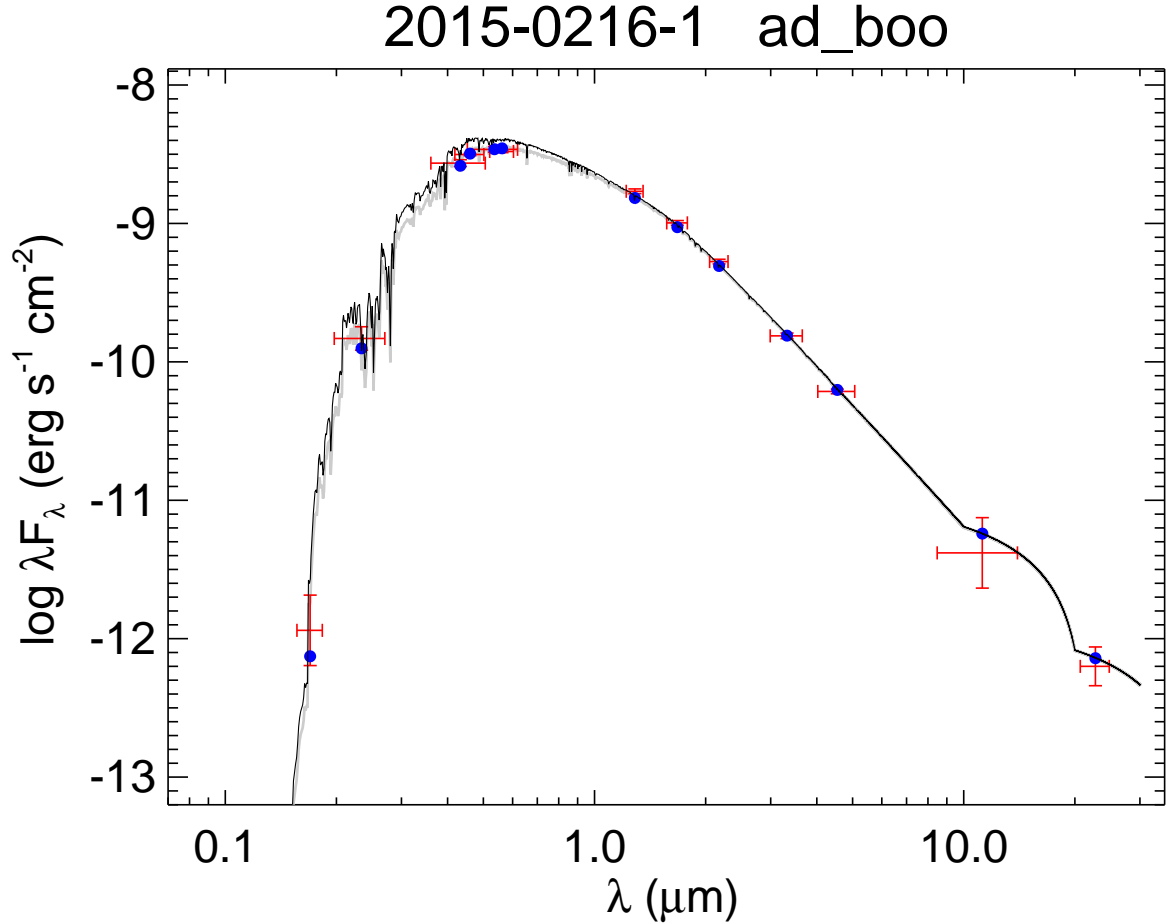


Fig. 11.— AD Boo is shown as example of the figure set. Each panel in the Figure Set is labeled at top by the *Tycho-2* ID and name of the EB, and shows the observed fluxes (in units of $\text{erg cm}^{-2} \text{s}^{-1}$) versus wavelength (in μm) as red error bars, where the vertical error bar represents the uncertainty in the measurement and the horizontal “error” bar represents the effective width of the passband. Also in each figure is the fitted SED model including extinction (light gray curve), on which is shown the model passband fluxes as blue dots. The discontinuity in the model SED at $0.1 \mu\text{m}$ among the hot stars is due to the blackbody extrapolation for $\lambda < 0.1 \mu\text{m}$ for stars with $T_{\text{eff}} > 15,000 \text{ K}$ (see the text). The corresponding un-extincted SED model is also shown (dark black curve); the reported F_{bol} is the sum over all wavelengths of this un-extincted model (see the text). The full figure set is displayed in Figures 13–39.

B. The uncertainties in the total bolometric luminosity

The uncertainty in the total bolometric luminosity L_{bol} of each of our EBs, which factors into the final error in the distances and parallaxes, depends on the radius and temperature uncertainties of both components. A naive approach to error propagation would consider the published primary and secondary temperature errors to be independent, and the radius errors to also be independent, whereas in reality they are not. For example, light curve analyses typically yield highly precise temperature *ratios* from the relative depth of the eclipses such that the secondary temperature essentially scales with the primary temperature (a positive correlation), and most of the uncertainty in the secondary value is inherited from the primary. The primary temperature and its error are usually determined from external information (e.g., spectroscopically) and held fixed in the photometric analysis. Similarly, light curves can often determine the radius *sum* very precisely from the total duration of the eclipses, whereas the radius *ratio* is less well constrained, as are the individual radii if solved for separately. This results in the primary and secondary radius errors being highly anti-correlated.

Given these correlations, propagating the temperature errors for the primary and secondary as if they were independent will cause the uncertainty in L_{bol} to be underestimated, and doing the same with the radius errors will tend to give an L_{bol} error that is too high, partially offsetting the temperature bias. However, as temperature errors dominate due to the fourth power dependence in the Stefan-Boltzmann law, and because they are typically larger (fractionally) compared to the radius errors, the net result will be an underestimate of the total luminosity error.

A more sensible approach would be to recast the published uncertainties in the secondary temperature $T_{\text{eff},2}$ in terms of the errors in the primary value and in the temperature ratio $t \equiv T_{\text{eff},2}/T_{\text{eff},1}$, which are usually uncorrelated, and the radius uncertainties in terms of those of their sum $r \equiv R_1 + R_2$ and their ratio $k \equiv R_2/R_1$, which are also uncorrelated, and to then propagate these new uncertainties independently to infer the error in L_{bol} . This should lead to more realistic errors for L_{bol} . However, in practice it is not possible to recover the uncertainties in t , r , and k accurately without access to the details of each light curve analysis, which are not always published, and the issue is further complicated by the sometimes subjective assignment of radius and/or temperature uncertainties in some of the original publications. For this work we have nevertheless attempted to estimate σ_t , σ_r , and σ_k in a statistical sense to match the ensemble of reported errors for the individual temperatures and radii as closely as possible. We proceed as follows.

Beginning with the radii, the individual component values may be expressed in terms of their sum and ratio as

$$R_1 = \left(\frac{1}{1+k}\right)r \quad , \quad R_2 = \left(\frac{k}{1+k}\right)r \quad (\text{B1})$$

(see Torres et al. 2000) in which the correlation between r and k is generally weak. Standard error propagation then gives

$$\sigma_{R_1} = \frac{1}{1+k} \left[\left(\frac{r}{1+k}\right)^2 \sigma_k^2 + \sigma_r^2 \right]^{1/2} \quad , \quad \sigma_{R_2} = \frac{1}{1+k} \left[\left(\frac{r}{1+k}\right)^2 \sigma_k^2 + k^2 \sigma_r^2 \right]^{1/2} \quad , \quad (\text{B2})$$

from which it can be seen that if the secondary is a smaller star, its uncertainty should in principle also be smaller. As mentioned above, many systems with smaller secondaries have reported σ_{R_2} values that are in fact larger than σ_{R_1} , which prevents one from solving Eqs.[B2] directly for σ_r , and σ_k . Since the expectation is that the radius sum should be better determined than the radius ratio, we introduce this condition by

defining

$$f_R \equiv \frac{\sigma_r/r}{\sigma_k/k} \quad (\text{B3})$$

where f_R , the ratio of the fractional uncertainties in r and k , should be smaller than unity. Solving for σ_k and inserting it in Eqs.[B2] leads to two expressions for σ_r in terms of the published errors, one based on σ_{R_1} and the other on σ_{R_2} :

$$\sigma_{r,1} = \sigma_{R_1}(1+k) \left[\left(\frac{k}{1+k} \right)^2 f_R^{-2} + 1 \right]^{-1/2}, \quad \sigma_{r,2} = \sigma_{R_2}(1+k) \left[\left(\frac{k}{1+k} \right)^2 f_R^{-2} + k^2 \right]^{-1/2}. \quad (\text{B4})$$

We adopt here a simple average of these two estimates, $\sigma_r = (\sigma_{r,1} + \sigma_{r,2})/2$. We then derive the uncertainty in k from Eq.[B3] as $\sigma_k = \sigma_r(k/r)f_R^{-1}$.

We apply a similar reasoning to the temperatures, assuming the uncertainties in the primary temperature and in the temperature ratio are largely independent. In that case, since $T_{\text{eff},2} = t T_{\text{eff},1}$, the uncertainty σ_2 in $T_{\text{eff},2}$ is expressed as

$$\sigma_2^2 = T_{\text{eff},1}^2 \sigma_t^2 + t^2 \sigma_1^2, \quad (\text{B5})$$

and as before we may define

$$f_T \equiv \frac{\sigma_t/t}{\sigma_1/T_{\text{eff},1}} \quad (\text{B6})$$

with the expectation that the fractional error in the temperature ratio will typically be smaller than that of the primary temperature. Solving for σ_1 and inserting it in Eq.[B5] leads to the required estimate of the uncertainty in the temperature ratio,

$$\sigma_t = \sigma_2 T_{\text{eff},1}^{-1} (1 + f_T^{-2})^{-1/2}. \quad (\text{B7})$$

Because of the ways in which individual temperature errors have sometimes been assigned to our eclipsing binaries, it is not always possible to use the above formalism to infer a value of σ_t or f_T for each system directly from the published uncertainties σ_1 and σ_2 . This is similar to the difficulty mentioned earlier for the radii. We have therefore chosen to adopt a single value of f_R and f_T for the entire sample, and to use the ensemble of published measurement errors for all 156 systems to tell us what the optimal values should be, such that when inserted into the expressions for σ_r , σ_k , and σ_t for each EB we obtain the closest match to the published individual radius and temperature errors using Eqs.[B2] and Eq.[B5]. Denoting the individual radius and temperature errors predicted by our prescription for given values of f_R and f_T as σ'_{R_1} , σ'_{R_2} , σ'_1 , and σ'_2 , we construct a figure of merit η for R and T_{eff} as follows:

$$\eta(f_R) = \sum \left(1 - \frac{\sigma'_{R_1}}{\sigma_{R_1}} \right)^2 + \sum \left(1 - \frac{\sigma'_{R_2}}{\sigma_{R_2}} \right)^2, \quad \eta(f_T) = \sum \left(1 - \frac{\sigma'_2}{\sigma_2} \right)^2. \quad (\text{B8})$$

Both statistics have a single absolute minimum yielding best-fit values $f_R = 0.56$ and $f_T = 0.46$ (see Figure 12). These factors are both smaller than unity, supporting our assumption that the radius sum is usually better determined than the radius ratio, and that the temperature ratio is typically more precise than the fractional error in the primary temperature. The fact that the f factors are not much smaller, as one might expect for canonical light curve solutions, is a reflection of the inhomogeneous nature of the published errors.

We used the above prescription to estimate the uncertainty in L_{bol} for each system by propagating the errors in r and k through a Monte Carlo procedure as if they were independent, and similarly with $T_{\text{eff},1}$

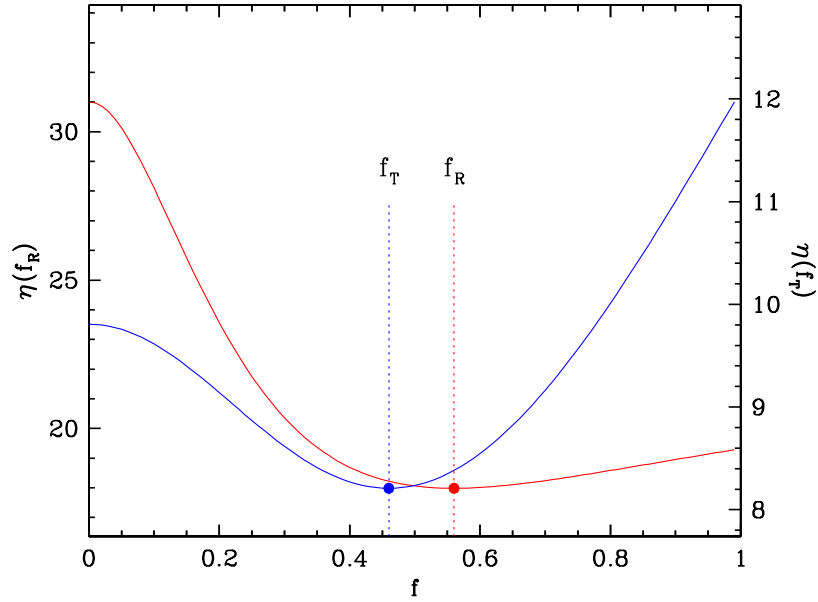


Fig. 12.— Illustration of how we estimated the scale factors f_R and f_T that provide the best overall fit to the ensemble of published errors in the radii and temperatures for the 156 EBs in our sample. The best-fit values that minimize the respective figures of merit η are indicated.

and t . Compared to the more simplistic approach in which the individual temperature errors and individual radius errors are considered to be uncorrelated, our approach results in typical luminosity uncertainties up to 50% larger, which we expect to be more realistic.

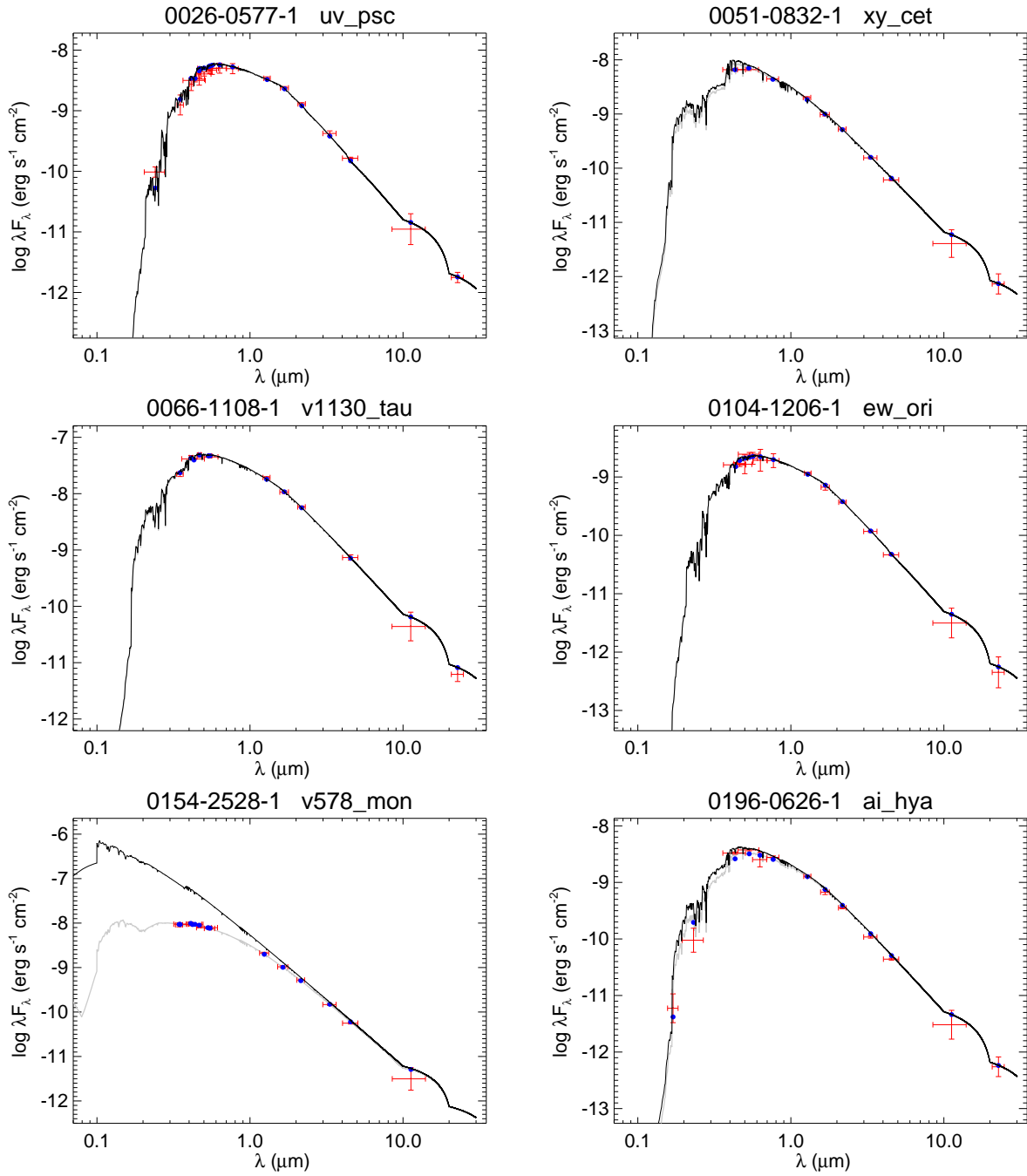


Fig. 13.— All labels, lines, symbols, and colors as in Figure 11.

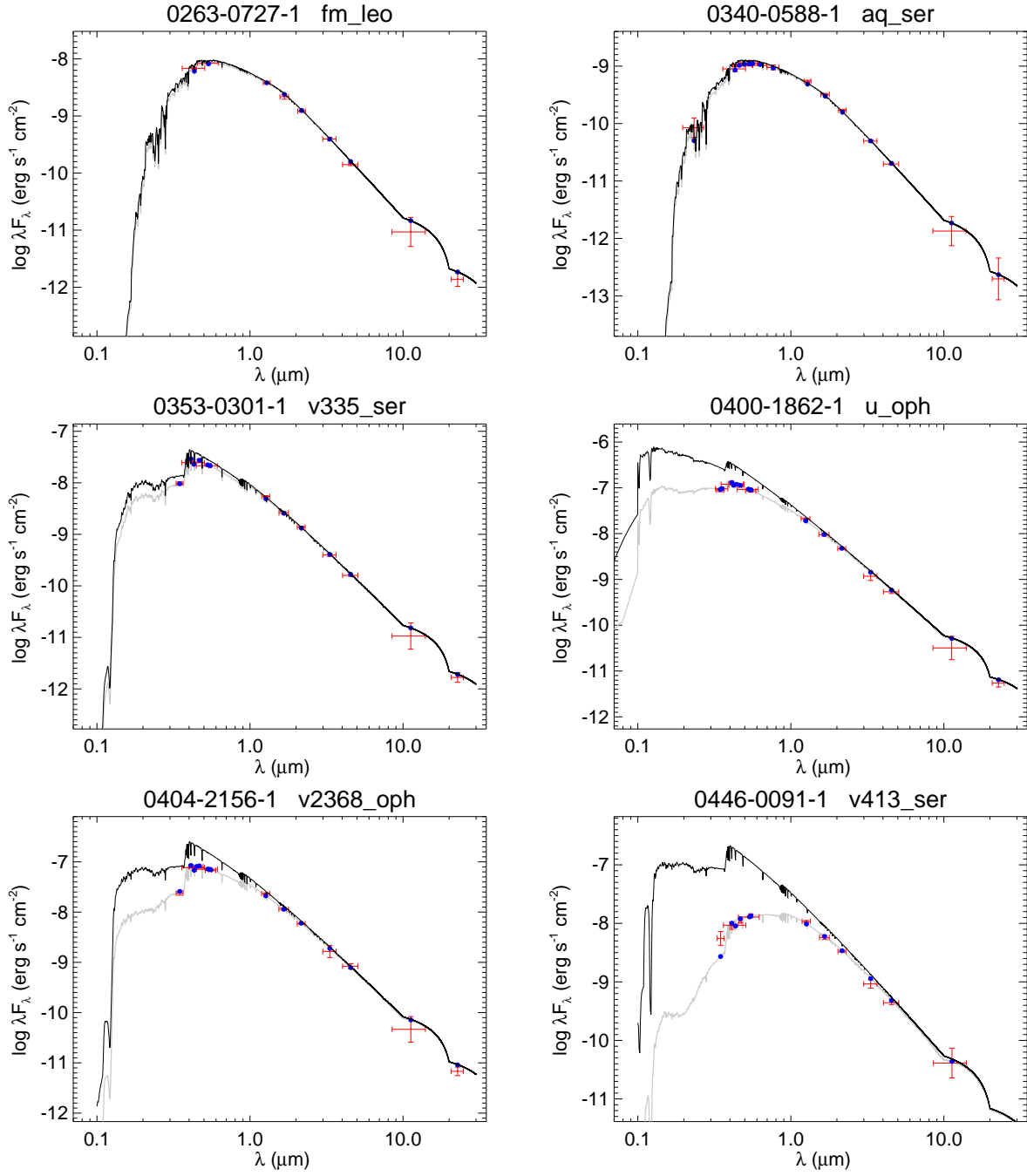


Fig. 14.— All labels, lines, symbols, and colors as in Figure 11.

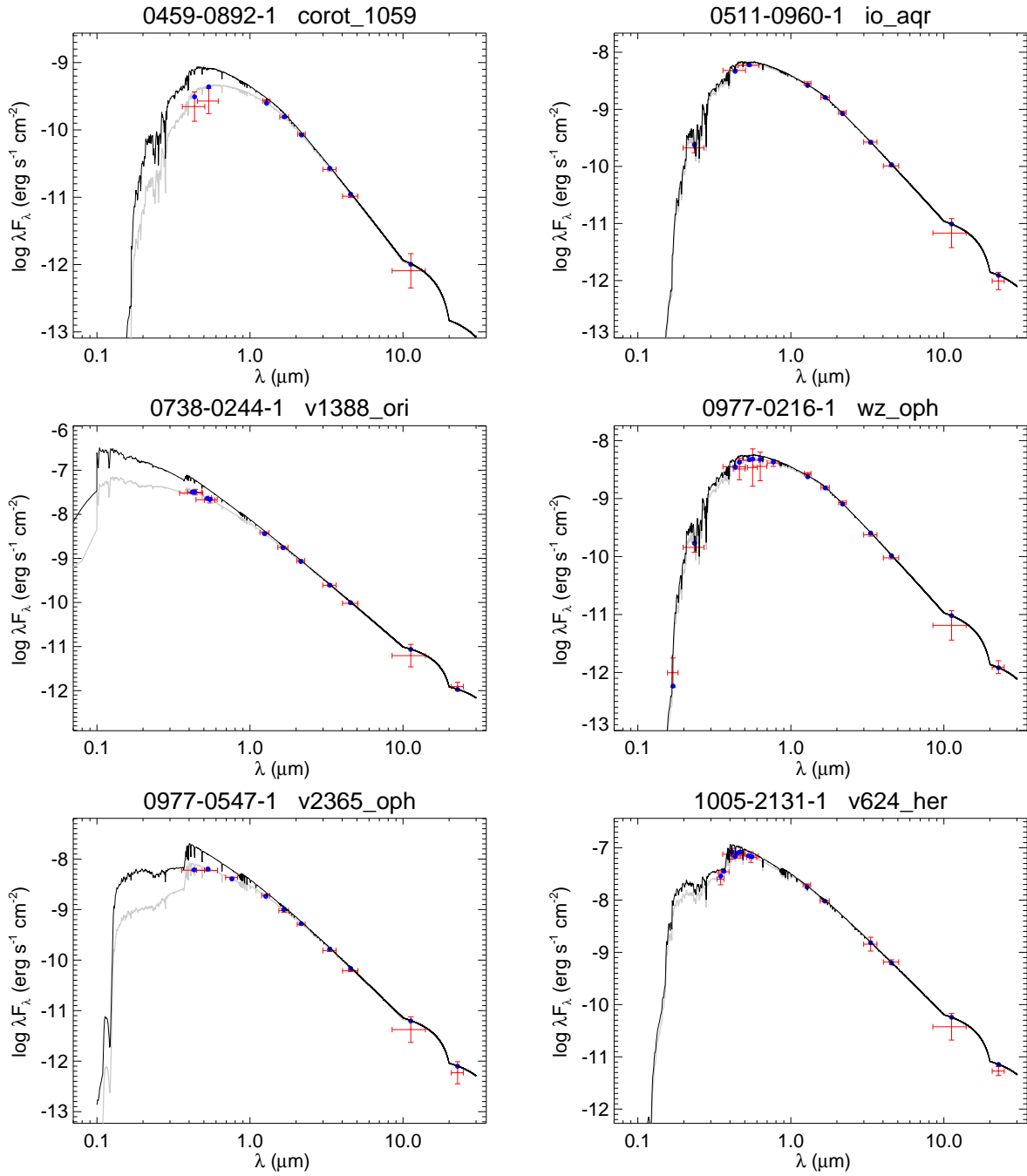


Fig. 15.— All labels, lines, symbols, and colors as in Figure 11.

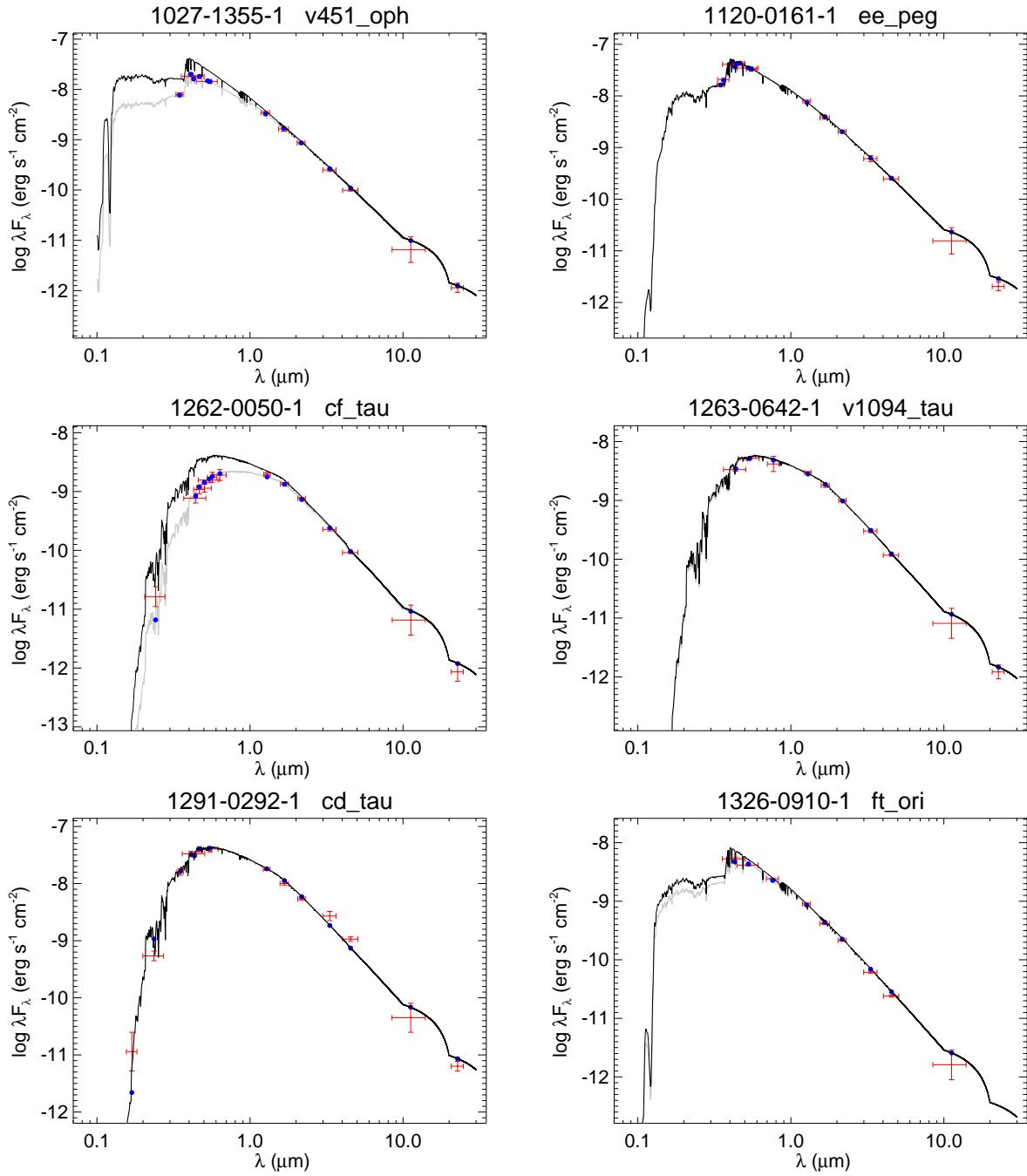


Fig. 16.— All labels, lines, symbols, and colors as in Figure 11.

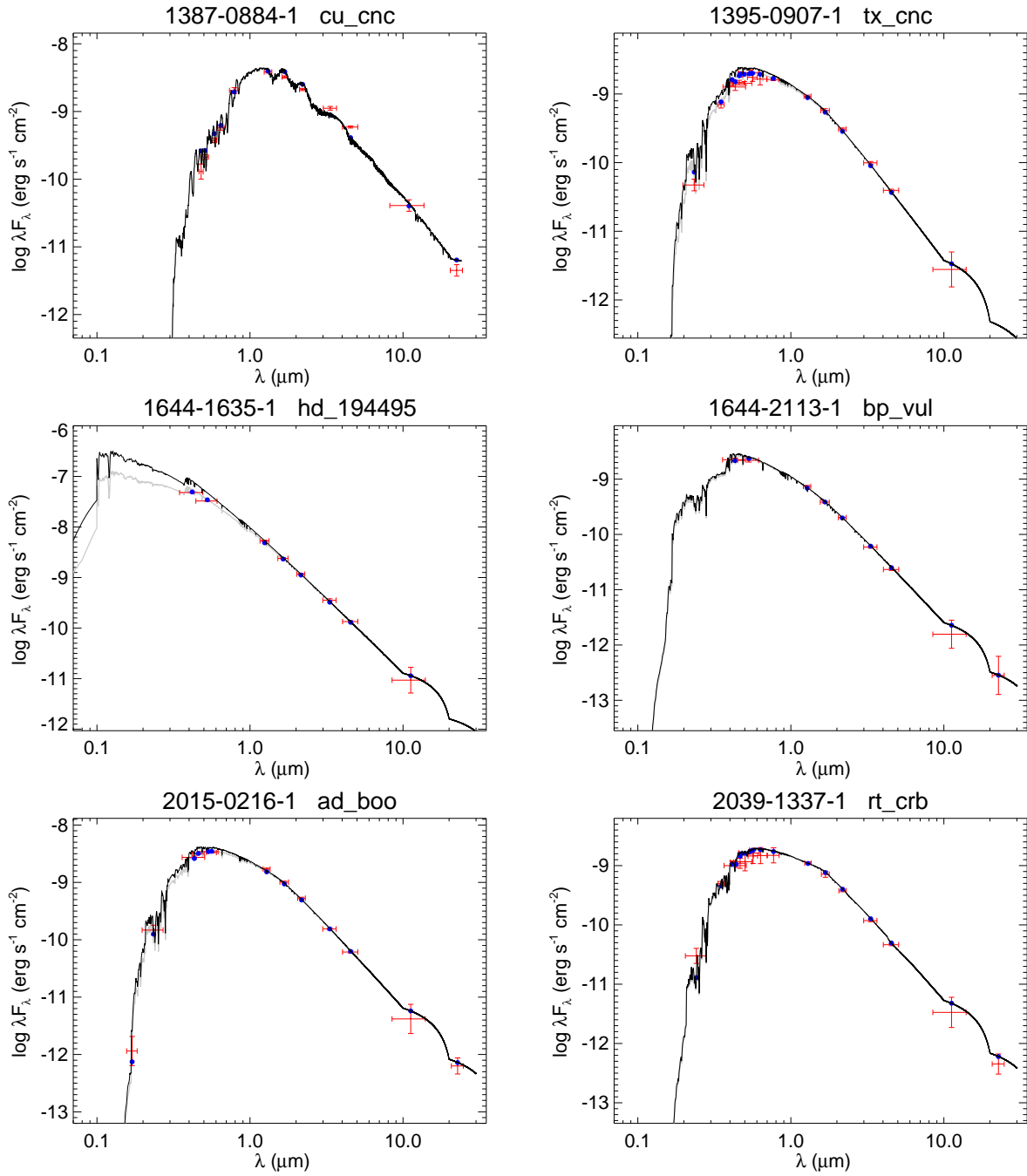


Fig. 17.— All labels, lines, symbols, and colors as in Figure 11.

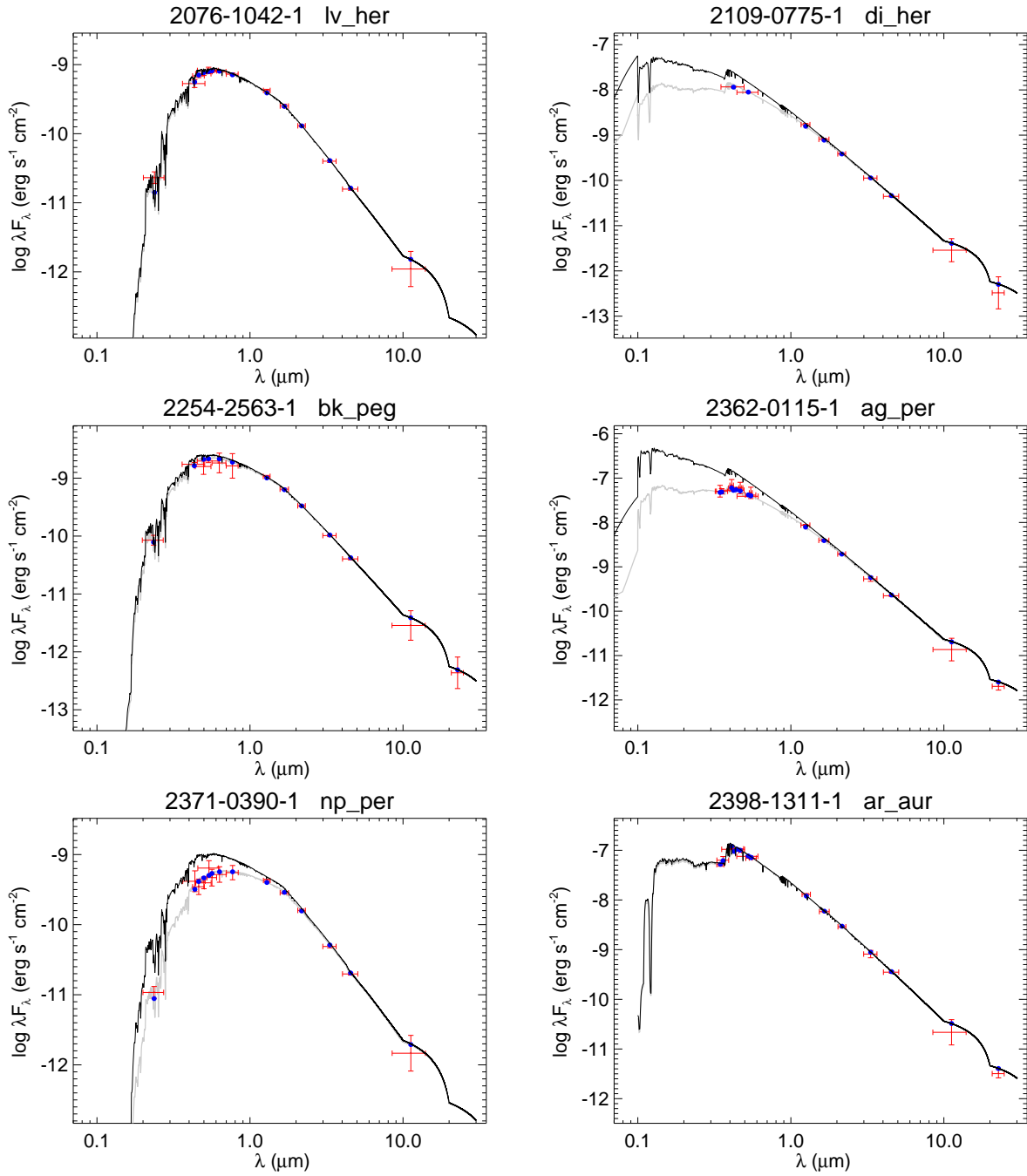


Fig. 18.— All labels, lines, symbols, and colors as in Figure 11.

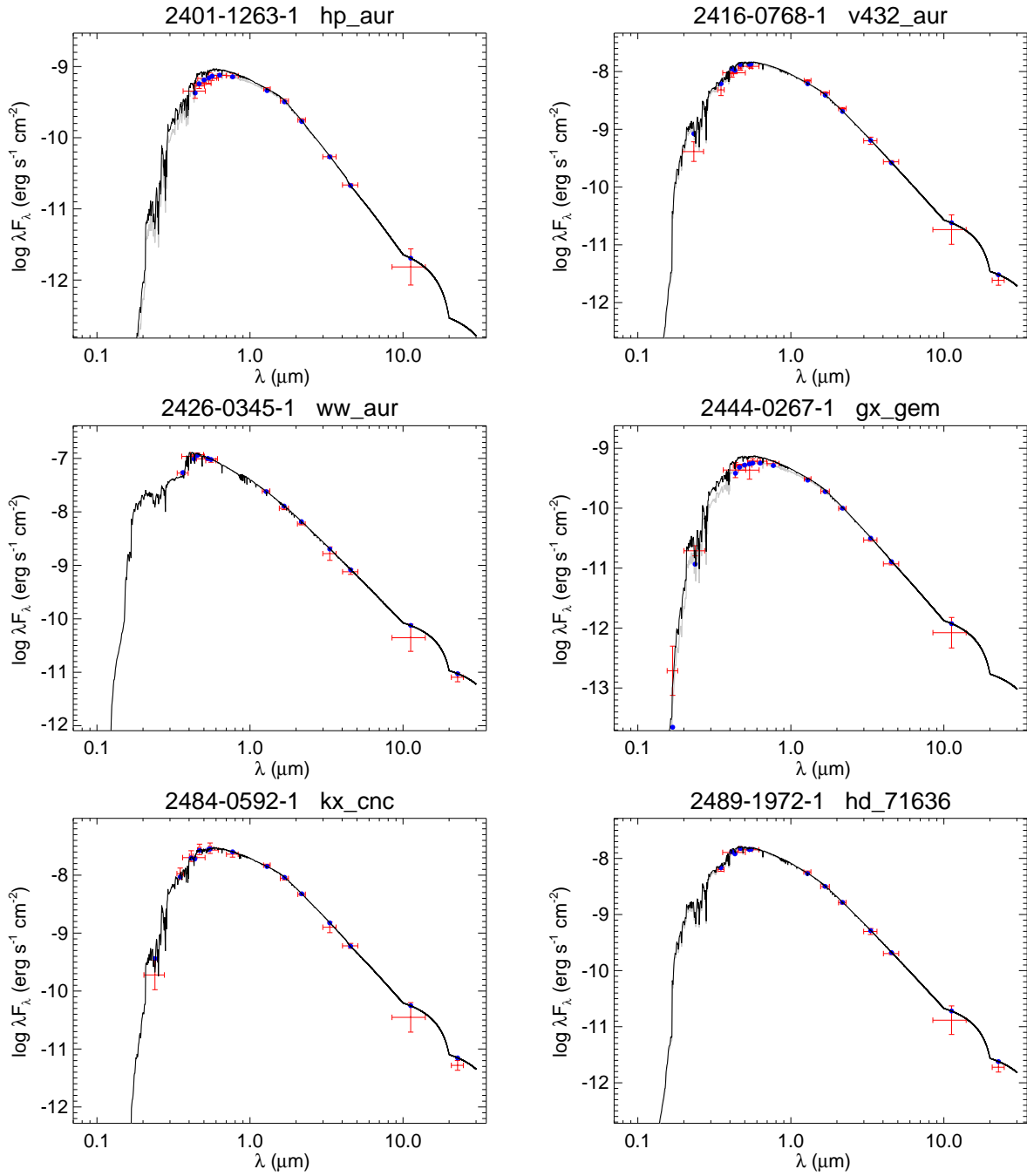


Fig. 19.— All labels, lines, symbols, and colors as in Figure 11.

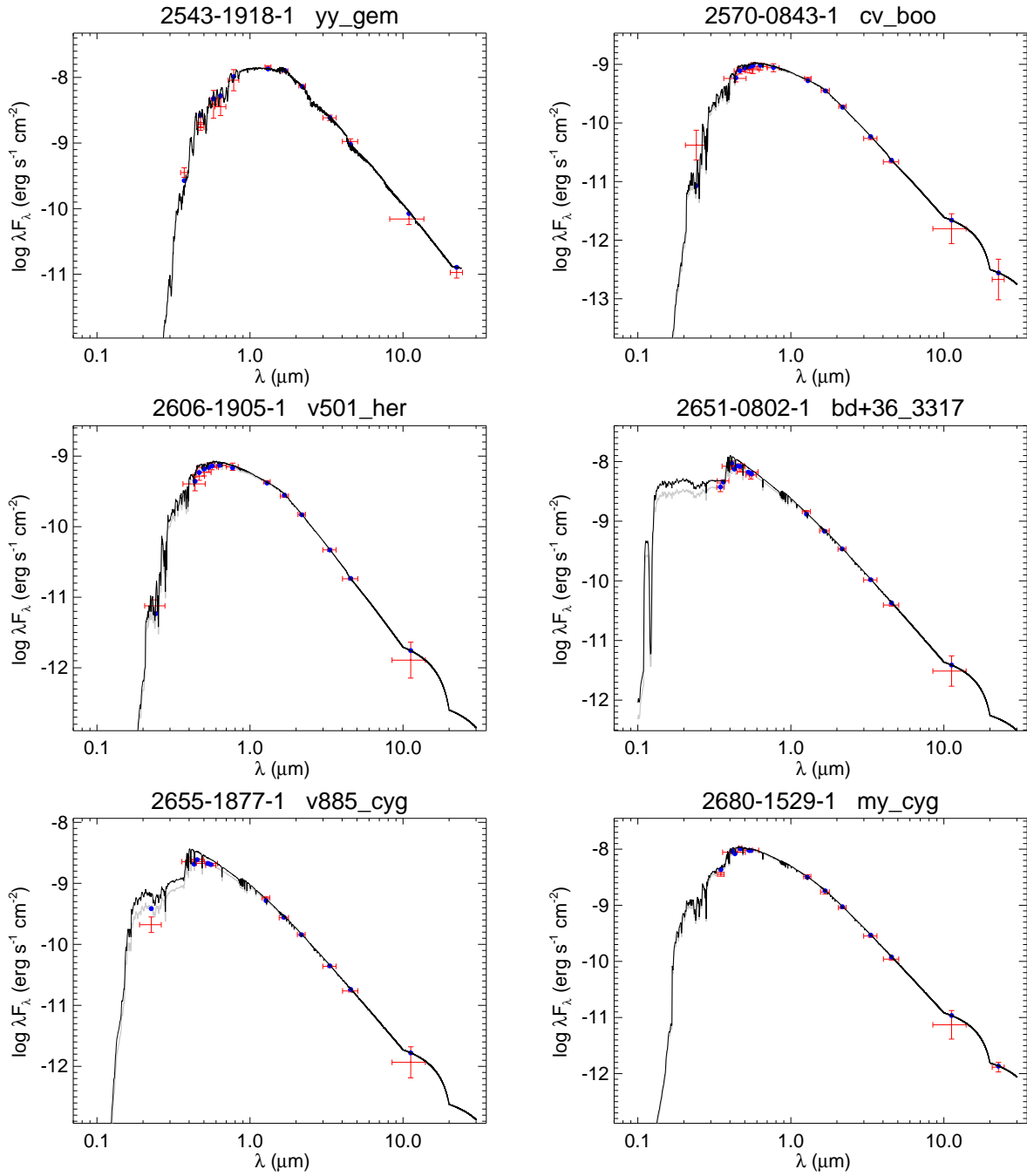


Fig. 20.— All labels, lines, symbols, and colors as in Figure 11.

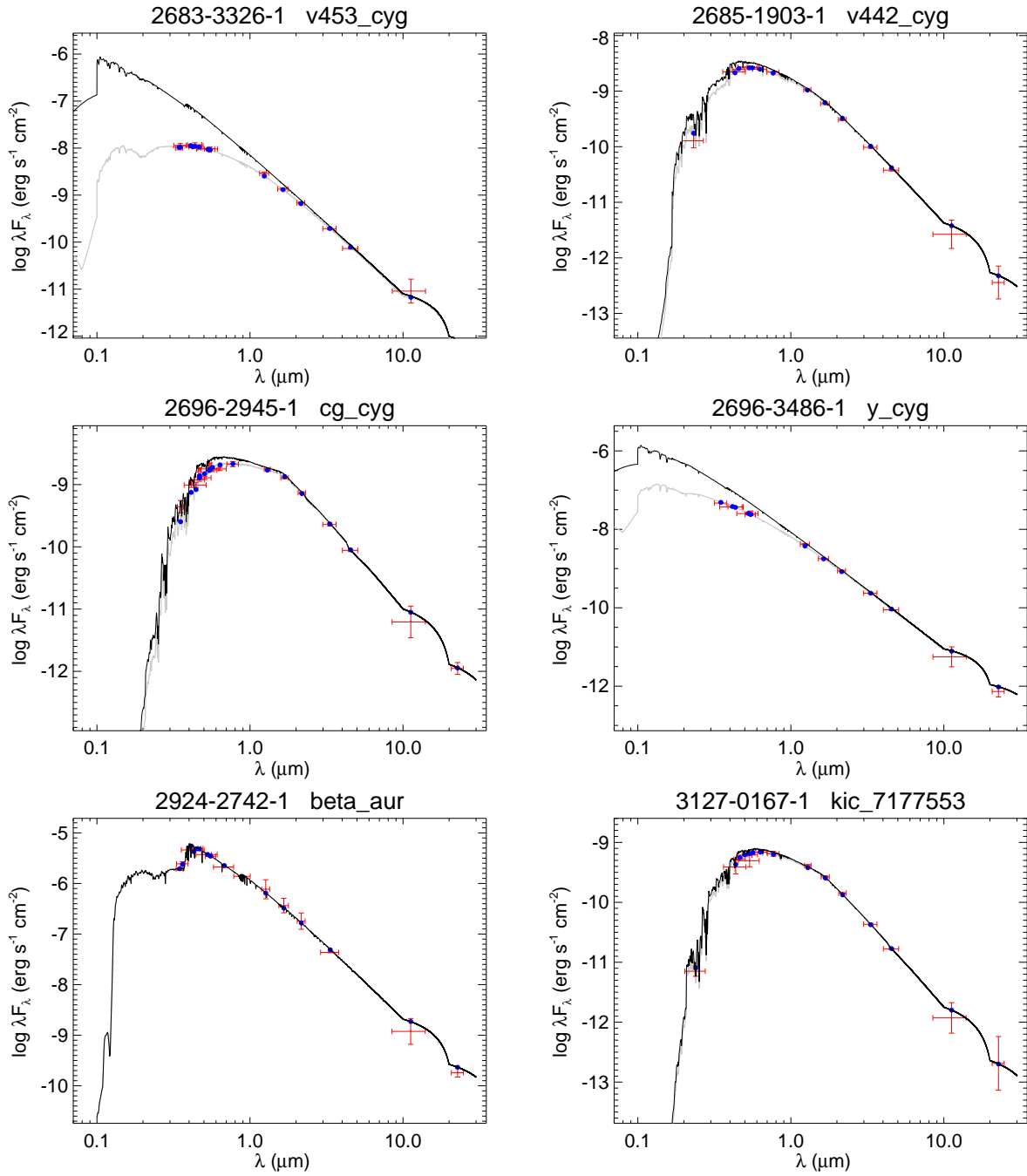


Fig. 21.— All labels, lines, symbols, and colors as in Figure 11.

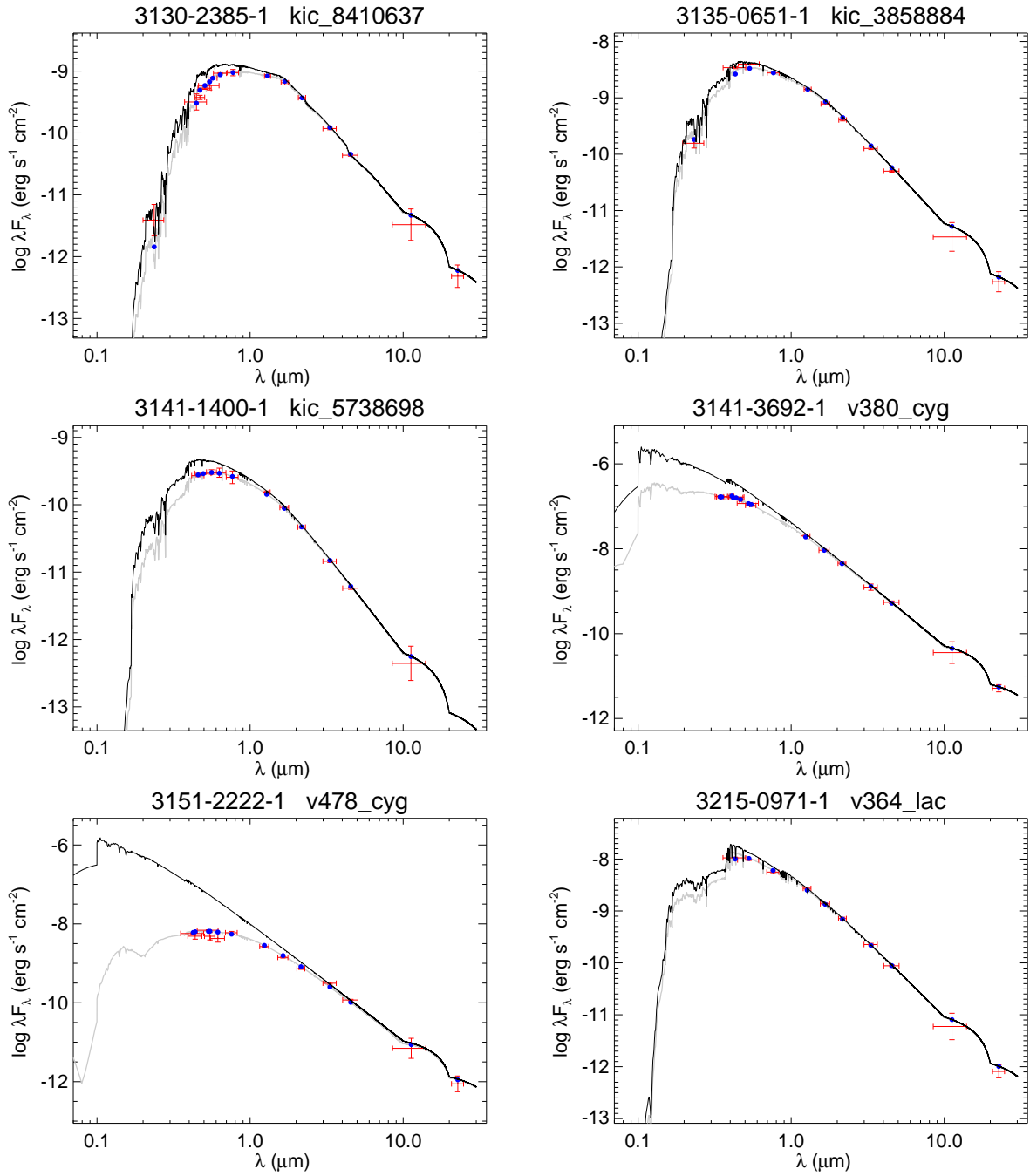


Fig. 22.— All labels, lines, symbols, and colors as in Figure 11.

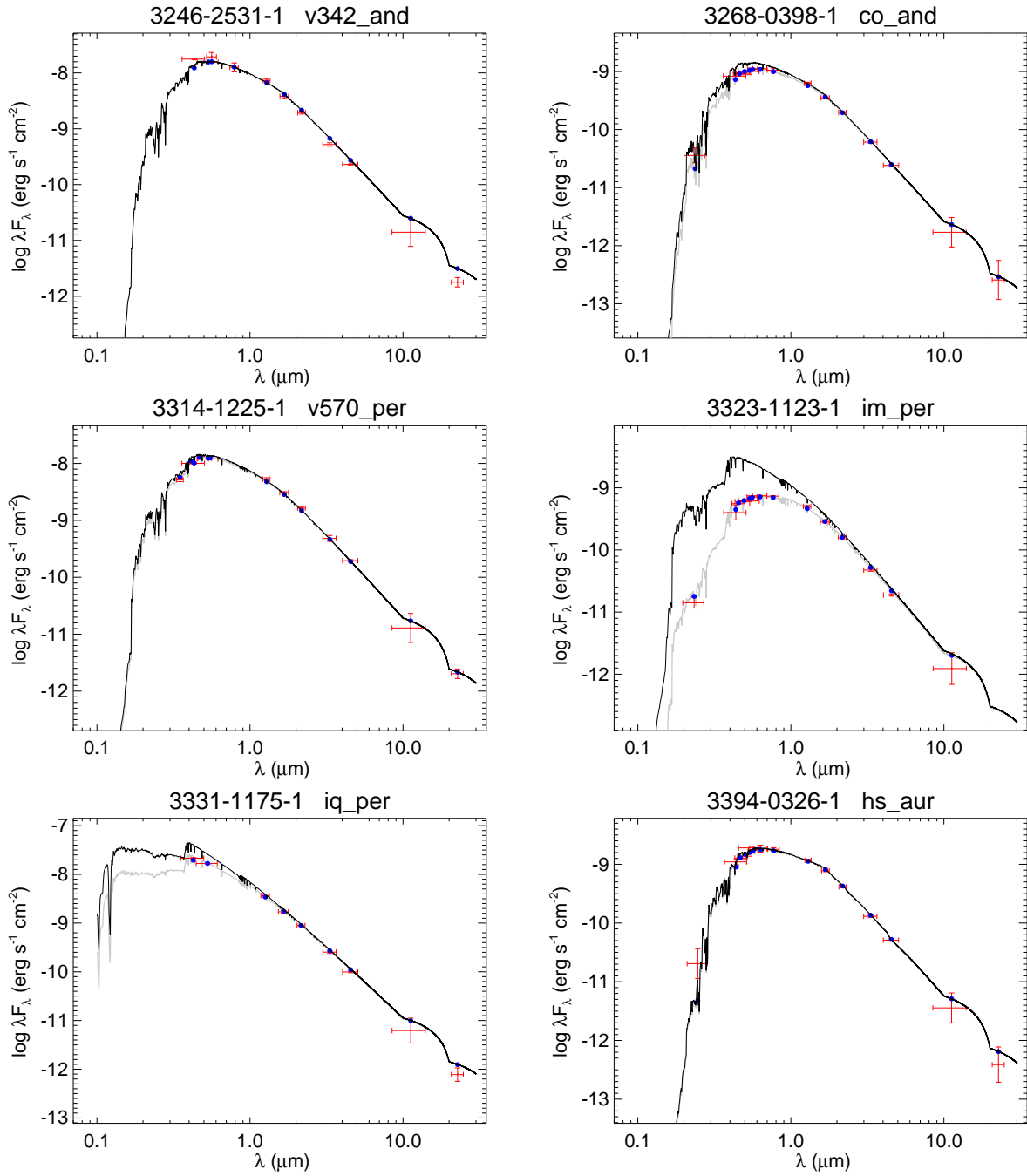


Fig. 23.— All labels, lines, symbols, and colors as in Figure 11.

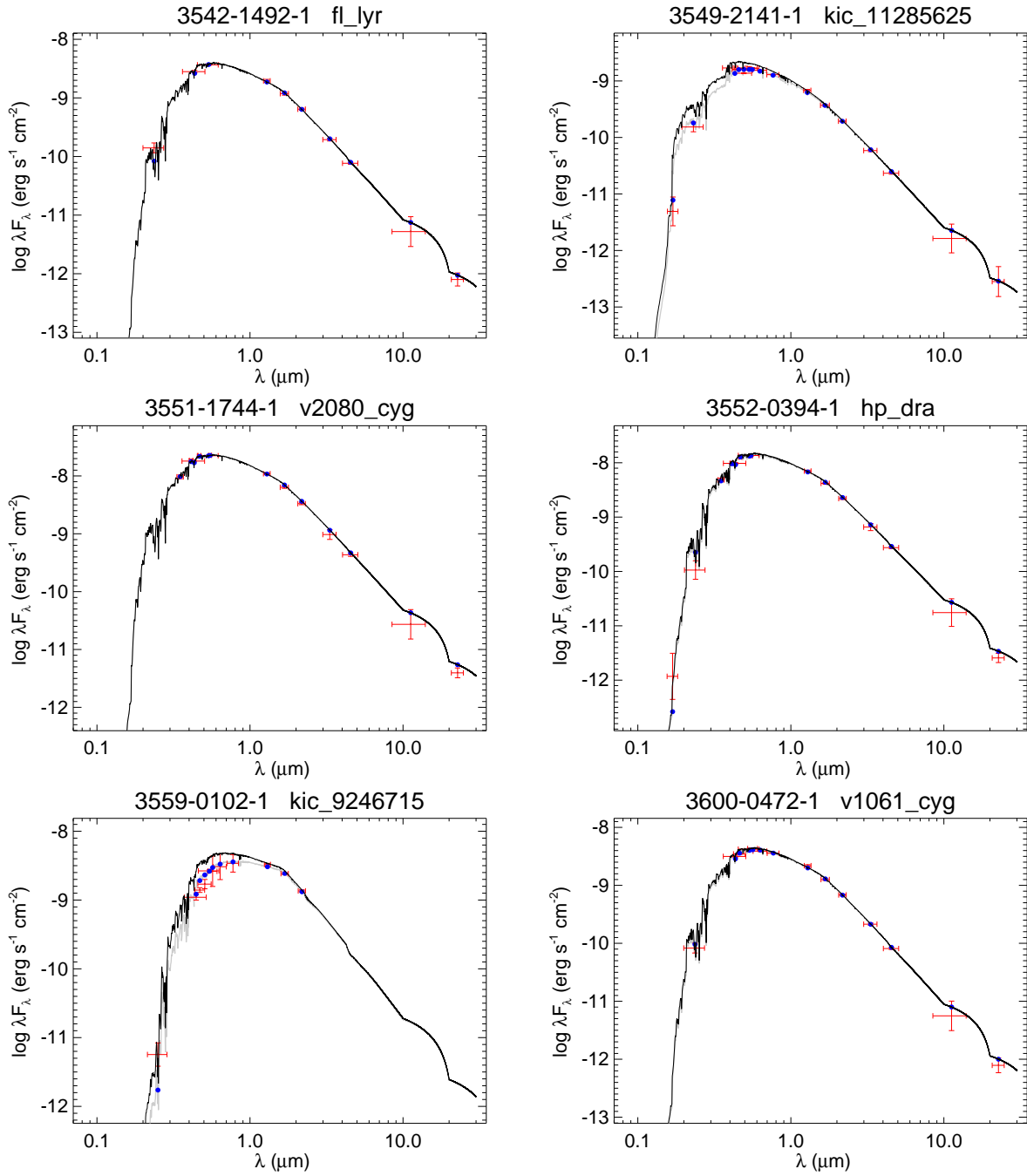


Fig. 24.— All labels, lines, symbols, and colors as in Figure 11.

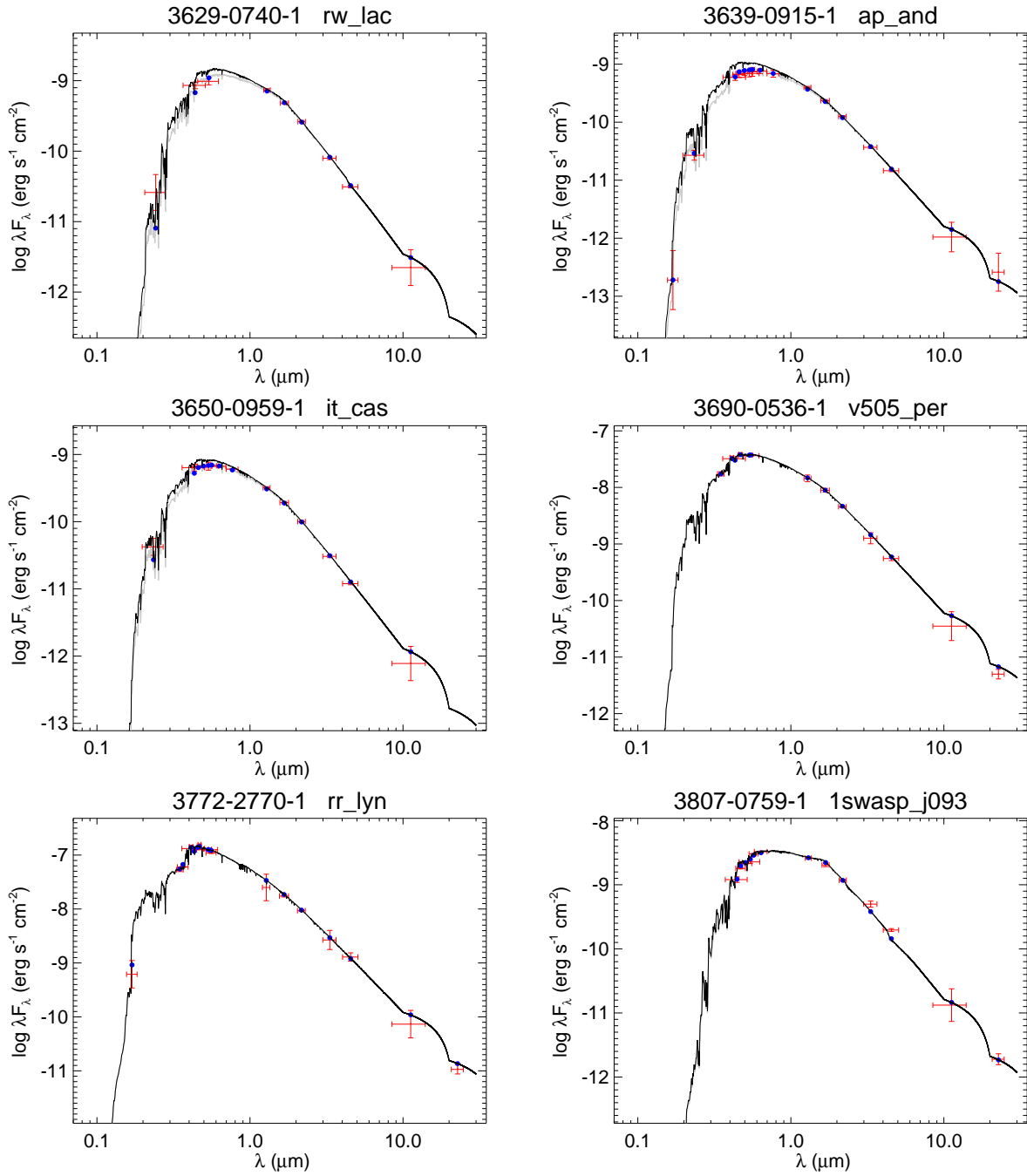


Fig. 25.— All labels, lines, symbols, and colors as in Figure 11.

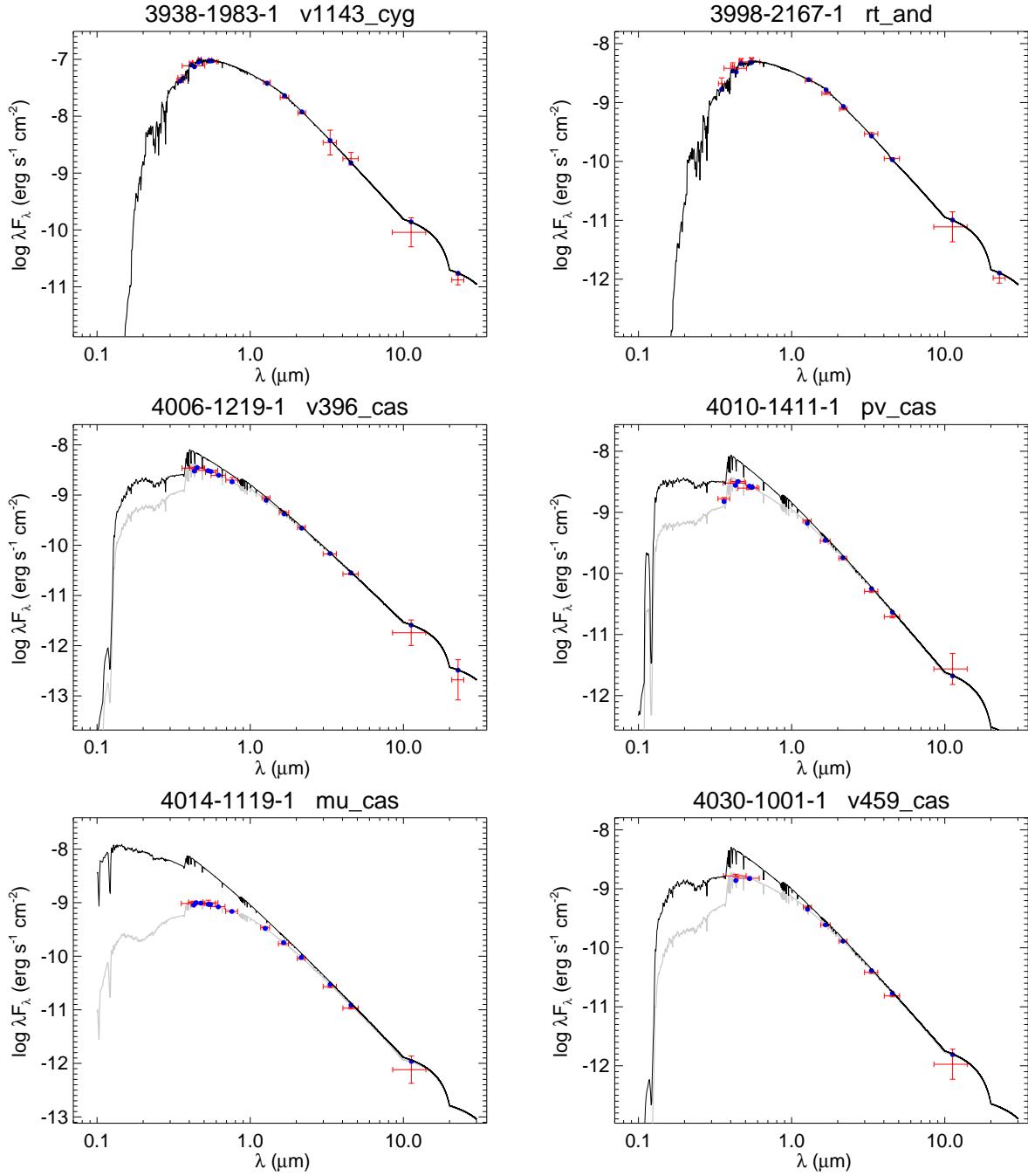


Fig. 26.— All labels, lines, symbols, and colors as in Figure 11.

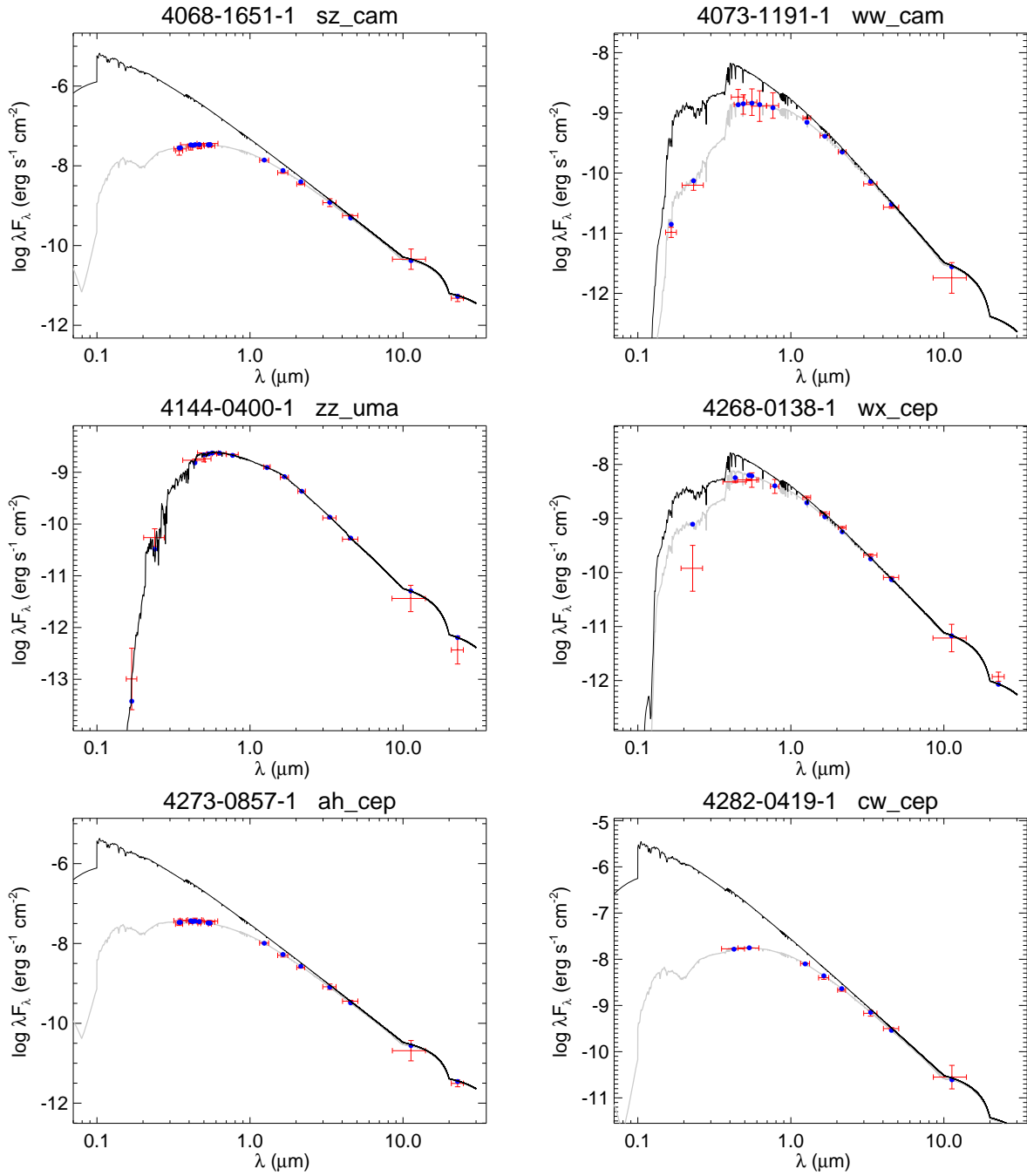


Fig. 27.— All labels, lines, symbols, and colors as in Figure 11.

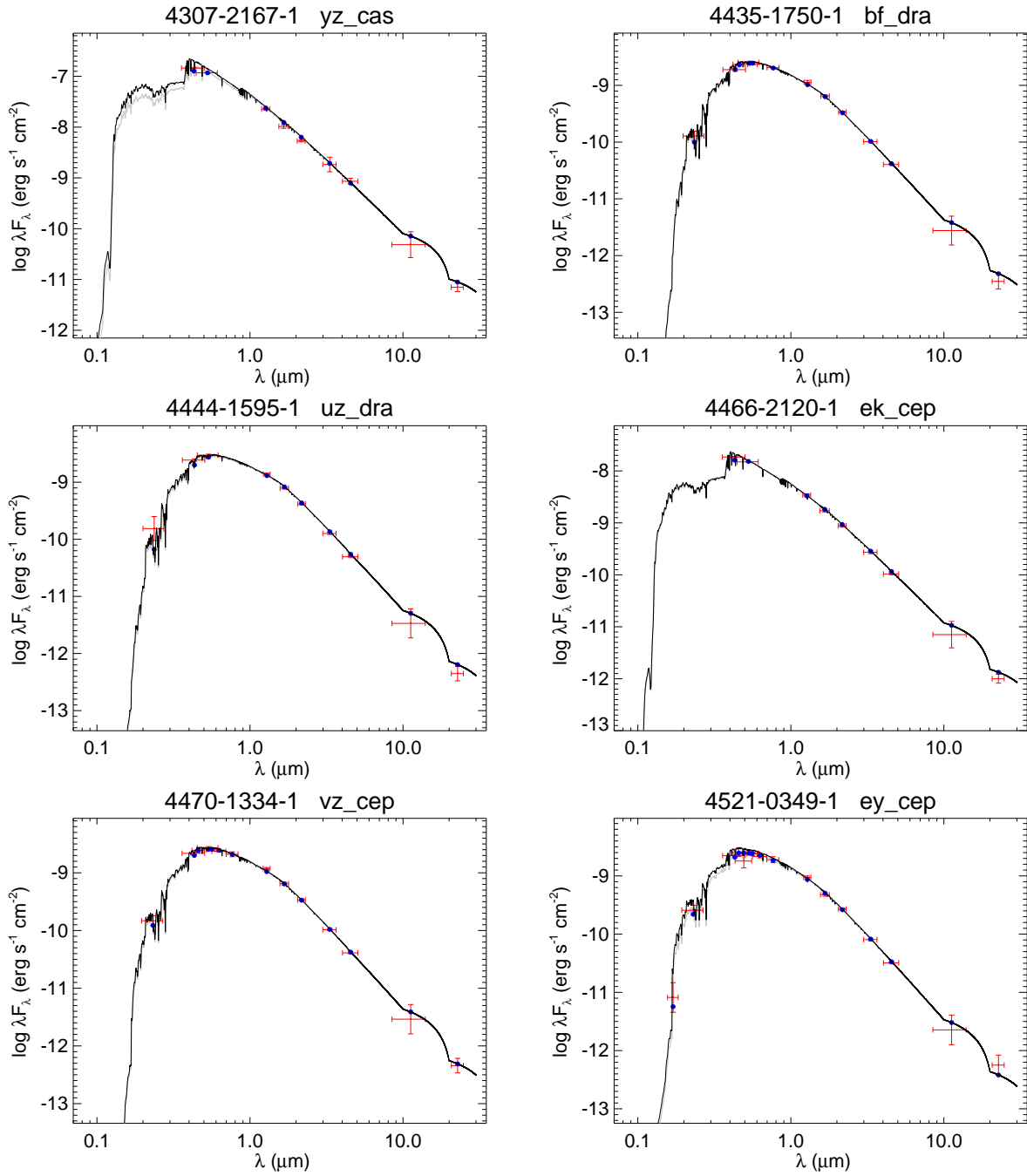


Fig. 28.— All labels, lines, symbols, and colors as in Figure 11.

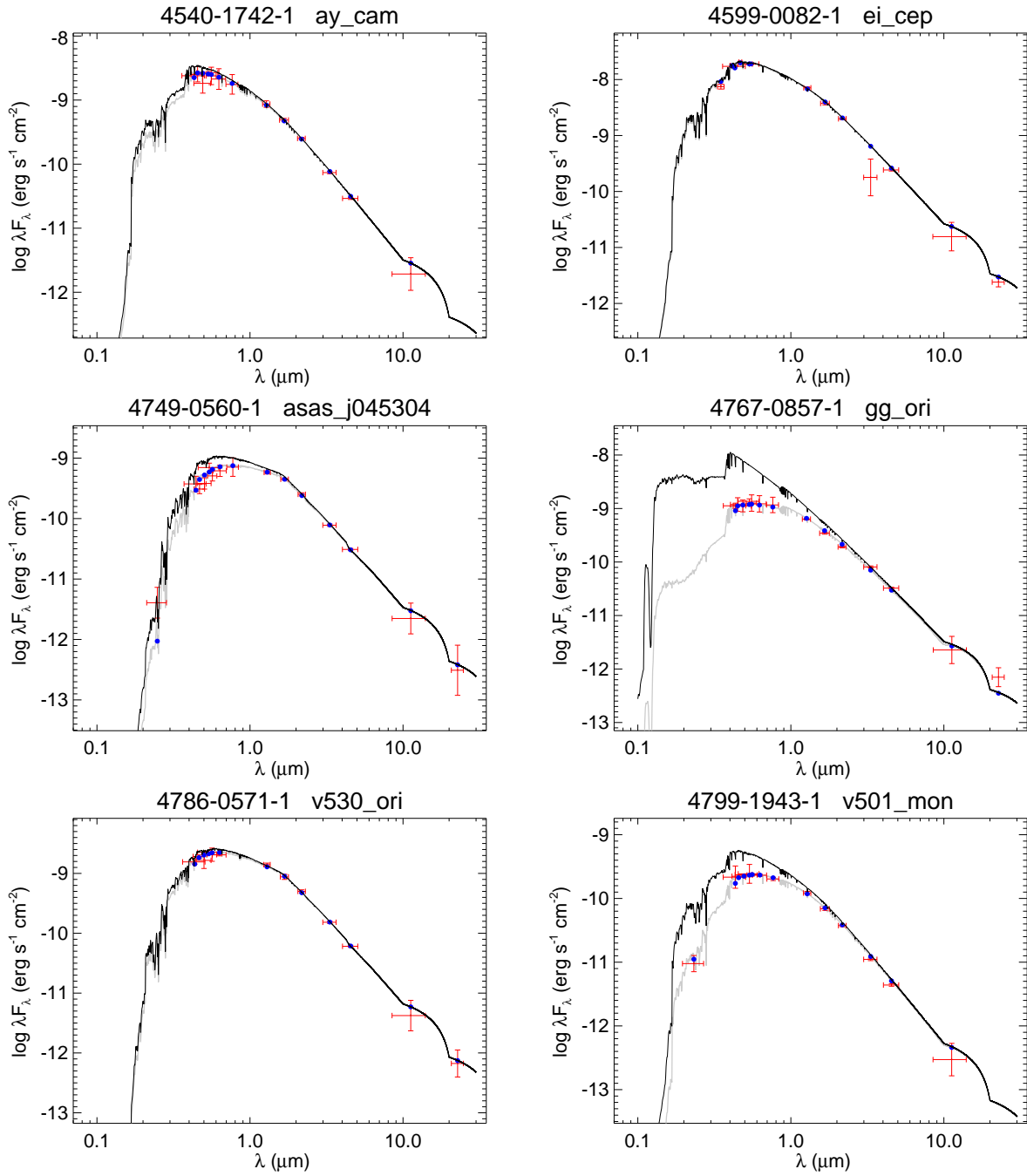


Fig. 29.— All labels, lines, symbols, and colors as in Figure 11.

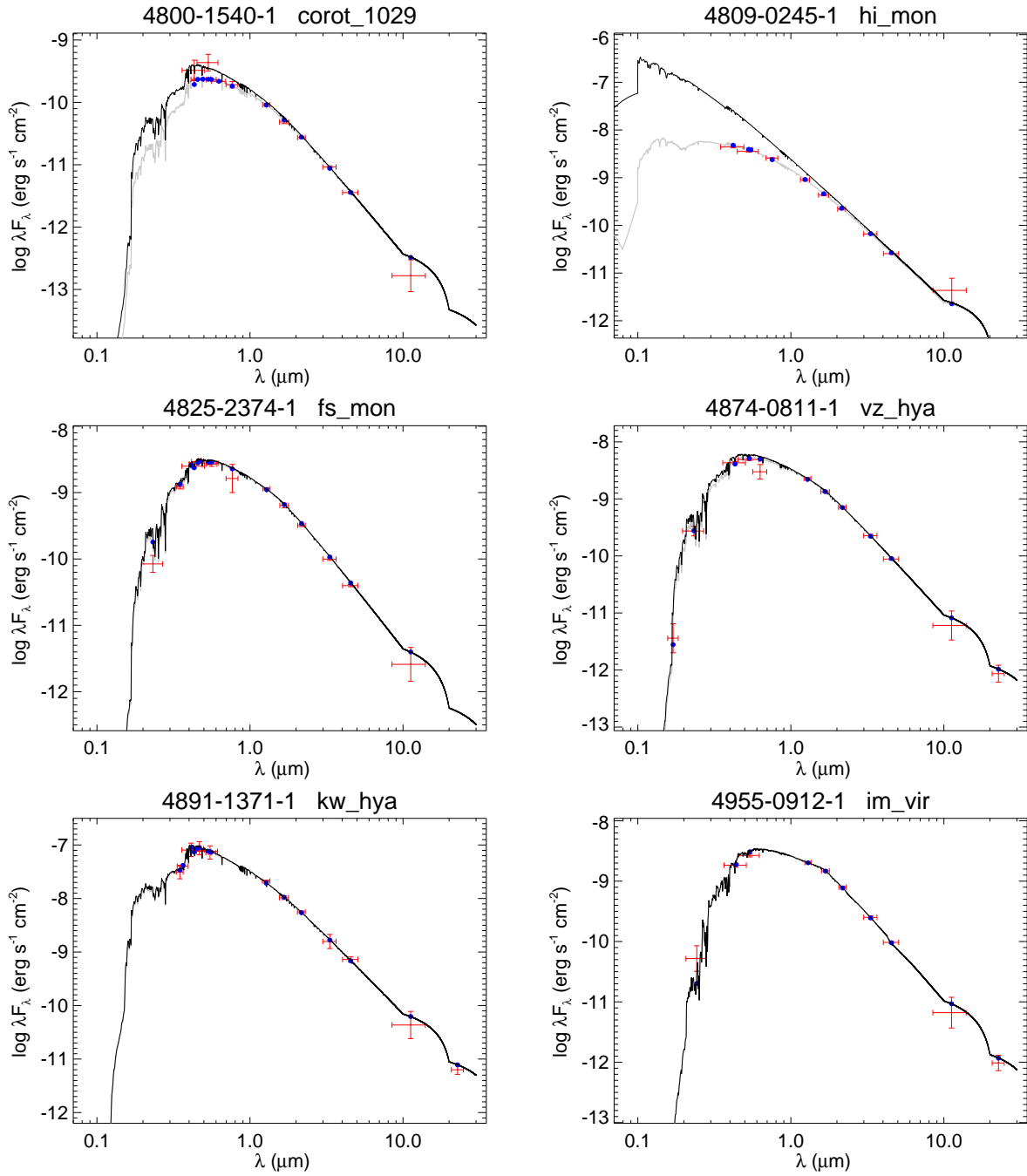


Fig. 30.— All labels, lines, symbols, and colors as in Figure 11.

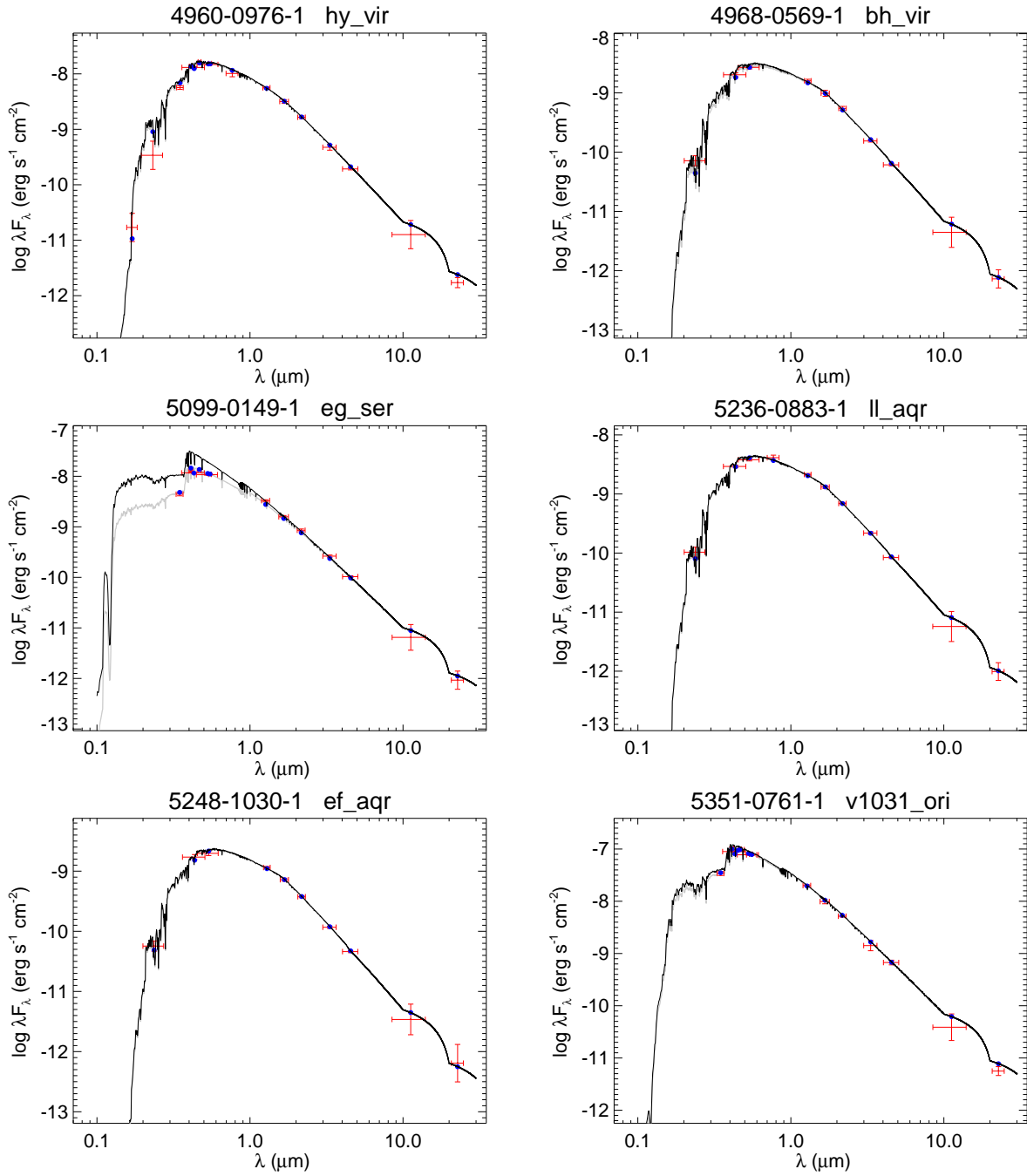


Fig. 31.— All labels, lines, symbols, and colors as in Figure 11.

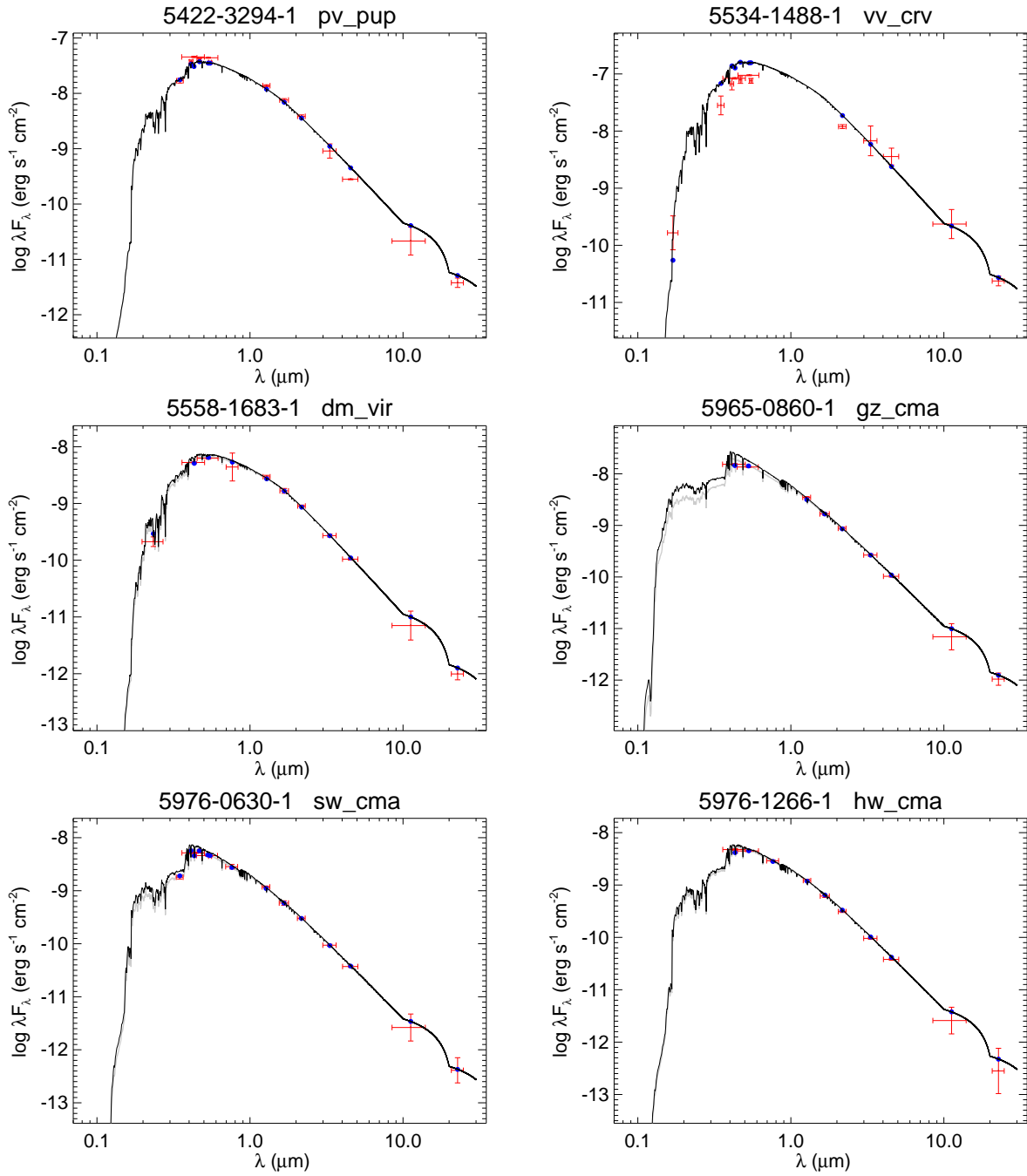


Fig. 32.— All labels, lines, symbols, and colors as in Figure 11.

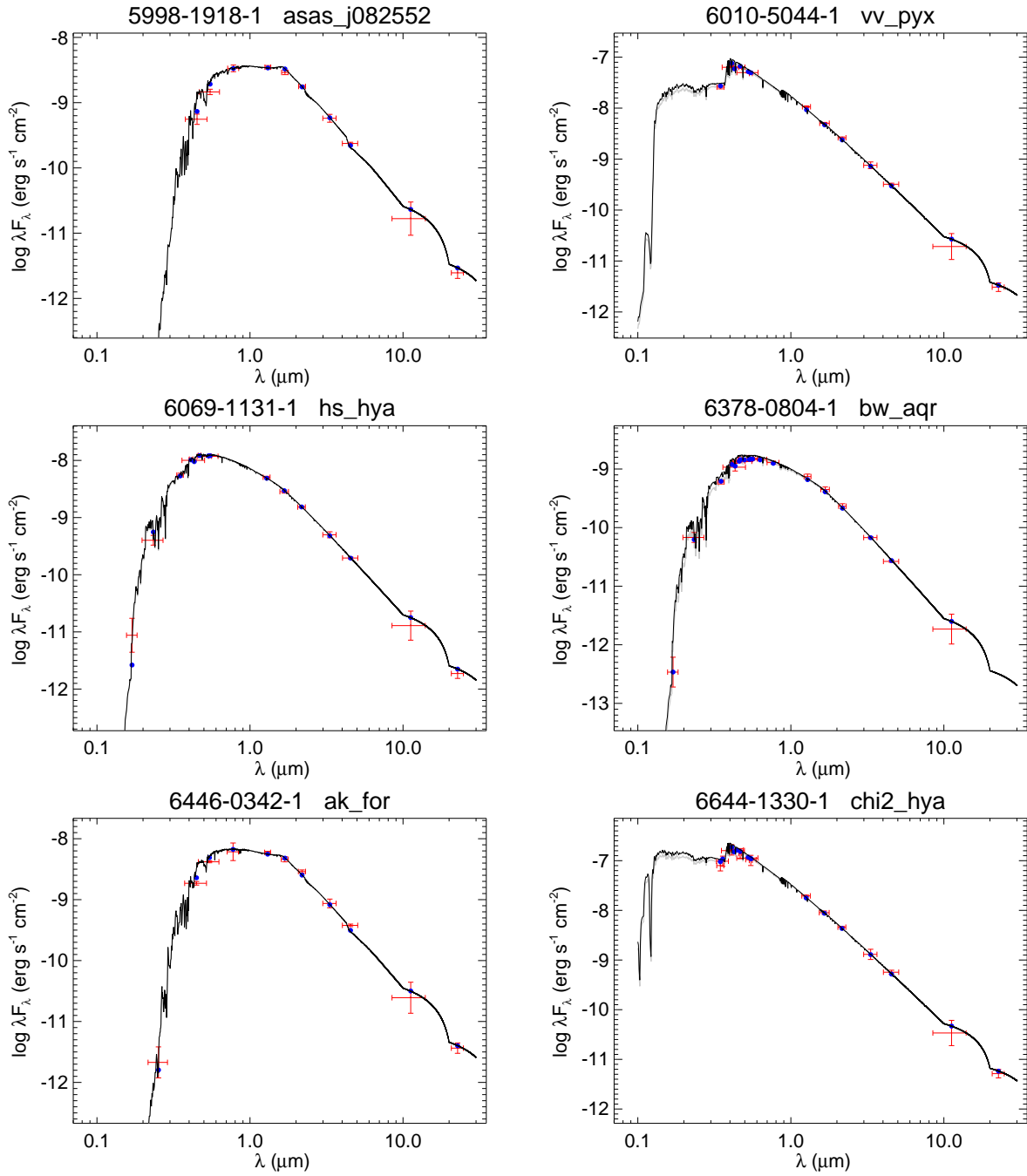


Fig. 33.— All labels, lines, symbols, and colors as in Figure 11.

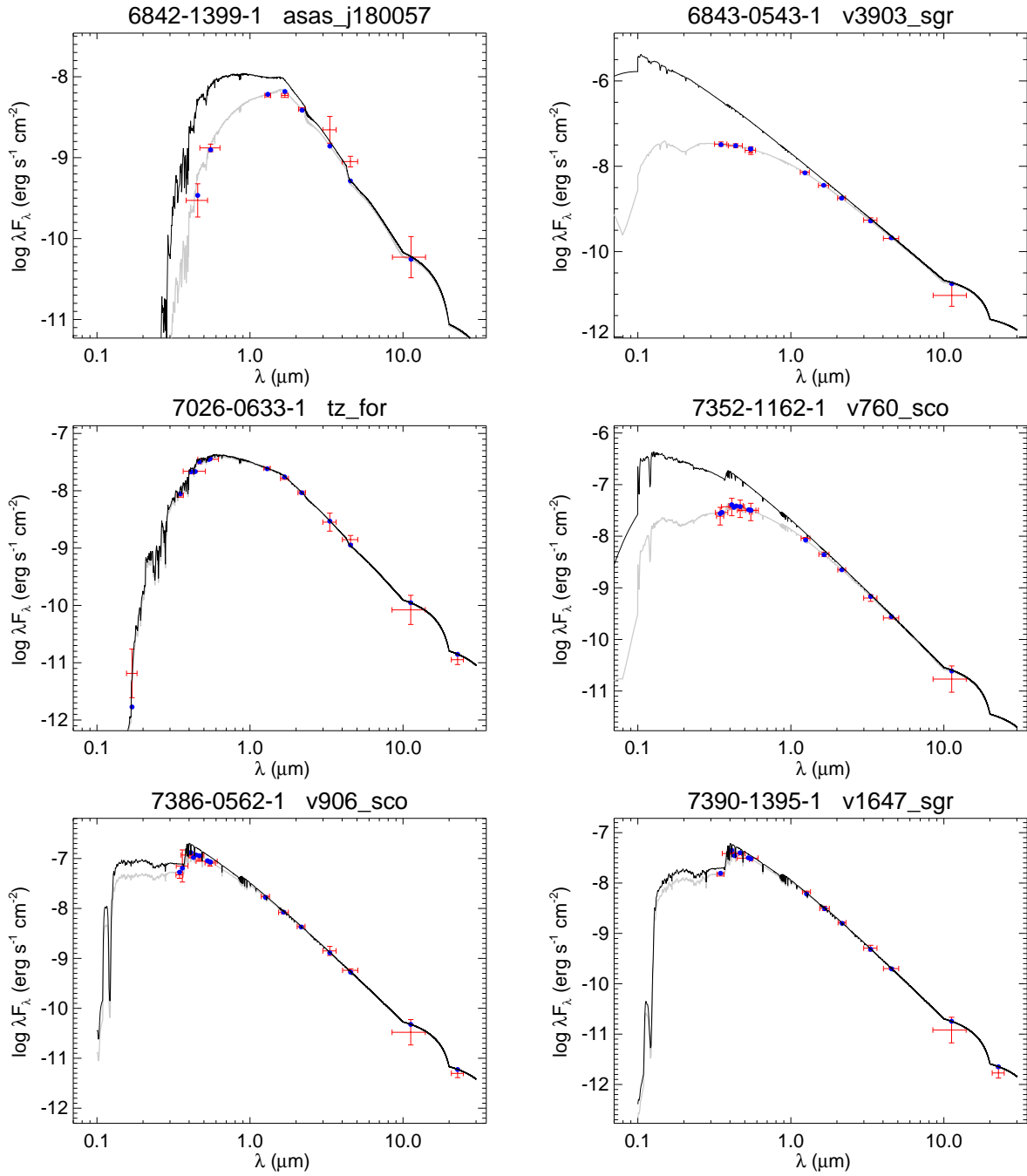


Fig. 34.— All labels, lines, symbols, and colors as in Figure 11.

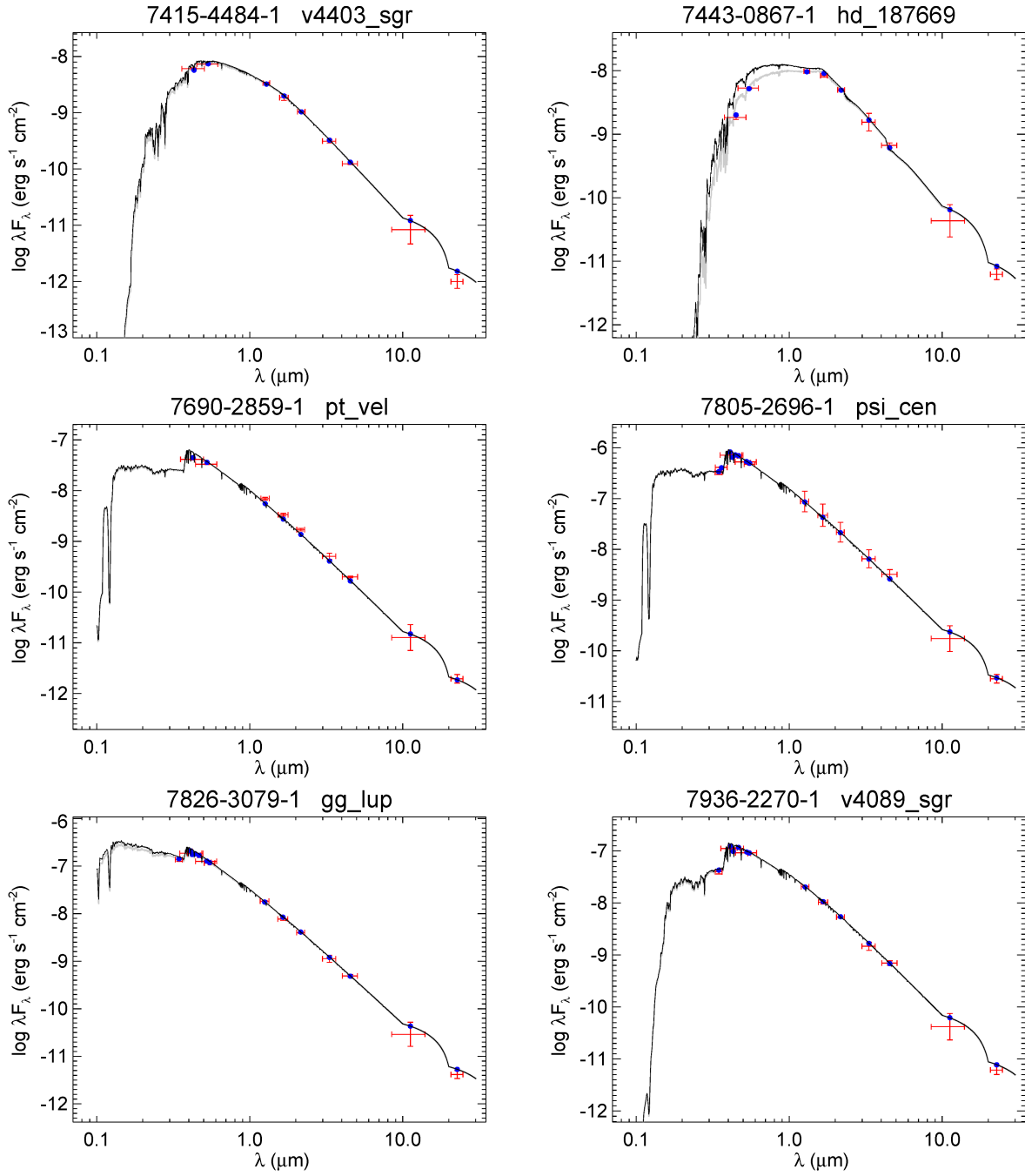


Fig. 35.— All labels, lines, symbols, and colors as in Figure 11.

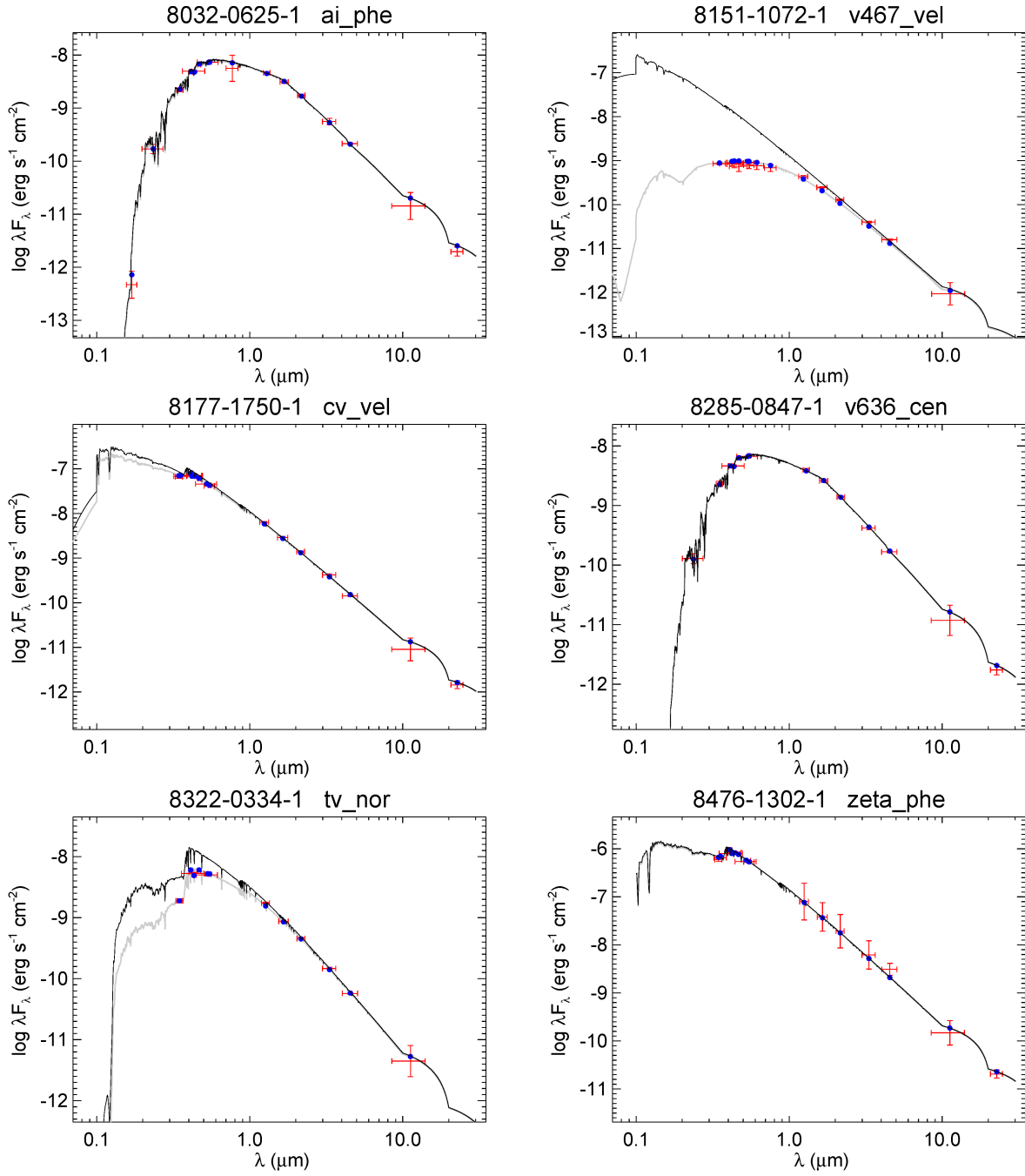


Fig. 36.— All labels, lines, symbols, and colors as in Figure 11.

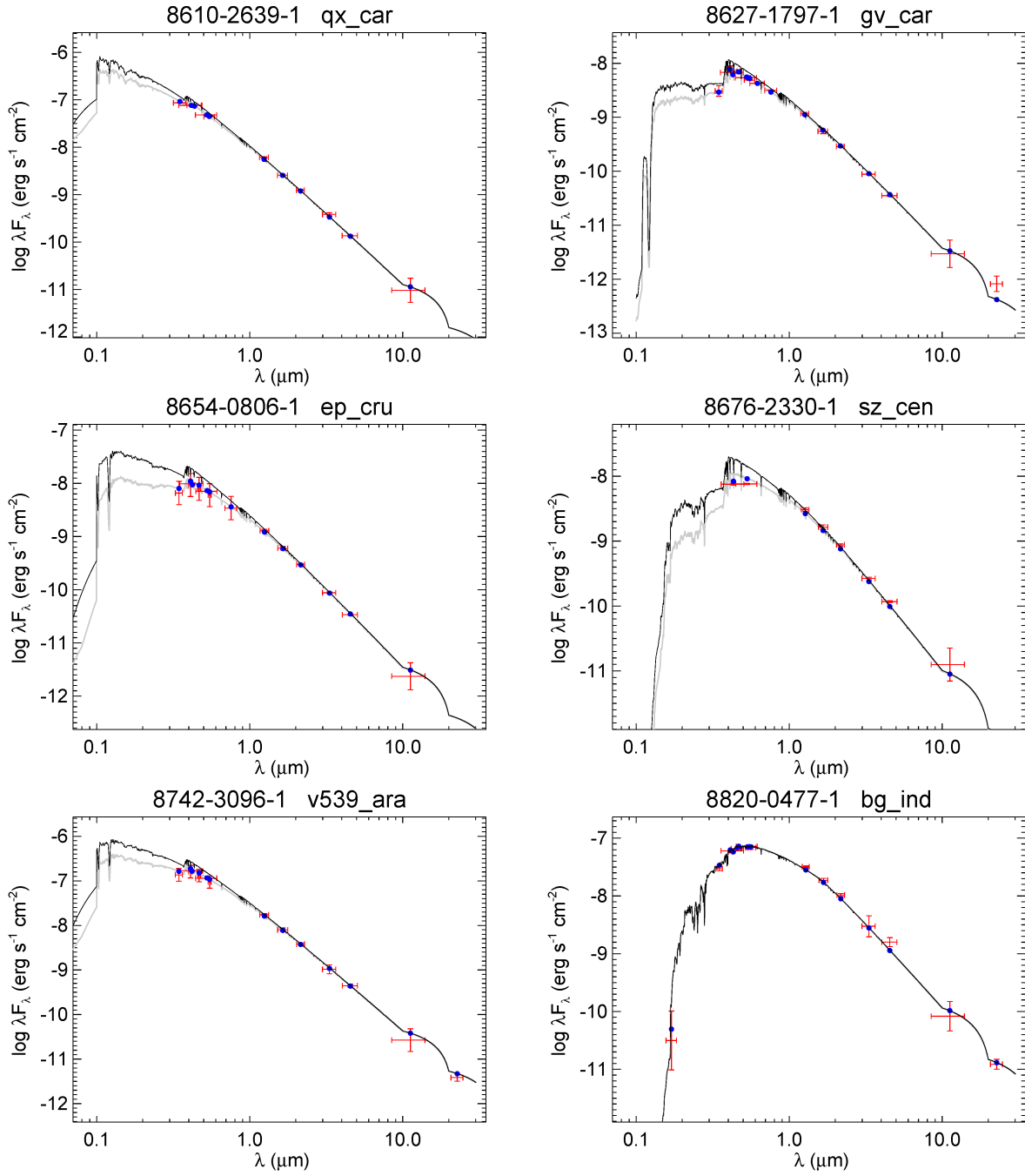


Fig. 37.— All labels, lines, symbols, and colors as in Figure 11.

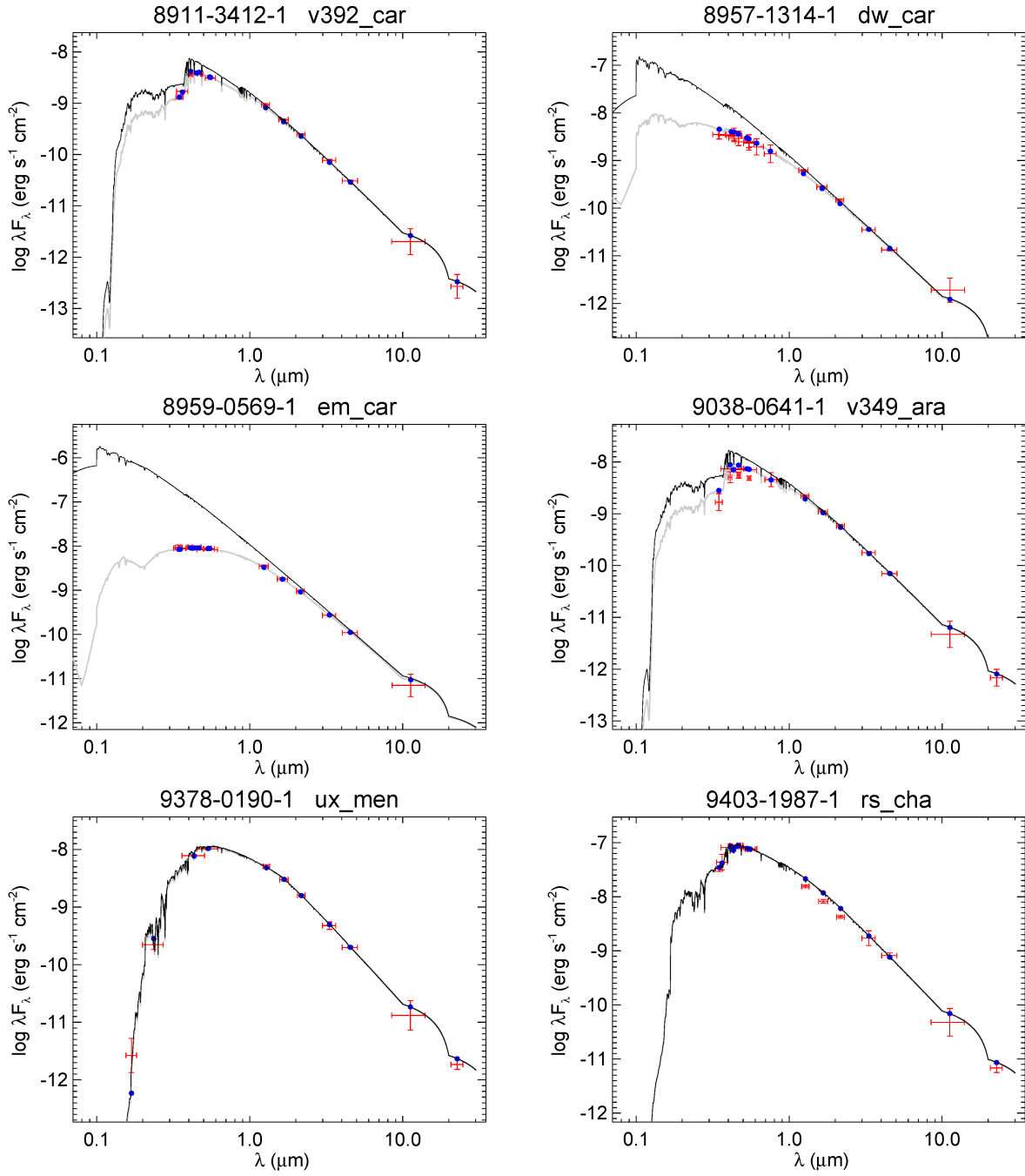


Fig. 38.— All labels, lines, symbols, and colors as in Figure 11.

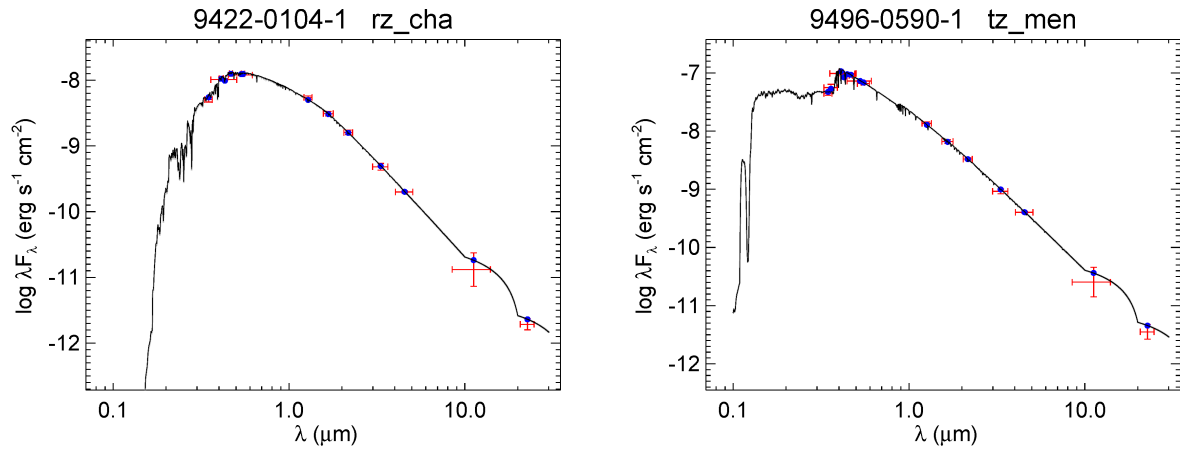


Fig. 39.— All labels, lines, symbols, and colors as in Figure 11.